Dissertation zur Erlangung des Doktorgrades

der Fakultät für Chemie und Pharmazie

der Ludwig-Maximilians-Universität München

Pattern recognition receptors are subset specific in dendritic cells

In vivo quantitative proteomic investigations using

label-free analysis and the SILAC mouse

Christian A. Luber

aus

Hirschau / Oberpfalz

2009

Table of Contents

1   Introduction

1.1   The immune system

The immune system (from Latin: *immunis* = free, untouched) is the entirety of all organs, cells and proteins, which are used by an organism to defend itself from the threat of pathogenic invaders including viruses, bacteria and parasites, and harmful substances. The immune system is also responsible for recognizing and destroying pathological, transformed cells and for keeping healthy cells untouched.

The first lines of defense against pathogens are natural barriers of the organism like epithelium of skin and mucosa. In case of failure of physical hurdles all vertebrates use innate and adaptive immune responses for recognition, clearance and protection from invading microorganisms.

1.1.1   Innate immune responses

The innate component of the vertebrate's immune system is the most universal and most rapidly acting branch of the immune response, consisting of the complement system, phagocytic cells and soluble factors like interferons. For example, the C3b molecule, a fragment of the complement component C3, becomes attached on the surface of invading microorganisms. Subsequently phagocytic cells, equipped with surface receptors for C3b, recognize these labeled invaders and remove them by engulfment. Most phagocytosis is conducted by specialized cells such as macrophages, granulocytes and dendritic cells (see also chapter 1.2). Macrophages and dendritic cells (DCs) are further equipped with specific receptors – so called *Pattern Recognition Receptors* (PRRs), which recognize conserved structural motifs of pathogenic microorganisms (see also chapter 1.3, (Janeway, 1989; Medzhitov and Janeway, 2000). Triggering of PPRs induces cytokine release, like the proinflammatory cytokines interleukin (IL)-1, IL-6, tumor necrosis factor (TNF)-α and type I interferons. A further important group of innate immune cells are natural killer (NK) cells. Even if NK cells seem not to express PRRs, they play an important role in the early response to tumors and infection with viruses or intracellular bacteria and.

Defense against infection is based on the described players of the innate immune system. These host-resistance mechanisms are thought to be responsible for the major part of host defense (Zinkernagel, 2003). However, as pathogens have developed their own immune evasion mechanisms during co-evolution with the host immune system, innate immunity alone is often inadequate for their clearance.

1.1.2   Adaptive immune responses

In case of failed elimination of invading microorganisms by the innate arm of the immune system, continuous production of inflammatory mediators leads to activation of adaptive immune responses. Unlike the innate component, which recognizes microorganisms via a limited number of germ line encoded receptors, pathogen detection of the adaptive immune system relies on a vast number of antigen receptors with unique specificities, which are generated via somatic recombination.

T-lymphocytes (T-cells) are the main mediators of cellular adaptive immunity. These T-cells only recognize antigenic peptides that are bound to Major Histocompatibility Complexes (MHC), via their T-cell receptors. This limitation is called MHC restriction (Zinkernagel and Doherty, 1974). According to their surface markers T-cells can be subdivided in $CD8^+$ T lymphocytes, also called cytotoxic T-cells (CTLs), which recognize antigens bound on MHC class I molecules for direct killing of virus infected or oncogenic transformed cells (Kagi et al., 1994; O'Rourke and Mescher, 1992; Squier and Cohen, 1994) and $CD4^+$ T-cells, also called T-helper-cells, which recognize antigenic peptides bound on MHC class II molecules. $CD4^+$ T-cells further develop into T_H1 or T_H2 helper-cells. T_H1 cells are mainly responsible for the activation of macrophages and the induction of inflammatory processes, whereas T_H2 cells are anti-inflammatory and activate B-lymphocytes (B-cells), which start to develop into antibody-secreting plasma cells or into memory cells. The humoral branch of adaptive immunity is based on B-cells. As the most striking feature B-cells possess membrane located antibodies, the so-called B-cell receptor. The developmental program of B-cells includes a variety of gene rearrangement steps, which potentially lead to receptor specificities for any antigens they may encounter. After recognition of the cognate antigen, receptor-antigen complexes are endocytosed, proteolytically digested, bound on MHC class II molecules and presented to T-cells (Parker, 1993). The successful recognition by T-cells, in the presence of secreted mediators leads to clonal proliferation and differentiation of B-cells into antibody-producing plasma cells or memory cells. In case of later infection with the same pathogen, the established immunological memory will induce a faster and more intensive immune response.

1.2   Dendritic cells

Dendritic cells are the most potent type of professional antigen presenting cells (APCs). DCs are central to the induction of innate and adaptive immune responses and are involved in inducing both $CD4^+$ and $CD8^+$ T-cell responses against antigens presented on MHC class I and MHC class II molecules, respectively (Steinman, 2007; Steinman and Banchereau, 2007). In contrast, other professional APCs like macrophages or B-cells (Table 1-1) and especially non-professional APCs like thymic cortical epithelial cells or glia cells in the brain, which only express MHC class II molecules after stimulation (e.g. IFN-γ) are less efficient in inducing primary immune responses. DCs are also involved in tolerance processes in central and peripheral lymphatic organs (Mellman and Steinman, 2001; Steinman and Nussenzweig,

2002; Stockinger, 1999) and support the survival of naïve T-lymphocytes in the periphery (Brocker, 1997; Muranski et al., 2000). Furthermore, in the adaptive arm of immunity, DCs decisively regulate the outcome of T-cell responses, whereas in innate immunity DCs influence NK- and NKT-cells via secretion of the cytokine IL-12 or type I and II interferons. How DCs fulfill these multiplex, partially contrary tasks is not yet fully understood.

Table 1-1 Specialization of different professional antigen presenting cells (adapted from (Belz et al., 2009)

	Dendritic cells	Macrophages	B cells
Antigen uptake	Phagocytosis, Macropinocytosis Receptor-mediated endocytosis	Phagocytosis, Receptor-mediated endocytosis	Receptor-mediated endocytosis via immunoglobulin
MHC II expression	Constitutive high levels, inducible	Low level expression, inducible	Constitutive expression, inducible
Antigen presenting function	Activation of naïve T cells	Recruitment of helper $CD4^+$ T cells, Activation of naïve B cells	Recruitment of helper T cells for antibody production

DCs are a rare cell population constituting about 0.05% of total body cells, however they form an extensive network covering all tissues and organs of the body. These cells are specialized in sampling invaded microorganisms in the periphery, travelling via lymphatic vessels or the blood to the draining lymphoid organs and presenting their antigens to the cognate lymphocytes (Banchereau and Steinman, 1998). DCs use macropinocytosis (Sallusto and Lanzavecchia, 1994), phagocytosis (Inaba et al., 1992; Reis e Sousa et al., 1993; Svensson et al., 1997) or receptor-induced endocytosis for uptake of antigens. In contrast to other phagocytes like macrophages, DCs sample their environment in a constitutive manner by uptake of high amounts of extracellular fluid. Additionally, DCs are equipped with specific uptake mechanisms using a variety of different receptors like DEC-205 (Jiang et al., 1995), Fc-receptors (Dubois and Caux, 2005), collagen type I receptor and heat shock receptors like CD91 (Binder et al., 2000). Endocytosed proteins are not presented in an intact form, but rather as short peptides generated from the antigen by proteolytic digestion (Dubois and Caux, 2005; Wykes et al., 1998). Generally, peptides from exogenous sources are presented via MHC class II for interaction with the T-cell receptor of $CD4^+$ T-cells, whereas intracellularly-derived peptides are bound in the groove of MHC class I and presented to $CD8^+$ T-cells.

DCs receiving any danger signal at the time of antigen acquisition convert from being specialized for antigen uptake to being antigen-presenting cells. This process, connected with a broad variety of phenotypic and functional changes, is called maturation (Banchereau et al., 2000). The 'danger signal' (Matzinger, 2001) for these changes can either come from microbial products like LPS or bacterial and viral nucleic acids (Cella et al., 1999; Rescigno et al., 1999). It can also originate from the host inflammatory response itself, for example stimulation by pro-inflammatory cytokines interleukin (IL)-6, IL-1β and TNF-α (Banchereau et

al., 2000). The levels of surface MHC-class II – peptide complexes then increase substantially and the half life of such complexes on the surface is prolonged from 10 to 100 hours (Cella et al., 1997). Simultaneously the expression of T-cell costimulatory molecules like CD80 (B7.1) and CD86 (B7.2) is induced, converting DCs to an activated, mature state. Subsequently DCs are no longer able to take up antigens via endocytosis. Thus they provide a snapshot of the hazardous antigen encountered initially (Pierre et al., 1997; Wilson et al., 2004). Therefore, depending on the maturation state, DCs can lead to either T-cell tolerance or to T-cell activation, which will result in adaptive immunity (Heath and Carbone, 2001).

1.2.1 The Langerhans cell paradigm

The previously described life history of dendritic cells, transforming from highly endoytotic immature cells in the periphery into strongly T-cell activating, but poorly endocytotic cells in the lymphoid organs, was originally derived from Langerhans cells (LCs), a DC type in the epidermis (Schuler and Steinman, 1985). Immature LCs exist in the skin dedicated to capture antigens and as a mature phenotype in the subcutaneous lymph nodes dedicated to present antigens to T-cells. The phenotypic changes during maturation together with specific tissue localization have been considered as a paradigm for all existing DCs. However, the life of DCs seems to be more complicated and most DC subtypes do not follow this simple "two-phase – two location" model. According to the LC paradigm, only immature DCs should be found in lymph nodes of infection-free mice. In reality even lymph nodes of such germ-free mice contain both immature and mature DCs, which is clearly in contradiction to the LC paradigm and may reflect distinct pathways of DC life history (Wilson et al., 2008). Indeed, recent research has revealed that DCs are not a homogeneous cell population but rather a network of different subtypes that are functionally and spatially distinct. Understanding diverse functionality of different DC subsets is not only of academic interest, but also becomes important for DC targeted immune therapies. Especially after the unsuccessful use of monocyte-derived DCs in immunotherapy, it has become clear that an increased knowledge of DC subsets and their function in health and disease will be of high importance for their clinical application.

1.2.2 Dendritic cell subsets of the mouse: a classification

As described above, DCs are a rare cell type located in blood, skin and all lymphoid tissues. These cells play a crucial role in normal immune responses, because mice depleted of DCs, display severe defects during bacterial and viral infections (Ciavarra et al., 2006; Jung et al., 2002). Mouse lymphoid organs and blood contain two distinct subtypes of DCs: conventional and playmacytoid DCs. Here I will focus mainly on DCs from the spleen.

1.2.2.1   Plasmacytoid dendritic cells

The family of circulating DCs consists of plasmacytoid DCs (pDCs), which exist in steady state as rounded cells, and which are characterized by expression of CD45RA and intermediate levels of CD11c (O'Keeffe et al., 2002a). Phenotypically distinct subsets have been reported, which can be separated by CD4 and CD8α expression (O'Keeffe et al., 2002a; Yang et al., 2005). They are found both in lymphoid and peripheral tissues and circulate within the blood stream (O'Keeffe et al., 2003). Upon activation pDCs acquire the typical DC morphology, which is accompanied by the secretion of large amounts of type I interferon (IFN) and are hence known as interferon-producing cells (Liu, 2005). This activation is caused by exposure to viruses, DNA, RNA or synthetic mimetics thereof in the form of TLR ligands like CpG-DNA (Krug et al., 2001) or single stranded (ss)RNA (Diebold et al., 2004), TLR9 and TLR7 agonists, respectively. There are indications that pDCs in different tissues function differentially: TLR9 was reported to be crucial for detection of herpes simplex virus 1 (HSV-1) in splenic pDCs, whereas pDCs of the bone marrow (BM) can respond both in a TLR9 dependent and independent manner (Hochrein et al., 2004).

There is no doubt that pDCs have an important function in innate immune responses due their outstanding ability to rapidly produce high levels of type I IFN (Barchet et al., 2005a; Barchet et al., 2005b). How pDCs are able to stimulate naïve T cells is still controversial and discussed at length in the literature. New potential roles of pDCs in antigen capture, processing, presentation and presentation to T cells at sites of infection have recently been reported (Villadangos and Young, 2008; Young et al., 2008).

1.2.2.2   Resident, conventional dendritic cells of the spleen

Around 1% of total splenocytes are DCs, of which approximately 80% belong to conventional (cDCs) and the remaining 20% to pDCs. Resident cDCs can be divided into three subsets according to their expression of the CD8α homodimer and the CD4 molecule: $CD4^+CD8\alpha^-$, referred to as $CD4^+$ cDCs, $CD4^-CD8\alpha^+$, referred to as $CD8\alpha^+$ cDCs, and $CD4^-CD8\alpha^-$, referred to as double negative (DN) cDCs (Vremec et al., 2000; Vremec et al., 1992). The resident DCs from the spleen develop directly from bone marrow derived precursors within the lymphoid organs without any trafficking through peripheral tissues and keep – in the absence of any infection – an immature phenotype throughout their entire lifetime (Wilson et al., 2003). The "immature" phenotype still expresses high levels of MHC class II on the cell surface relative to other hematopoietic cells.

1.2.2.2.1 $CD8\alpha^+$ conventional dendritic cells

CD8α expression can be found on around 25% of all $CD11c^{hi}$ cDCs as an αα homodimer rather than as an αβ heterodimer expressed on T cells (Vremec et al., 1992). These $CD8\alpha^+$ cDCs reside, unlike other cDCs, in the T cell area of the spleen in the steady state (De Smedt et al., 1996), and correspond most probably to the interdigitating cell (IDC), which has been

described earlier (Agger et al., 1992; Veerman and van Ewijk, 1975). With a life span of about 3 days, CD8α^+ cDCs are the shortest lived splenic cDC population. One hallmark of CD8α^+ cDCs is their ability to secrete enormous amounts of the pro-inflammatory cytokine IL-12p70 upon activation (Hochrein et al., 2001; Reis e Sousa et al., 1997). This cytokine leads to T_H1 priming of CD4$^+$ T cells (Maldonado-Lopez et al., 1999). Additionally CD8α^+ cDCs secret IL-6 and TNF-α (Proietto et al., 2004), and under certain circumstances even type I IFNs (Hochrein et al., 2001).

CD8α^+ cDCs play a unique role in the maintenance of peripheral tolerance. During negative selection of T cells in the thymus, not all tissue specific antigens are expressed potentially leading to autoreactive T cells (Starr et al., 2003). For the prevention of autoimmunity, peripheral mechanisms of tolerance are mediated by dendritic cells (Hawiger et al., 2001). There are indications that CD8α^+ cDCs are involved in this process (O'Keeffe et al., 2005a).

In the classical pathway endogenous antigens are presented via MHC class I molecules and exogenous antigens via MHC class II molecules. However, this model does not explain how exogenous self-antigen can access the MHC class I pathway for induction of immunity and tolerance. One unique key feature of CD8α^+ cDCs is their exclusive ability to "cross-present" antigens. In this process exogenous antigens are directed towards the MHC class I pathway, enabling presentation to the TCR of CD8$^+$ T cells (den Haan et al., 2000; Villadangos and Schnorrer, 2007). Cross-presentation clearly plays an important role in the context of CD8 T cell priming towards infection with lytic and non-lytic viruses and intracellular bacteria, tumor surveillance and maintenance of peripheral tolerance (Belz et al., 2005; Belz et al., 2004; Chen et al., 2004; Heath et al., 2004). However the precise molecular mechanisms are still ill defined and remain controversial (Groothuis and Neefjes, 2005; Lin et al., 2008).

CD8α^+ cDCs, unlike other cDCs of the spleen, absolutely require interferon response factor 8 (IRF8, also known as ISCBP) for development and normal immune function (Tamura et al., 2005). Additionally CD8α^+ cDCs uniquely express TLR3, enabling these cells to recognize dsRNA viruses.

1.2.2.2.2   CD4$^+$ conventional dendritic cells

CD4$^+$CD8α^- cDCs comprise around 50% of all splenic cDCs. In contrast to T cell area located CD8α^+ cDCs, CD4$^+$ cDCs tend to be found in the marginal zones of the spleen (Agger et al., 1992; Metlay et al., 1990). However, upon stimulation with TLR agonists like LPS, these cells redistribute to the T cell areas of lymphoid organs (Reis e Sousa et al., 1997).

Compared to other cDCs, CD4$^+$ cDCs produce the highest level of chemokines like Mip3α, Mip3β and RANTES (Proietto et al., 2004), even in a resting state. The functional significance of this chemokine secretion is still not fully understood.

Contrary to CD8α^+ cDCs, CD4$^+$ cDCs have been reported to induce T_H2 response (Hammad et al., 2004; Maldonado-Lopez et al., 1999). The cross-presentation capability of CD4$^+$ cDCs is

also very poor. However, CD4$^+$ cDCs are the most potent presenters of antigens loaded on MHC class II molecules to CD4$^+$ T cells (Pooley et al., 2001). Furthermore, CD4$^+$ cDCs efficiently induce CD4$^+$ T cell responses after antigen targeting via C-type lectin receptors such as Dectin-1 and DCIR-2 (Carter et al., 2006; Dudziak et al., 2007).

Only a few reports are published analyzing the role of CD4$^+$ cDCs in immunity against intracellular pathogens. It has been proposed that CD4$^+$ cDCs play a role in immunity against microbes due their capability to produce TNF-α and iNOS (Serbina et al., 2003). However, the recent observation of de novo-formed DCs during inflammation make it is most likely that these functions have been incorrectly attributed to CD4$^+$ cDCs (Lopez-Bravo and Ardavin, 2008). Therefore, it remains elusive whether or not CD4$^+$ cDCs are crucial for the control of any particular infection.

1.2.2.2.3   CD4$^-$CD8α^- conventional dendritic cells

It has become common to group DN cDCs, about 25% of splenic cDC, which express neither CD4 nor CD8α, together with CD4$^+$ cDCs and define this "new" subset as CD8α^- cDCs. This is mainly justified due to similar gene expression profiles (Edwards et al., 2003a) and similar production of Mip3α, Mip3β and RANTES (note that the levels produced in the steady state are considerably lower than those produced by CD4$^+$ cDCs). Consistently DN cDCs are also poor in cross-presenting exogenous antigens, although they are as efficient as CD4$^+$ cDCs in direct MHC class II presentation (Schnorrer et al., 2006). It was earlier believed that DN cDCs are able to produce high levels of IFN-γ, but this was later revealed to derive from a small population of precursor cells, which are frequently contaminants in DC preparations (Vremec et al., 2007).

In spite of this evidence of close similarity between CD4+ and DN cDCs, IRF4, IRF2 (Tamura et al., 2005) or NF-κBp50 knockout mice (O'Keeffe et al., 2005b) show heavily reduced numbers of CD4$^+$ cDCs, but much less reduction of DN cDCs. Moreover, mice treated with Flt3-ligand show a large increase in cell numbers of CD8α^+ cDCs and DN cDCs, but not CD4$^+$ cDCs. It has to be mentioned, that these studies were performed when little solid knowledge of lineage development of functionally specialized DC subsets existed. The discovery that DN cDCs preparations can contain around 10% "contaminations" of precursor cells en route to the CD4$^-$CD8α^+ cDC subtype, however not yet expressing CD8α homodimer, makes a careful reinvestigation of the functional properties of DN cDCs necessary (Vremec et al., 2007). Many of the above mentioned studies should be repeated using published antibodies like Sirp-alpha (CD172α) (Naik et al., 2005) to get a "real" CD11c^{hi}CD4^{neg}CD8α^{neg}Sirpα^{hi} DN cDC population.

1.2.3   In vitro models of dendritic cells

Because dendritic cells are a very rare population in vivo it quickly became apparent that *in vitro* generation systems would greatly speed up research. Several cell culture methods have been developed.

1.2.3.1   GM-CSF derived dendritic cells (GM-DC)

In the human system in particular, difficulties in handling human tissues make an *in vitro* generation method for dendritic cells highly desirable. In both humans and mice, monocytes can differentiate into DCs. This fact has widely been taken advantage of by culturing human peripheral blood mononuclear cells (PBMCs) with the cytokines GM-CSF and interleukin-4 (IL-4) (Sallusto and Lanzavecchia, 1994). Similarly, mouse bone marrow cells can differentiate in the presence of GM-CSF with or without IL-4 into $CD11^{hi}$ cells (Inaba et al., 1992; Lutz et al., 1999). The resulting human and mouse "monocyte-derived dendritic cells" are similar to each other and show a quite mature phenotype with relative high levels of MHC class II surface expression and co-stimulatory molecules. This method has become the standard for the generation of DC in vitro and as a consequence, monocytes or earlier precursors have long been acknowledged to be precursors of dendritic cells.

While this method of generating DCs has undoubtedly enhanced knowledge of DC biology, nowadays it is becoming more and more obvious that these "monocyte-derived DCs" do not mimic the steady state cDC in vivo in all aspect. In fact, GM-CSF expression levels are basically undetectable in healthy humans and steady state mice. Therefore it is unlikely that low concentrations of GM-CSF can significantly contribute to the steady state generation of DCs from monocytes (Cheers et al., 1988; Metcalf, 1988). Also knockout mice lacking either GM-CSF or the receptor for GM-CSF show normal numbers of DC in spleen and thymus. Furthermore, the expected distribution of cDCs subsets in these knock out mice was indistinguishable from WT mice (Vremec et al., 1997). This means that monocytes can differentiate into dendritic cells, however in the steady state, this differentiation pathway is not used.

The first clear evidence for an *in vivo* equivalent of "monocyte derived"-DCs emerged when a novel dendritic cell type was described in the spleen of Listeria monocytogenes infected mice. This DC type produced high levels of TNF-α and iNOS (inducible nitric oxide synthase) and was therefore named Tip-DC (Serbina et al., 2003). The phenotype of Tip-DCs is described as $CD11c^{int}CD11b^{+}Mac\text{-}3^{+}$, clearly different from the $CD11c^{hi}CD11b^{low}Mac\text{-}3^{-}$ phenotype of steady state cDCs. Importantly, chemokine receptor 2 (CCR2) knockout mice could not generate Tip-DC, whereas cDC were not impaired. It is known that CCR2 is selectively expressed on a specific $Ly6C^{hi}$ monocyte subset (Geissmann et al., 2003), which is now acknowledged to be the precursor of inflammatory Tip-DCs. Finally, a recent study revealed that GM-CSF driven "monocyte-derived" DCs represent inflammatory Tip-DCs, rather than cDCs of the steady state (Xu et al., 2007).

1.2.3.2   Flt3-derived dendritic cells (FL-DCs)

Another in vitro system uses Flt3-ligand (FL) to drive mouse bone marrow precursors into steady state DCs. Following the observations that FL treatment caused heavily increased DC numbers in living mice (Maraskovsky et al., 1996), and that FL knockout mice had abrogated DC numbers (McKenna et al., 2000), a novel cell culture system was devised using total BM cells supplemented with FL to generate high numbers of immature mouse DCs (Brasel et al., 2000). Later it was found, that these cultures contain a large number type I interferon-producing B220 positive cells, which were proposed to be equivalents of pDCs (Brawand et al., 2002). The recent finding that DCs of these cultures closely represent pDC as well as both CD8$^+$ and CD8$^-$ conventional subsets of mouse spleens, strongly suggests the use of this system as the most representative model of splenic subsets (Naik et al., 2005). Using Sirpα, an already proven marker in splenic DC research, easily separates FL-driven DC cultures into CD11c$^+$CD45RA^{hi} , CD11^{hi}CD24^{hi}Sirpα^- and CD11^{hi}CD24^{lo}Sirpα^+ as bona fide equivalents of splenic pDCs, CD8$^+$ and CD8$^+$ cDCs, respectively (Vremec and Shortman, 2008).

1.3   Pathogen recognition

Charles Janeway published a prescient paper in 1989, proposing that APCs and other innate immune cells possess pattern recognition receptor (PRRs) enabling the recognition of molecular signatures of possibly infectious organisms (Janeway, 1989).
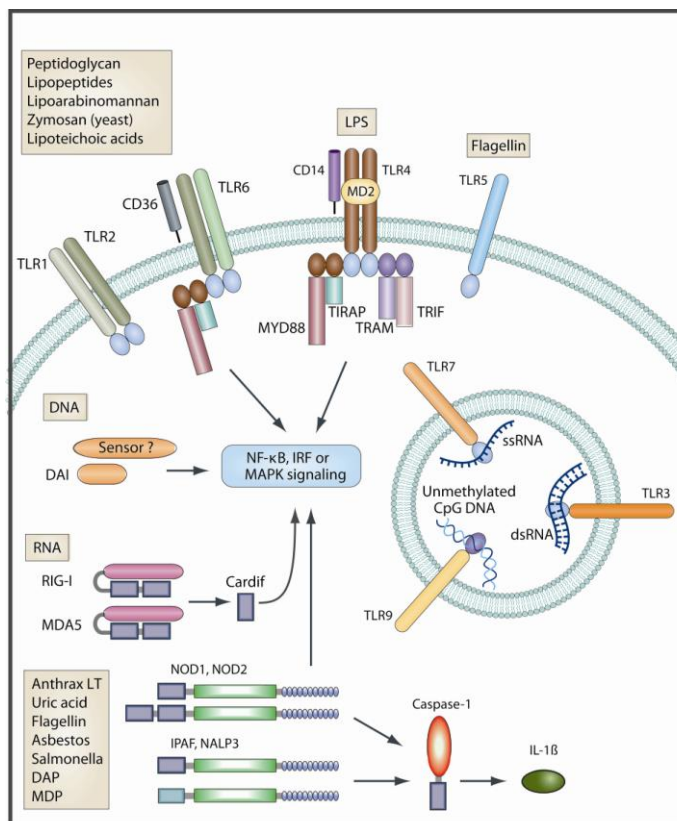

Figure 1-1 Schematic representation of the structure and main signaling pathways of the PRR families (adapted from (Rakoff-Nahoum and Medzhitov, 2009)

The target of PRRs is often referred to as "pathogen associated molecular patterns" (PAMPs), although they are also present on non-pathogenic microorganisms.

PAMPs are very important for the innate immune system for three main reasons. First, PAMPs are invariant among microorganisms of a certain class. Second, PAMPS represent products unique to microorganisms, allowing discrimination between self and non-self molecules. Third, PAMPS play an essential role in microbial physiology, restricting the opportunities of microorganisms to evade immune recognition via evolutionary adaption. Charles Janeway was years ahead of the rest of the immunology field and it took until 1996 that the first molecular component of a PRR was identified in drosophila adults and called "Toll" (Lemaitre et al., 1996). Just one year later, the first bona fide PRR, a human toll-like receptor (TLR), was cloned (Medzhitov et al., 1997). Today, various classes of PRRs have been identified besides TLRs, like nucleotide binding and oligomerization domain (NOD)-like receptors (NLRs), retinoid acid-inducible gene I (RIG-I)-like helicases (RLHs) and DNA receptors (Figure 1-1). TLRs are located on the cell surface and in endosomes, whereas NLRs, RLHs and the DNA receptors detect foreign components in the cytosol. Recognition of PAMPs by PRRs activates intracellular signaling cascades leading to DC maturation and type I IFN and proinflammatory cytokine production, which mediate the innate and adaptive immune response.

1.3.1   Toll-like receptors

The TLR family members recognize nucleic-acid, lipid, carbohydrate and peptide signatures which are broadly distributed in microorganisms. To date, a total number of 13 TLRs have been identified in mouse and man (Takeda et al., 2003). TLR1-9 are common to mice and humans, whereas TLR10 seems only to be functional in humans. TLR11-13 occur only in the mouse. TLR1, TLR2, TLR4, TLR5 and TLR6 are expressed on the cell surface, whereas TLR3, TLR7 and TLR9 are localized in the endoplasmic reticulum (ER) and move to endosomes or lysosomes upon stimulation. All TLRs are comprised of luminal leucine-rich repeats (LRRs) that sense PAMPS, a transmembrane domain and a cytoplasmic Toll/interleukin-1 (IL-1) receptor (TIR) homology domain. The TIR domain couples the TLRs to four adaptors molecules, MyD88, TIRAP/MAL, TRAM and TRIF through homophilic interactions (Takeda et al., 2003).

The first TLR to be discovered was TLR4, the cellular receptor for lipopolysaccharide (LPS), responsible for mediating the inflammatory response to Gram-negative bacteria (Hoshino et al., 1999). The lipid portion of LPS, called "lipid A" is known to be one of the most potent immunostimulants causing endotoxic shock. After invasion of Gram-negative bacteria, LPS associates with acute phase proteins present in the bloodstream and binds to CD14, expressed on the cell surface of phagocytic cells and in conjunction with MD-2 activates TLR4 (Poltorak et al., 1998; Shimazu et al., 1999). But not only Gram-negative bacteria activate the innate immune system. The bacterial cell wall of Gram-positive bacteria contains lipoteichoic acid (LTA) instead of LPS (Takeuchi et al., 2000). In this case, TLR2, together with TLR1 and

TLR6, is mainly responsible for recognition (Ozinsky et al., 2000). Table 1-2 gives a basic overview of several bacterial components recognized by a defined set of TLRs.

Table 1-2 TLRs and their cognate bacterial ligands

TLR	Bacterial component	Species
TLR1/TLR2	Triacyl lipopeptides	Bacteria / Mycobacteria
TLR2	Peptidoglycan	Gram-positive bacteria
TLR2	Porins	Neisseria
TLR2	Lipoarabinomannan	Mycobacteria
TLR2/TLR6	Lipoteichoic acid	Streptococcus
TLR2/TLR6	Diacyl lipopeptides	Mycoplasma
TLR4	Lipopolysaccharide	Gram-negative bacteria
TLR5	Flagellin	Flagellated bacteria
TLR9	CpG-DNA	Bacteria / Mycobacteria

TLRs also recognize virus associated molecules. Viruses contain either DNA or RNA that encode structural components and enzymes, which are necessary for replication and further infection of cells. Various structural components, including, double-stranded (ds)RNA, single-stranded (ss)RNA and viral DNA are recognized by TLR3, TLR7, TLR8, TLR9, whereas TLR2 and TLR4 recognize surface glycoproteins of viruses (Table 1-3).

TLR3 was found to detect dsRNA by specifically recognizing purified genomic dsRNA (and the synthetic ligand poly(I:C)) (Alexopoulou et al., 2001) resulting in induction of IL-12, IL-6, TNF-α and IFN-ß. dsRNA is a PAMP which can be generated during viral infection as a replication intermediate of ssRNA viruses or as a transcriptional by-product of DNA viruses.

TLR3 is expressed in a broad variety of epithelial cells, such as airway, vaginal, uterine and intenstinal epithelial cells, which function as barriers to infections. Unlike specialized immune cells like DCs, which express TLR intracellularly, these cells express TLR3 on their cell surface. Furthermore, astrocytes and glioblastome cell lines strongly express TLR3, indicating a specific role for TLR3 in the brain. Confusingly, TLR3 seems not be involved in the initial phase of viral recognition. Several reports showed, that TLR3 knockout mice did not show increased susceptibility to many viral infections like murine cytomegalovirus (MCMV), vesicular stomatitis virus (VSV), lymphocytic choriomeningitis virus (LCMV) and reovirus (Edelmann et al., 2004). Instead, interactions of West Nile virus with TLR3 seems even to be beneficial for the spread and survival of the virus (Wang et al., 2004). Further complicating the role of TLR3 in viral infection, it has been reported that TLR3 promotes crosspresentation of virus-infected cells (Schulz et al., 2005).

TLR7 and TLR8 are both expressed in the endosomal membrane in human and mice, however mouse TLR8 appears to be non-functional. The key activator for these TLRs of both species are uridine-rich, or uridine-guanine-rich viral ssRNA (as well as synthetic compounds like antiviral imidiazoquinolines like R848 or imiquimod). The endosomal location seems to

be evolutionary 'well chosen', because many enveloped viruses traffic into the cytosol through the endosomal compartment and can be discovered in such way. Additionally, the proteolytic environment in endosomes digests the viral particles leading to release of ssRNA which can be recognized by TLR7 and TLR8.

TLR9 is located in acidified, intracellular compartments and activated by ssDNA oligonucleotides bearing unmethylated CpG base pairs (Bauer et al., 2001) from viruses including herpes simplex virus 1 and 2 (HSV-1, HSV2) and MCMV. Optimal CpG motifs of synthetic compounds for murine TLR9 activation were found to be unmethylated CpG dinucleotides flanked by 5' purines and two 3' pyrimidines. Recently, the strict dependence of TLR9 on non-self CpG motifs was challenged by the discovery that 2' deoxyribose is sufficient – independently of base sequences – to confer signaling specificity by TLR9 for DNA (Haas et al., 2008).

For reasons of completeness it should be noted that besides the key viral activators of the immune system, viral DNA and RNA, some viral envelope proteins can also be recognized, mainly by TLR2 and TLR4. However, detection via TLR2 and TLR4 leads to induction of proinflammatoriy cytokines rather than to type I IFNs. For example, the fusion protein of Respiratory Syncytial Virus (RSV) or the envelope protein (ENV) of mouse mammary tumor virus (MMTV) activates TLR4 (Burzyn et al., 2004; Kurt-Jones et al., 2000).

Table 1-3 TLRs and their cognate viral ligands

TLR	Viral component	Species
TLR3	dsRNA	Viruses
TLR7/TLR8	ssRNA	RNA viruses
TLR9	DNA	Viruses
TLR2	Hemaglutinin protein	Measles virus
TLR4	Envelope proteins	MMTV, RSV

1.3.2   RIG-like helicases

Another family of PRRs shown to be involved in the recognition of viral RNA are the members of the RIG-like helicase (RLH) family, namely retinoic-acid-inducible gene I (RIG-I, also called DDX58), melanoma-differentiation-associated gene 5 (MDA5, also called Helicard) and laboratory of genetics and physiology-2 (LGP2) (Yoneyama and Fujita, 2007). Whereas RIG-I and MDA5 both contain a DExD/H box RNA helicase domain and two N-terminal caspase recruiting domain (CARD)-like domains, which is essential for downstream signaling, LGP2 lacks the CARD-like domains completely (Yoneyama et al., 2005).

Several studies reported differential involvement of RIG-I and MDA5 in antiviral responses, whereas LGP2 was suggested to serve as a negative regulator of RIG-I (Rothenfusser et al., 2005; Saito et al., 2007). RIG-I recognizes a wide variety of ssRNA viruses which include members of the paramyxoviridae like, Newcastle disease virus and Sendai virus,

rhabdoviridae like, VSV, and members of the flaviviridae like Japanese encephalitis virus (JEV) and hepatitis C virus (HCV). Picornaviruses, such as encephalomyocarditis virus (EMCV) and Theiler's virus are specifically recognized by MDA5, as shown in MDA5 knockout mice. (Kato et al., 2006; Xagorari and Chlichlia, 2008).

It has been reported that RIG-I and MDA5 recognize distinct types of RNA (Figure 1-2). The critical determinant for type I IFN induction by RIG-I stimulation through RNA was recently determined to be a 5'-triphosphate moiety, independently of single or double strandedness. Similarly, in vitro described RNA also contains a 5'-triphosphate and therefore leads to RIG-I activation (Hornung et al., 2006; Pichlmair et al., 2006). This strict requirement of 5'-triphosphates also explains why RIG-I does not activate innate immune responses against host RNA. Cellular ssRNAs are normally capped or processed and therefore absent for the recognition motif. However not only 5'-triphosphate specifically activates RIG-I but also dsRNA, lacking any 5'-triphposphates, initiates type I IFN secretion by RLHs. It has been shown, that poly(I:C), an artificial dsRNA generate by annealing pI and pC, which does not bear any 5'-triphosphates, activates cytosolic RLHs in a length dependent fashion: MDA5, the originally described agonist of p(I:C) (Gitlin et al., 2006) binds to long poly(I:C), whereas RIG-I preferentially binds shortened poly(I:C) (Kato et al., 2008). Furthermore long dsRNA, produced by EMCV infection trigger a MDA5-dependent IFN production.
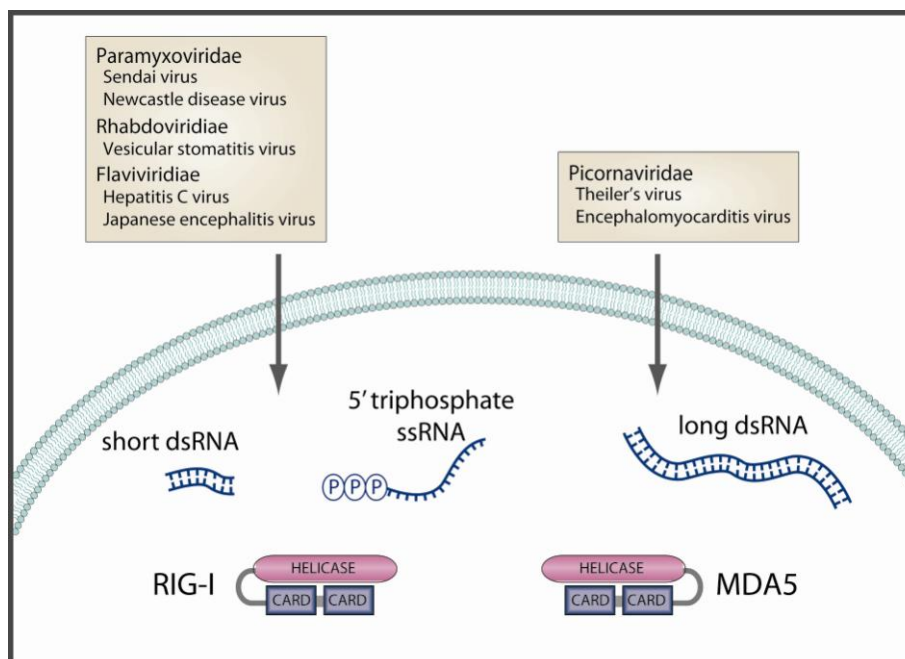
Figure 1-2 Differential recognition of RNA by RLHs receptors

A recent report suggested that RIG-I also requires a polyuridine motif at the 3'-non-translated region for recognition of HCV infection (Saito et al., 2008). If this applies also to the recognition of other viruses remains still to be determined.

1.3.3   NOD-like receptors

The murine nucleotide oligomerization domain-like (NOD) receptor family comprises at least 34 members, which are expressed in many different cell types, including immune and epithelial cells. NLRs were first identified in plant, where they play a crucial role in resistance against microbial and parasite pathogens (Dangl and McDowell, 2006). NLRs are in general composed of variable N-terminal domains, like caspase recruitment domains (CARDs), baculovirus inhibitor repeats (BIRs) or pyrin domains (PYD), which also define the subfamily classes (Inohara and Nunez, 2003). These are connected to a centrally located NOD (also called NACHT-domain), which plays a critical role in activation, and C-terminal leucine-rich repeats (LRRs), responsible for pathogen sensing (Figure 1-3). The NOD-domain shows similarities to the oligomerization module of ATPases, indicating that nucleotide hydrolysis is essential for activation (Hanson and Whiteheart, 2005). Indeed, mutations in conserved regions of the NODs NOD1, NOD2, NLRP3 and NLRP12 abolished signaling (Duncan et al., 2007; Ye et al., 2008).
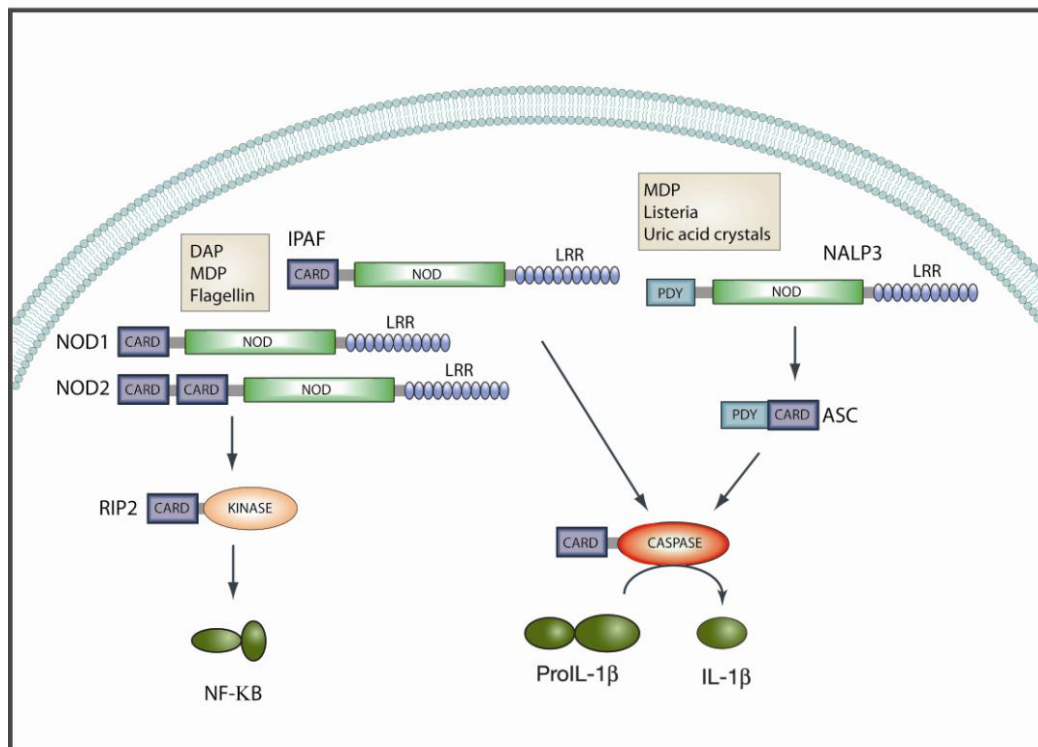
Figure 1-3 Activation of inflammatory immune responses by NOD-like receptors

Both NOD1 and NOD2 recognize bacterial molecules produced during degradation, synthesis or remodeling of peptidoglycan (PGN), a major component of bacterial cell walls. Specifically, NOD1 senses meso-diaminopimelic (meso-DAP)-containing PGN-fragments (Chamaillard et al., 2003), which are produced by most Gram-positive and a few Gram-negative bacteria, including Listeria and Bacillus species (Hasegawa et al., 2006). NOD2 is activated by all types of muramyl dipeptide (MDP), which is found in the PGNs of nearly all bacteria. Following microbial sensing NOD1 and NOD2 recruit the serine-threonine kinase

RIP2, which is essential for signal transduction, as shown in RIP2 null mice (Kobayashi et al., 2002), leading to NF-κB activation.

Deregulation of NOD1 and NOD2 signaling is involved in a variety of human diseases. There is mounting evidence that several NOD2 variants cause increased susceptibility to Crohn's disease, a chronic disorder characterized by inflammation of the intestine (Hugot et al., 2001; Ogura et al., 2001) and to Blau syndrome, an autosomal dominant disorder characterized by inflammation of the eyes, skin and joints (Miceli-Richard et al., 2001).

Besides the activation of inflammatory cytokines and interferons via NF-κB, certain members of the NLR family trigger caspase-1, an inflammatory molecule. Tschopp and colleagues coined the term "inflammasome" to describe a multiprotein complex leading to caspase-1 activation. Depending on the stimulus, at least three inflammasomes of distinct composition are formed *in vivo*: the IPAF inflammasome triggered by Salmonella, Legionella and flagellin (Franchi et al., 2006; Mariathasan et al., 2004; Miao et al., 2006), the NALP1 inflammasome triggered by B. anthracis (Boyden and Dietrich, 2006), the NALP3 inflammasome triggered by non-microbial signals like uric acid crystals, asbestos and silica (Cassel et al., 2008; Dostert et al., 2008; Hornung et al., 2008; Mariathasan et al., 2006). Biochemical analysis revealed that IPAF directly binds caspase-1, whereas NALP1 and NALP3 associate with caspase-1 via the adaptor molecule ASC, both leading to subsequent processing of proinflammatory pro-IL-1ß.

1.3.4   Dendritic cell subsets and pathogen recognition

The separation of DCs into several subsets is based on their differential expression of surface markers, but these diverse subsets in most cases also correlate with functional differences. These functional differences amongst phenotypically different subsets are of major importance in understanding DC biology especially for manipulating the immune response to tumors, autoimmune diseases and pathogens. Functional diversity is thought to be mainly based on differential expression of certain PRRs. Especially TLRs, an ancient and highly conserved family of PRR involved both in pathogen recognition (Hochrein and O'Keeffe, 2008) and autoimmune pathologies (Fischer and Ehlers, 2008) are known to be distinct distributed amongst mouse DC subsets (Table 1-4), as revealed by microarray analysis (Edwards et al., 2003a).

As shown in Table 1-4 all DC subsets express a wide array of extra- and intracellular TLRs. However, some of them are more abundant in pDCs or cDCs, or even between cDC subsets. All cDCs express TLR2, TLR4 and TLR6, enabling them to respond to a variety of extracellular bacterial products such as LPS and lipopeptides, and also some coat proteins from different viruses like HSV-1, HCMV, RSV or MMTV.

Within the TLR family for nucleic acid recognition TLR7 and TRL9 are more abundant in pDCs, enabling them to respond to a broad variety of viruses by producing high levels of type I IFNs. cDC subsets also express TLR9 and partially TLR7, however only pDCs are able to produce very high levels of IFNs. TLR3 is mainly expressed by CD8α^{+} cDCs, which also

corresponds to their unique cytokine and chemokine secretion profile after stimulation with cognate ligands. The activation of TLR3 in CD8α^+ cDCs also enhances crosspresentation, a unique feature of this specific DC subset (Schulz et al., 2005).

Table 1-4 Variation of TLR expression amongst different splenic DC subsets of mice (adapted from (Hochrein and O'Keeffe, 2008)

	pDCs	CD4$^+$ cDCs	CD8α^+ cDCs	DN cDCs
TLR1	++	++	++	++
TLR2	++	++	++	++
TLR3	low	+	+++	++
TLR4	+	+	+	+
TLR5	+	++	low	+
TLR6	++	+++	++	++
TLR7	+++	++	neg	+
TLR8	++	++	++	++
TLR9	+++	++	++	++

In addition to TLRs, other PRRs have been identified to be differentially involved in pathogen recognition amongst DC subsets. An example is the involvement of the cytosolic RNA helicases RIG-I and MDA5. It was shown recently that DC subsets use different mechanisms to sense direct viral infections: pDCs predominately detect viral infections via the TLR system (TLR7 and TLR9), whereas all cDC subsets use the cytosolic helicases RIG-I and MDA5 (Kato et al., 2005). This shows that RIG-I and TLRs exert antiviral responses in a dendritic cell type-specific manner.

1.4   Mass spectrometry in the field of protein analysis

Mass spectrometry (MS) has emerged as a central analytical technique for protein research (Aebersold and Mann, 2003; Cravatt et al., 2007). After the discoveries made by whole genome sequencing it was clear that the nucleic acid data needed to be used to understand protein sequences and protein functions. However, this turned out to be not a trivial task! The systematic analysis of all proteins expressed in a cell or complete tissues was popularized under the term "proteomics" by Marc Wilkins at the Siena-meeting in 1994, when he was looking for a crisper alternative to the term "the protein complement of the genome"(Wilkins et al., 1996). In the early proteomics era (really the era of protein chemistry), even as this term had not been coined yet, chemical and enzymatic methods were typically used to identify highly purified proteins. Edman degradation was the method of choice to readout the sequence of small proteins in a stepwise manner starting from the N-terminus and proceeding towards the C-terminus (Edman, 1970). However, the need of highly purified proteins and the limited sequencing depth of less than 50 amino acids never qualified this laborious work-flow for characterization of the entire protein complement of

biological systems. Furthermore, the traditional separation of proteins by two-dimensional gel electrophoresis in the proteomic field never fully delivered on its promises.

Amongst all proteomic techniques, mass spectrometry has emerged as the method of choice for proteome-wide expression analysis. A prerequisite for analyzing molecules by MS is the ionization of the analyte as only ions can be detected by mass spectrometers. This requirement restricted MS for a long time to small and thermally stable compounds, because effective techniques for gentle ionization without immediate fragmentation were still to be invented. The development of soft ionization methods for intact biomolecules by John B. Fenn and Hillenkamp and Karas two decades ago opened the field of mass spectrometric analysis for complex biological samples and has became of tremendous success. The development of electrospray ionization was honored with the share of the Nobel Prize in chemistry (Fenn, 2003) .

MS has revolutionized the field of proteomics and matured into the most important technology in proteomics today, because it encompasses several unique and highly desirable features at once. First, MS is a relatively 'unbiased' method and therefore well suited for analyzing mixtures of unknown compounds. This unbiased nature is of great advantage when compared to other protein detection methods like western blotting which uses antibodies: in that case, one can only detect what one is looking for, because of the specific nature of antibodies (Mann, 2008). Second, consistent with genomics, MS posseses the power of high-throughput and is capable of detecting thousands of peptide sequences per hour providing information in a global manner. Finally, modern mass spectrometers can deliver data of excellent quality regarding mass accuracy, sensitivity and reproducibility.

1.4.1   Fundamentals of MS-based proteomics

Every MS-based proteomic experiment consists of distinct steps (Figure 1-4):

(i) Protein samples are isolated from their biological source and optionally fractionated, e.g. by one-dimensional gel electrophoreses (1D-PAGE). Individual bands can be excised or more usually the entire lane can be sliced into 14-20 parts. Proteins in the gel slices are proteolytically digested into peptides using different enzymes like trypsin, LysC or AspN. Trypsin has proven to be an especially well suited degradation enzyme because it yields peptides with C-terminally protonated amino acids (Arginine and Lysine), which fragment well in the mass spectrometer. It is also possible to digest protein mixtures in solution.

(ii) The peptides are analyzed qualitatively or quantitatively in the mass spectrometer. Before peptides mixtures are sprayed into the mass spectrometer, they are separated in an on-line set up with the instrument. The most common method is reversed-phase (RP) liquid chromatography (LC), which separates peptides according to their hydrophobicity. As an additon to RP chromatography, strong cation exchange chromatography (SCX) can be used. It is also possible to combine both RP and SCX resins in series offline or in one or two columns to achieve even better separation. The peptide mixture, separated via nano flow

chromatography, is then directly electrosprayed into the mass spectrometer. The spray contains small droplets that contain the peptides or proteins of the sample. While entering the mass spectrometer the droplets become desolved while keeping the charged acquired in the electrospray process. The mass spectrometer analyzes the protein mixture in two stages. First, the survey or MS scan accurately determines the mass and signal of the peptide. In a second step, these peptide ions are fragmented to produce amino acid sequence related data (MS/MS). Subsequently, the resulting large data sets have to be analyzed by software tools to figure out the amino sequences, to map peptide sequences to parent proteins, and, if applicable, to quantify the proteins within the samples.
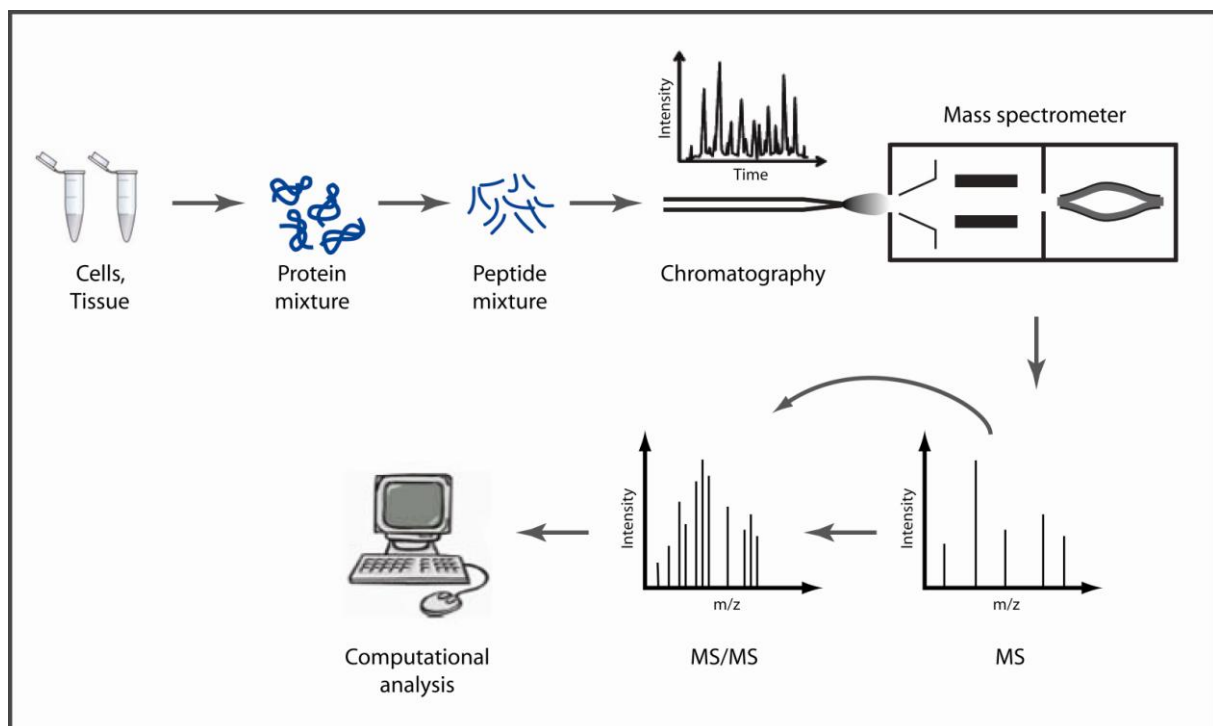
Figure 1-4 Workflow in MS-based proteomics

1.4.2   Mass spectrometric instrumentation and parameters

Mass spectrometers are instruments that determine the mass of ions derived from molecules, in principle acting like a conventional balance. However this picture is oversimplified, instead the MS instruments produce gas-phase ions in the ion source, which are later filtered and separated according to their mass-to-charge ratio (m/z) in mass analyzers and finally recorded using a detector. The resulting data are mass spectra containing the relative abundances of ions as a function of their m/z ratios (Figure 1-4). Every peptide and every modification has its characteristic mass. Together with its distinct fragmentation pattern exact amino acid sequence and modification information can in principle be achieved. Before introducing the currently most powerful mass spectrometers, a description of some key performance parameters is necessary.
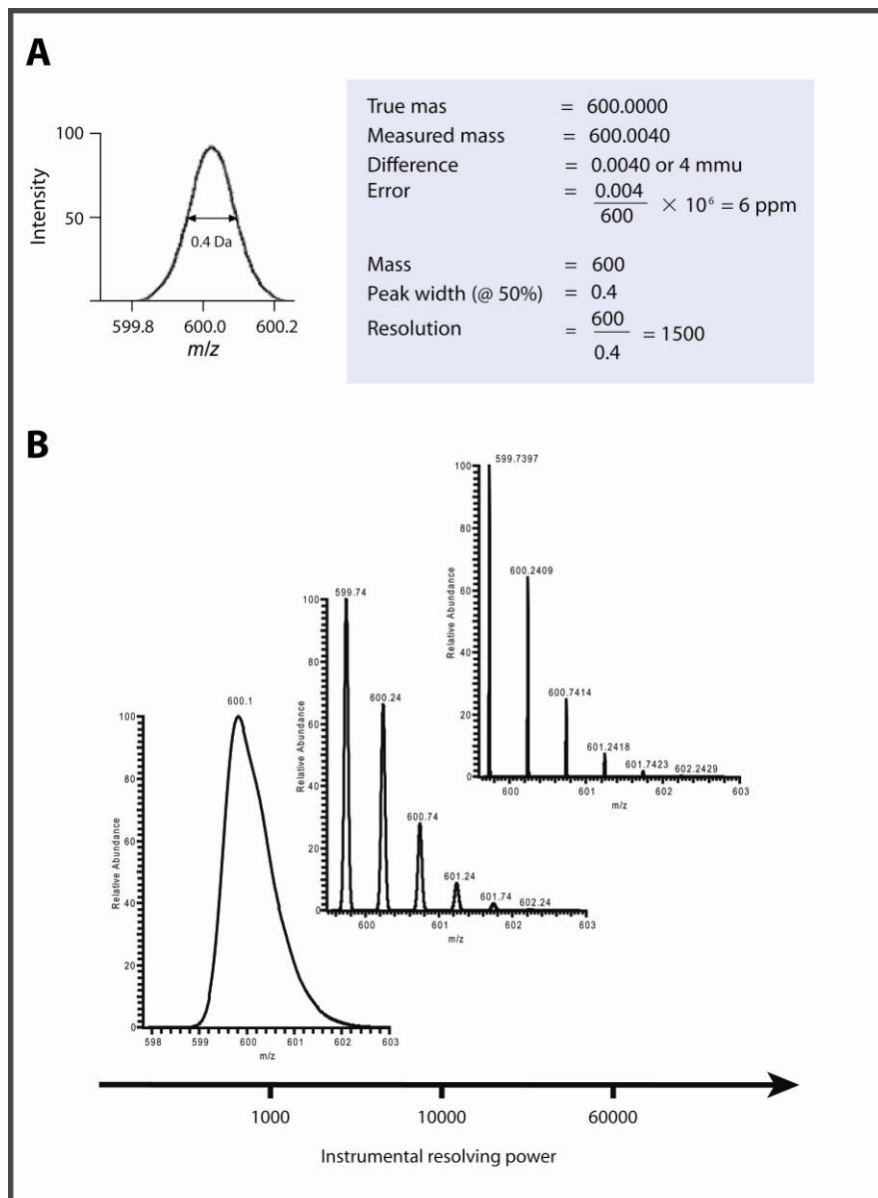
Figure 1-5 Mass accuracy determination and the need for resolving power

(i) Mass accuracy: The mass of a gas-phase ion can only be measured as accurately as the mass analyzers and detectors allow. Usually expressed in parts per million (ppm), the measurements indicates the deviation of the measurement from a known monoisotopic mass (Figure 1-5A). Clearly, as the mass of an analyte increases, the absolute mass error corresponding to a given ppm error will increase proportionally. The most powerful MS instrumentats in common use now have around 2-5 ppm mass accuracy, achieved by external calibration or internal mass standard (lock mass (Olsen et al., 2005)).

(ii) Resolution: Resolution can be defined as the ability to "image" a detected ion in a mass spectrometer and differentiate it from other similar, but not identical masses. Only with high resolution instruments can ion peaks be visualized as isotope patterns which is of particular value for charge state information and accurate quantitation as illustrated in Figure 1-5B.

(iii) Dynamic range: The range of peptide concentrations of interest in proteomic measurements can vary more than six orders of magnitude. One crucial factor for the performance of a mass spectromter is its dynamic range, in other words, the ability to discern low abundance peptide peaks from the most highly abundant signals. Current mass spectrometers, like the LTQ-Orbitrap™ have a dynamic range or around 5000 in single scans for binary mixtures, which means that peaks 5000-fold less intense than a peak can still be detected.

(iv) Acquisition speed: A major parameter of a mass spectrometer is the time necessary for acquisition of MS- and MS/MS spectra. Especially in the analysis of proteomics samples, the speed of the mass spectrometer determines how much information can be gained.

(v) Sensitivity: This parameter is a value for the minimal amount of sample that can be detected. It is important for analyzing small numbers of cells and is limited by the need to trigger a recognition event at the mass detectors.

1.4.3   Hybrid mass spectrometer: the LTQ-Orbitrap™

Because proteomic analyses has become more and more complex, it is of great interest to develop instrumentation that are able to acquire information in an accurate manner, with respect to mass accuracy, acquisition speed, sensitivity and resolution power. Unfortunately, a single kind of mass analyzer is not able to combine all these three requirements. However, it turned out that a combination of different mass analyzers with different characteristics in the same instrument enhanced performance greatly: this realization led to the concept of hybrid mass spectrometers.

The introduction of the LTQ-Orbitrap™ (Hu et al., 2005) in 2005 was a major breakthrough in the field of MS-based proteomic instrumentation. This hybrid mass spectrometer consists of a linear ion trap (LTQ) coupled to a C-trap and a novel Fourier transform mass analyzer, called the Orbitrap. The Orbitrap works very well as a high resolving, accurate mass detector with high dynamic range, whereas the LTQ is the ideal partner instrument with its exquisite sensitivity, very fast scanning rates and its MS^n capability. One operation cycle consists of an accurate determination of the parent ions in the Orbitrap (full scan, MS) and consecutive fragmentation and detection steps of typically the five most abundant precursor ions in the LTQ (MS/MS). In this, the hybrid nature of the instrument is of great importance, because both types of scans can be done largely in parallel, which makes the Orbitrap superior in speed. Together with its capabilities of internal calibration, called lock mass, where omnipresent ions from ambient air are used to improve mass accuracy (Olsen et al., 2005), the LTQ-Orbitrap is the most powerful instrument for any proteomic experiment today.

1.4.4   Quantitative MS-based proteomics

Mass spectrometry is widely applied to identify components in a qualitative manner. To gain deeper insights into biological systems there is a clear trend to study protein changes quantitatively. MS itself is inherently not quantitative because peptides exhibit a broad range of different proprieties like size, charge, hydrophobicity, etc. which alter their ionization capabilities and which lead to large differences in their MS responses. Therefore many chemical and metabolic labeling strategies have been developed to obtain the needed quantiative information. Basically all labeling strategies rely on stable isotope dilution (Jonckheere et al., 1980): stable, non-radioactive isotopes like deuterium (D), carbon13 (^{13}C), nitrogen15 (^{15}N) are introduced in one of the samples and directly compared to sample with the native counterpart of these isotopes. As MS can distinguish and resolve mass differences both samples can be analyzed together and directly quantified by comparing the labeled and the unlabeled peptide signals. Besides quantitation methods based on integration of stable isotopes, either chemically or metabolically, alternative strategies, called label-free quantitation methods, have emerged. These methods directly compare peptide intensities from different experiments.

1.4.4.1   Isotope coded affinity tag (ICAT)

The very first approach of using isotope coded mass tags for quantitative proteome analysis was developed in 1999 by Ruedi Aebersold and coworkers (Gygi et al., 1999). In pioneering work, they targeted cysteine residues in proteins using a thiol-specific anchor group combined with a biotin moiety for affinity purification. The crucial step was to connect those two functionalities with a mass-encoded linker group containing either zero or eight deuterium atoms in the light or heavy form respectively, resulting in a well-detectable mass shift (Figure 1-6).
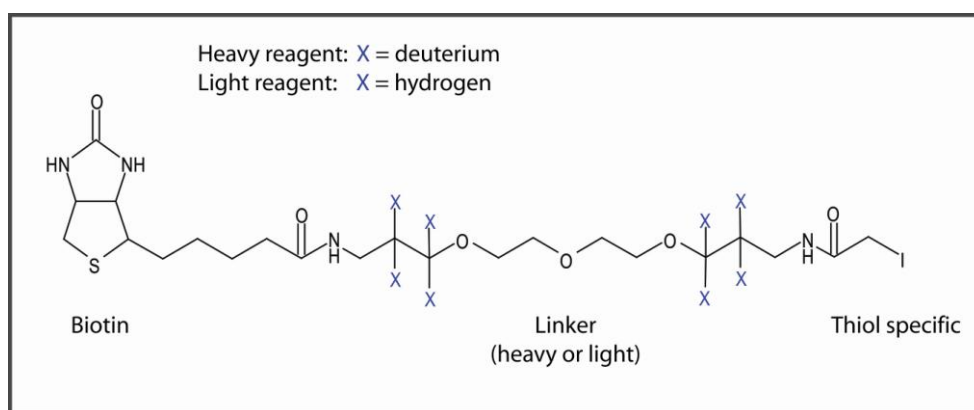
Figure 1-6 ICAT reagent

In the original Isotope coded affinity tag (ICAT) experiment, two batches of proteins were reduced, alkylated, modified with each ICAT reagent and combined. After digestion, ICAT-labeled peptides were enriched using avidin-affinity columns and, after elution, analyzed by

MS. Although the affinity enrichment decreases the complexity of the sample dramatically, which is undoubtfully of advantage for quantitation, this approach has some severe disadvantages. Some proteins may contain only a few or even no cysteines and are therefore excluded from accurate quantitation. The fact that only a few peptides can be quantified in general reduces the reliability of quantitation. In addition, the separation using RP-chromatography is not trivial because the deuterium atoms cause a retention time shift compared to their light counterparts complicating correct quantitation. It should also be noted that the original ICAT tag generates very abundant peaks in MS/MS spectra making database searches more difficult. The next-generation ICAT reagents were significantly improved using ^{13}C atoms instead of deuterium improving the chromatography properties or acid-cleavable biotin taq, however the caveats about targeting only cysteine-residues still remain and the ICAT method is not in general use today.

1.4.4.2   Isobaric tags for relative and absolute quantitation (iTRAQ)

The isobaric tag for relative and absolute quantitation (iTRAQ) method has been developed for quantitation of up to 4 samples (4-plex), but 8-plex implementations have also become commercially available. iTRAQ uses NHS (N-hydroxysuccinimide) chemistry to target all free N-termini and free amines in lysine side chains of peptides (Ross et al., 2004). The innovative concept of iTRAQ is based on a tag that generates specific reporter ions (m/z 114, 115, 116 and 117) for quantitation in the low mass region on the MS/MS spectra level. Combined with a balance group, which varies also in mass, the combined masses of reporter and balance groups remain constant, forming isobaric peptides with indistinguishable mass at the MS level, which precisely co-elute in liquid chromatography separations (Figure 1-7A).
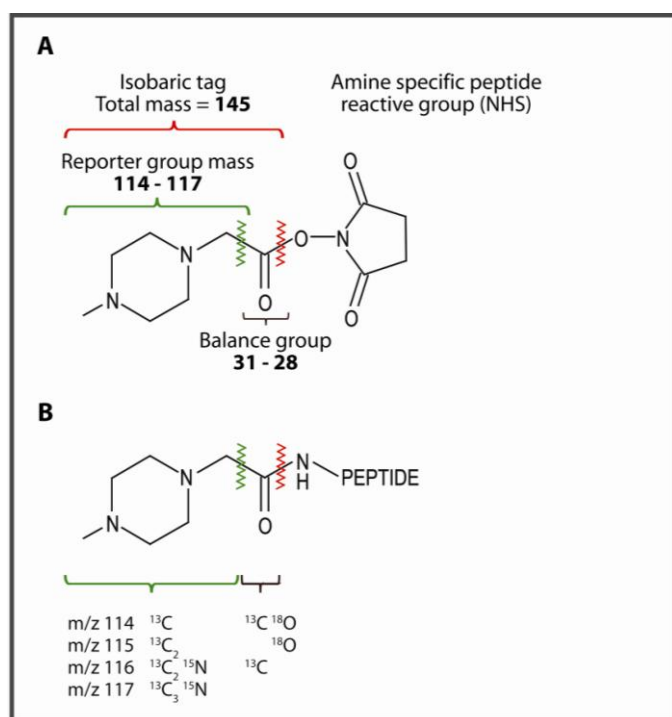
Figure 1-7 iTRAQ reagent

With this approach peptides of samples to be compared are labeled with different sets of iTRAQ reagents after enzymatic digestion (Figure 1-7B) and separated via RP chromatography. Upon peptide fragmentation, the different mass tags also fragment giving rise to the reporter signals, which can be easily quantified. However, it should be noted, that, as the label is introduced at a late stage of the sample preparation, controlling the reproducibility of the measurements is challenging.

1.4.4.3   Stable isotope labeling by amino acids in cell culture (SILAC)

The SILAC approach is the most prominent methods for introducing heavy isotopes into samples by metabolically labeling (Figure 1-8).
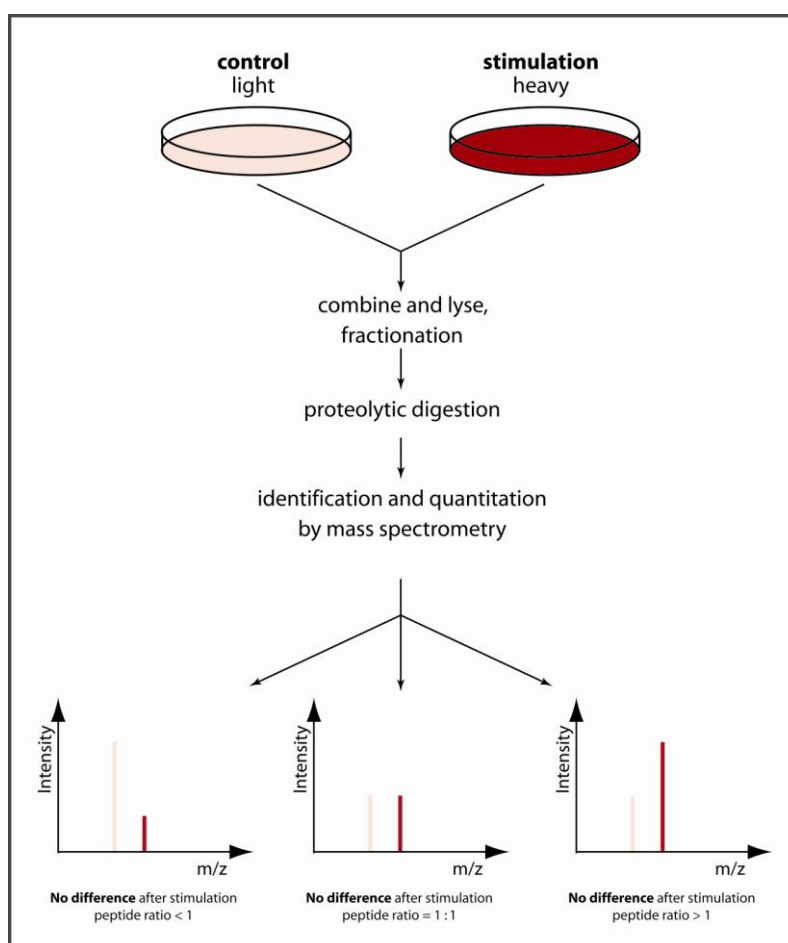
Figure 1-8 SILAC-based quantitation workflow

In SILAC this is achieved by providing heavy isotopes to a cell culture system, so that these isotopes are exclusively incorporated into newly synthesized proteins (Ong et al., 2002). Typically, cells are grown in culture media containing either the naturally occurring form or the heavy stable isotope form of the amino acids lysine or arginine. Both lysine and arginine are labeled in different combinations of ^{13}C, ^{15}N and ^{3}H in order to generate distinguishable mass shifts. The differentially labeled samples are combined, mixed and digested with a suitable protease, before being analyzed by mass spectrometry. The combination of the

amino acids lysine and arginine together with trypsin as a digestion enzyme is especially advantageous because trypsin cleaves C-terminally to both amino acids, which ensures that that in principle all observed peptides are also quantifiable (except the C-terminal peptide of the protein) (Olsen et al., 2004).

The incorporation of the mass tags happens very early, already during cell culture and prior to any sample fractionation, minimizing potentials biases due to separate handling of the samples. This makes SILAC superior to chemical labeling strategies. However, an important constraint is its limitation to cells growing in cell culture.

1.4.4.4   Quantitation without stable isotopes ("label-free" quantitation)

Stable isotope based approaches for quantitation are not always practical and might be relatively expensive. It should also be considered, that all these methods are limited by the available tags, which might not be sufficient for comparative analysis of multiple samples in a simultaneous way. Despite the success of isotope labeled methods, label-free quantitation is potentially the simplest and most economical method. It would also be ideal for certain types of samples such as clinical material and *in vivo* material. The main advantage of metabolic labeling is its much greater accuracy and robustness, which is mainly due to its tolerance towards irreproducibility in sample processing steps. Furthermore, peptide quantitation is performed pair wise within each MS full scan, excluding any bias between measurements.

A vast literature, as well as associated methods already exists on the topic of label-free quantitation (see for example (Bantscheff et al., 2007; Listgarten and Emili, 2005; Mueller et al., 2008)). One possible estimation of protein abundance in a label-free manner is that the number of peptides identifying a protein scales with protein amount. Yet, the number of detected peptides is also dependent on the size of the protein itself. This has lead to the definition of the "protein abundance index" (PAI), where the number of observed peptides, normalized against the number of identifiable peptides for a certain protein, is regarded as a measure of protein abundance (Rappsilber et al., 2002). However, as the number of identified peptides and protein abundance in a defined sample is logarithmic, a modified version of PAI, called "exponentially modified PAI" (emPAI) has been introduced (Ishihama et al., 2005a).

A more elegant way to quantify proteins amongst different samples would be the use of the extracted ion current (XIC), which is the volume under the curve generated by plotting the signal intensity of a peptide over the elution time. This information should be available for every peptide, if high mass resolution is provided.

The comparison of subsequent MS runs is very challenging. In the absence of internal controls (such as exist automatically in a SILAC experiment), XIC-based quantitation is still regarded as inaccurate and unreliable at the current time.

1.5   Prologue to this thesis

This study was conducted with two major goals in mind. The main focus was the in-depth characterization of dendritic cell subsets. These rare cells have great influence on our immune system, uniquely connecting innate and adaptive immune responses and controlling 'magic spots' of the immune system. However, laborious workflows for the isolation of sufficient cell numbers of each subset in high purity prevented their characterization on a proteome level so far. A further drawback of using cells directly isolated from mice is the incompatibility with the SILAC approach for accurate MS-based quantitation. This issue directly relates to the second objective of my thesis, done in collaboration with Juergen Cox, namely the development of a robust, proteome-wide quantitation approach without any need of stable isotopes, to make it applicable for quantitative analysis of rare *in vivo* cells. The third main topic of my thesis was the extension of the SILAC approach from *in vitro* to *in vivo*. I was involved in the development of a stable isotope labeled mouse, which can be used for accurate quantitation of *in vivo* samples.

2 Dendritic cells differ from viral recognition

Abstract

Dendritic cell populations consist of multiple subsets that are essential orchestrators of the immune system. However their functional relationships and properties are not completely defined. Technological limitations have so far prevented systems-wide, accurate proteome comparison of rare cell populations in vivo. Here we used high resolution mass spectrometry-based proteomics combined with newly developed label free quantitation algorithms to determine the proteome of mouse conventional dendritic cell subsets to a depth of 5,780 proteins. We found mutually exclusive expression of pattern recognition pathways not previously known to be subset specific. Our experiments assign key viral recognition functions, thought to be mainly mediated by CD8α$^+$ dendritic cells, to be exclusively expressed in CD4$^+$ and DN dendritic cells. Thus robust label free quantitation is feasible for proteome wide comparisons of rare in vivo cell populations and provides direct insight into specific functions of closely related cell types.

This work is included in a manuscript under revision:

Quantitative proteomics reveals subset-specific viral recognition in dendritic cells

Christian A. Luber*, Jürgen Cox*, Ben Fancke, Matthias Selbach, Jurg Tschopp, Shizo Akira, Hubertus Hochrein, Meredith O'Keeffe and Matthias Mann

*: These authors share first authorship

2.1   Introduction

Dendritic cells (DCs) are a highly specialized master regulators of the immune system involved in responses ranging from resistance to infection to self-tolerance. Mouse spleen contains two major subsets of DCs, plasmacytoid DCs (pDCs) and conventional DCs (cDCs). cDCs can be further segregated according to different expression of surface markers into $CD4^+$ cDCs, $CD8\alpha^+$ cDCs and $CD4^-CD8\alpha^-$ cDCs (double-negative (DN) (Shortman and Naik, 2007; Vremec et al., 2000)). Importantly, different DC subsets appear to have specialized roles in immune responses (Villadangos and Schnorrer, 2007; Villadangos and Young, 2008). pDCs, also called natural interferon-producing cells, uniquely secrete very large amounts of type I interferons (IFN I) directly upon activation and therefore play an important role in response to viral infections (Fuchsberger et al., 2005). Amongst the cDC subsets, $CD8\alpha^+$ DCs appear to be particularly important in the context of different viral infection models (Allan et al., 2003; Belz et al., 2005; Belz et al., 2004). $CD8\alpha^+$ DCs have the ability to cross-present antigens, a process in which exogenous antigen is presented to T cells by MHC class I molecules to activate cytotoxic CD8+ T cells (Heath et al., 2004). In addition, $CD8\alpha^+$ DCs are mainly associated with a T_H1 inducing profile due to their ability to secrete extremely high amounts of the pro-inflammatory cytokine IL-12 (Maldonado-Lopez et al., 1999). $CD4^+$ DCs and DN DCs are particularly potent in stimulating CD4+ T cells via MHC II-antigen complexes. In contrast to $CD8\alpha^+$ DCs, $CD4^+$ DCs and DN DCs are mainly involved in stimulating a T_H2 response (Maldonado-Lopez et al., 1999).

Innate immunity largely depends on the recognition of highly conserved structures of pathogens that are distinct from the host, so called pathogen-associated molecular patterns (PAMPs) (Janeway and Medzhitov, 2002). These PAMPs comprise two broad classes of biochemical compounds (Beutler et al., 2006). The first category includes products of microorganisms such as lipopolysacchride and lipotechoic acid. The second category consists of nucleic acids derived from pathogens, particularly viruses. Receptors involved in recognition of nucleic acids from viruses activate type I interferon secretion, which places the host in a state of general alert (Stetson and Medzhitov, 2006). DCs express a great variety of pattern recognition receptors (PRRs), such as toll-like receptors (TLRs), RIG-like helicases (RLHs) or NOD-like receptors (NLRs) (Akira et al., 2006). Whereas the majority of TLRs are expressed on the cell surface, the TLRs recognizing nucleic acids namely TLR3 (sensing double-stranded RNA [dsRNA]), TLR7 and TLR8 (sensing single-stranded RNA [ssRNA] and TLR9 (sensing CpG-DNA), are located in endosomal/lysosomal compartments within the cytosol (Alexopoulou et al., 2001; Heil et al., 2004; Hemmi et al., 2000). TLRs in general elicit cellular responses by recruiting several adaptor molecules such as MyD88 and TRIF, leading to the expression of inflammatory genes (Kawai and Akira, 2008).

Recently it has been shown that DC subsets differ in their ability to sense viral infections. pDCs rely on the TLR system, namely TLR7 and TLR9, whereas cDCs mainly uses the cytoplasmic virus sensors retinoic-acid-inducible gene I (RIG-I) and melanoma differentiation antigen 5 (MDA5) (Kato et al., 2005). Several studies, using mice lacking RIG-I and MDA5,

reported the importance of both cytoplasmic sensors for different virus infection models *in vivo* and *in vitro* (Kato et al., 2008; Kato et al., 2006). On binding to their cognate ligands, RIG-I and MDA5 recruit adaptor molecules like Cardif (also called IPS-1, VISA or MAVS) (Meylan et al., 2005) that are distinct from those that mediate TLR signaling, although both pathways converge on interferon regulatory factors (IRFs) and NF-κB for the production of inflammatory cytokines and interferons (Kawai and Akira, 2008).

The molecular basis for the functional segregation of cDC subsets is still incompletely defined. Although microarray experiments provided first insights (Dudziak et al., 2007; Edwards et al., 2003a), there is no systems-wide information about differences in protein composition between cDC subsets. We reasoned that differences in protein abundance might provide us with direct insights into functional differences between cDC subsets.

Mass spectrometry (MS)-based proteomics can identify thousands of proteins in complex samples (Aebersold and Mann, 2003). In addition a variety of methods are available to quantitatively compare changes in protein abundance at a proteomic scale (Bantscheff et al., 2007; Ong and Mann, 2005; Panchaud et al., 2008). Most quantitative MS methods rely on differential labeling of protein samples with stable isotopes. These introduce a mass difference between differentially labeled peptides that can be differentiated by MS. Our laboratory developed stable isotope labeling with amino acids in cell culture (SILAC) as a metabolic strategy that can accurately determine protein expression ratios (Ong et al., 2002). We showed recently that the SILAC approach can also be used to label entire mice (Kruger et al., 2008). Unfortunately, comparison of DC subsets *in vivo* would require pooling of cells isolated from a significant number of labeled animals and therefore be prohibitively expensive.

An alternative to stable isotope labeling is 'label-free' quantitation. In this case, peptide intensities measured during individual LC runs are compared across runs (Bantscheff et al., 2007). In general, label-free quantitation is very attractive because it can be applied to any proteomic sample material without need of introducing isotopes for quantitation. However, label-free methods are generally much less accurate than isotope-based methods and proteome-wide quantitation has not yet been possible (Schiess et al., 2008; Xu et al., 2008). Major challenges in label free quantitation are matching of thousands of peptides across samples, variability in LC-MS resulting in retention time shifts and errors introduced by slight differences in sample fractionation steps.

Here we studied the differences in abundance of proteins in cDCs subsets using a novel algorithm for label-free quantitation, which we have recently developed (Cox et al., submitted and attached). We here introduce this MS-based label-free quantitation approach to profile protein abundance differences of cDC subsets to a depth of more than 5000 proteins requiring only 1.5 - 2.0 x10^6 FACS purified cells. This technology now makes it possible to study closely related cell types *in vivo*. Expression profiles show substantial overlap but also highly informative differences in protein composition between the three cDC subsets. Our analysis reveals mutually exclusive expression of pattern recognition

pathways not previously known to be subset specific. We show that members of the NOD-, TLR and RLH signaling pathways are differentially expressed in cDC subsets. Amongst these, RIG-I and MDA5 are significantly higher or uniquely expressed by CD4^{+} and DN cDCs. This lack of viral recognition receptors in CD8α^{+} cDC is surprising, because CD8α^{+} cDC are thought to be the main mediators of antiviral defense amongst cDC subsets. In agreement with their selective expression of RIG-I and MDA5, only CD4^{+} and DN cDC subsets, but not CD8α^{+} cDCs, were able to recognize and produce type I interferon in response to direct RNA virus infection. Thus label-free, proteome-wide quantitation assigns key viral recognition functions to CD4^{+} and DN cDCs.

2.2   Experimental Procedures

2.2.1   Mice

All mice were bred and maintained either in the animal facility at Bavarian Nordic GmbH (BN) or the Max Planck Institute of Biochemistry (MPIB) according to institutional guidelines. Experiments were generally done between 8-12 weeks of age. Mutant mice lacking MyD88 were generated by S. Akira (Adachi et al., 1998) and backcrossed on a C57BL/6 background by H. Wagner. Cardif deficient mice on a C57BL/6 background were provided by J. Tschopp (Meylan et al., 2005). C57BL/6 wildtype were obtained from the animal facility of MPIB.

2.2.2   Cells, Flow Cytometric Analysis and Sorting

cDC subsets were isolated from pooled mouse spleens from wild type, MyD88^{-/-} and Cardif^{-/-} C57BL/6 mice as described (Vremec et al., 2007). Briefly, spleens were chopped, digested with collagenase (Worthington Biochemical) and DNase (Roche) at room temperature, and treated with EDTA. Low-density cells were enriched by density centrifugation (1.077 g/cm^3, Progen Biotechnik, adjusted to 308 mOs mouse osmolarity). Non-DC lineage cells were coated with mABs (anti-CD3, KT3-1.1; anti-Thy-1, T24/31.7; anti Gr-1, 1A8; anti-CD19, ID3; anti-erythrocytes, TER119 and anti-NK cells, DX5). pDCs were depleted by adding anti-B220 (RA3-6B2) in the mAb depletion cocktail. Depletion was done using anti-rat Ig magnetic beads (Qiagen). Dead cells were stained with propidium iodide (PI) and gated out. For purification and segregation of the populations of cDCs, the pre-enriched DC preparations were fluorescent cell sorted based on the expression of CD11c, CD45RA, CD4 and CD8α (all BD Biosciences) using a FACS Aria instrument (BD Biosciences).

Activation of cDC subsets was determined by CD86 expression using a FACS Calibur instrument (BD Biosciences). Analysis of FACS data was performed with WEASEL software (The Walter and Eliza Hall Institute of Medical Research, Melbourne, Victoria, Australia).

Flt3-ligand derived dendritic cells were prepared as described (Naik et al., 2005). Briefly, bone marrow (BM) cells were flushed from femurs and tibiae of WT, MyD88^{-/-} and Cardif^{-/-} mice and depleted of red blood cells. Total BM cells were cultured at 1.5x10^6 cells/mL in

RPMI 1640 media supplemented with 10% fetal calf serum (FCS), 50µmol/L ß-mercaptoethanol, antibiotics and 35ng/mL recombinant mouse (recmu) FL for 8 days at 37°C. Recmu FL was expressed in Chinese hamster ovary cells and purified in house as described previously (O'Keeffe et al., 2002b). Fluorescent cell sorting into both eCD8^{+} and eCD8^{-}-cDC subsets was done based on expression of CD11c, CD11b, CD24, CD103 and CD45R (all BD Biosciences).

2.2.3   Sample preparation for mass spectrometry

FACS purified cDC subsets were washed two times in PBS and immediately frozen on dry ice. Cell lysates were boiled in 2x LDS-buffer, separated by 1D-SDS PAGE (4-12% Novex mini-gel, Invitrogen) and visualized by colloidal Coomassie staining. The gel was cut into 14 slices and each slice was subjected to reduction, alkylation and in-gel digestion with sequence grade modified trypsin (Promega) according to standard protocols (Shevchenko et al., 1996). After digestion peptides were extracted by 30% acetonitrile in 3% TFA, reduced in a *speed vac* and desalted using StageTips before analysis by mass spectrometry (Rappsilber et al., 2003).

2.2.4   Mass spectrometric analysis

All mass spectrometric (MS) experiments were performed on a nanoflow HPLC system (Agilent Technologies 1100 or 1200) connected to a hybrid LTQ-Orbitrap(Thermo Fisher Scientific, Bremen, Germany), equipped with a nanoelectrospray ion source (Proxeon Biosystems). Peptide mixtures were separated by reversed phase chromatography using in house-made C_{18} microcolumns (75 µm ID packed with ReproSil-Pur C18-AQ 3-µm resin, Dr. Maisch GmbH) with a 2h gradient from 5% to 60% acetonitrile in 0.5% acetic acid at a flow rate of 200nl/min and directly electrosprayed into the mass spectrometer. The LTQ-Orbitrap was operated in the data dependent mode with a full scan in the Orbitrap with a resolution R=60,000 at m/z 400 after accumulation of a target value of 1×10^6 ions. Meanwhile, the five most intense ions with charge states ≥ 2 were isolated (target value 5,000) and fragmented in the LTQ part by collisionally induced dissociation.

2.2.5   Data processing and analysis

The data analysis was performed with MaxQuant software (version 1.0.12.12) supported by Mascot as a database search engine for peptide identification as described (Cox and Mann, 2008). Label-free quantitation algorithms were added to MaxQuant by extracting isotope patterns for each peptide in each run. These isotope patterns were matched to each other across runs using peptide identifications, the very high mass accuracy and non-linearly re-mapped retention time. Total peptide signals within each run were normalized in order to make experiments comparable that were performed months apart. For label-free quantitation we compared the maximum number of peptides between any two samples, resulting in a matrix of protein ratios, calculated as the median of all ratios for common

peptides. We used least squares regression to solve the over-determined system of equations to obtain the best estimate for the protein ratios. Details of the algorithm will be described elsewhere (available upon request to reviewers). The proportion of kinases in the proteome and genome were determined using the GO term 0004672.

2.2.6 Virus infection

Purified Sendai virus (Cantell strain, Charles River laboratories) was used for *in vitro* infection of FACS purified DC subsets from wild type, MyD88$^{-/-}$ and Cardif$^{-/-}$ C57BL/6 mice. 1x10^6 DC subsets per ml were infected with virus at an optimal concentration for IFN-α induction in cDCs in RPMI 1640 medium supplemented with 10% FCS and antibiotics in the presence of IL-3 and GM-CSF. Cell culture supernatants were harvested 18 hours after incubation with the virus and secretion of IFN-α, IFN-ß and IL-6 was measured by ELISA reagents as described (Hochrein et al., 2004).

2.2.7 Data and software access notes

Identified Peptides and Proteins will be uploaded to MAPU 2.0 (proteome.biochem.de), a member of ProteomeCommons. Raw MS data files will be uploaded to Tranche (http://www.proteomecommons.org). Source code for label-free algorithms incorporated into MaxQuant are available at the MaxQuant.org web site upon publication.

2.3 Results

2.3.1 Quantitative proteomic analysis of cDC subsets

To identify differentially expressed proteins amongst cDC subsets we used a mass spectrometry based proteomics approach to quantitatively compare FACS purified cDC subsets of the spleen of uninfected steady-state mice. cDCs were subsequently purified from Collagenase and DNAse digested spleens by density centrifugation and magnetic depletion of non-cDC resulting in a 70-80% enriched cDC cell population, which was segregated into subsets according to the expression of CD8α and CD4 surface molecules using flow cytometry (Figure 2-1A). cDCs preparations from pooled spleens of 32 mice consistently yielded more than 2.5x10^6 cDCs per subset with purity higher than 95%, as estimated by FACS-reanalyses (Figure 2-1B).

Sorted CD4$^+$, CD8α$^+$ and DN cDCs, resulting in 20 to 25μg total protein each, were separated by 1D sodium dodecyl sulfate-polyacrylamide gel electrophoresis (SDS-PAGE) and after tryptic in-gel digestion analyzed by LC-MS/MS (LTQ-Orbitrap). We repeated this experiment twice with different pools of spleens resulting in biological triplicates.

LC-MS/MS data from all 126 gel slices of the three independent large scale experiments were combined and analyzed by MaxQuant (Cox and Mann, 2008).
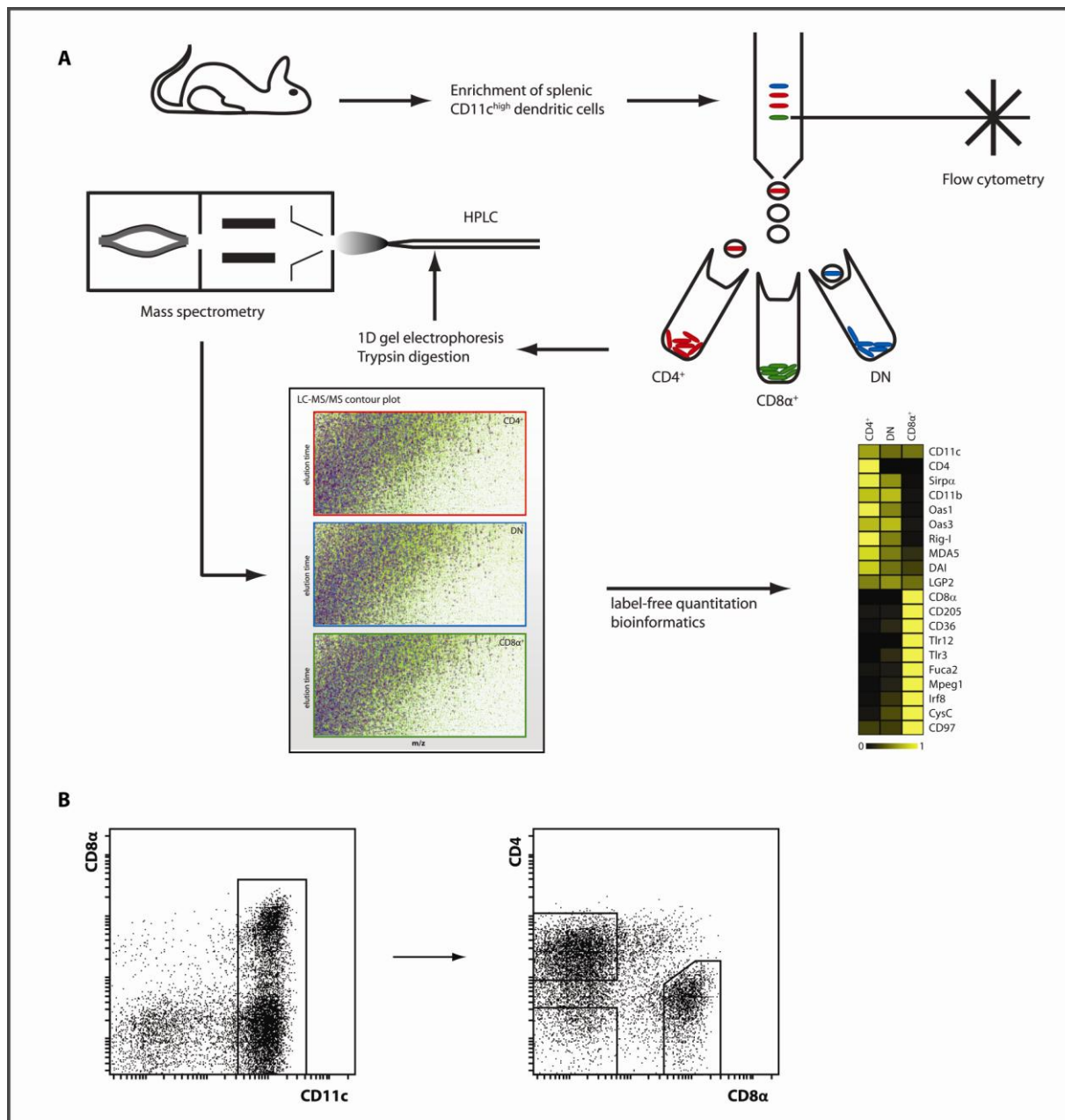
Figure 2-1 Experimental strategy for *in vivo* cDC subset proteomics (A) and FACS purification (B)

We incorporated new algorithms for label-free quantification into MaxQuant, which allows us to quantify peptides across individual LC-MS/MS runs (Cox et al., submitted and attached). Analysis of the entire dataset using uniform statistical criteria identified 1,283,676 peptides (99,228 non-redundant sequences), corresponding to 5359, 5642 and 4830 proteins in CD4$^+$, CD8α$^+$ and DN cDCs with 99% certainty, respectively.

Summed peptide intensity is a good proxy for absolute protein abundance (de Godoy et al., 2008b) and by this measure we covered the cDC proteomes across more than four orders of magnitude. The cDC proteome of 5780 proteins shows no bias against low level regulatory proteins such as kinases (209 identified or 3.6% of our proteome vs. 4.2% in the genome).

Relative label-free quantitation was highly reproducible between biological replicates and correlation between normalized protein intensities was between 0.84 and 0.96 (Figure 2-2). Hence, label free quantitative proteomics provides an accurate means of comparing differences in protein expression between cDC subsets *in vivo* for thousands of proteins.
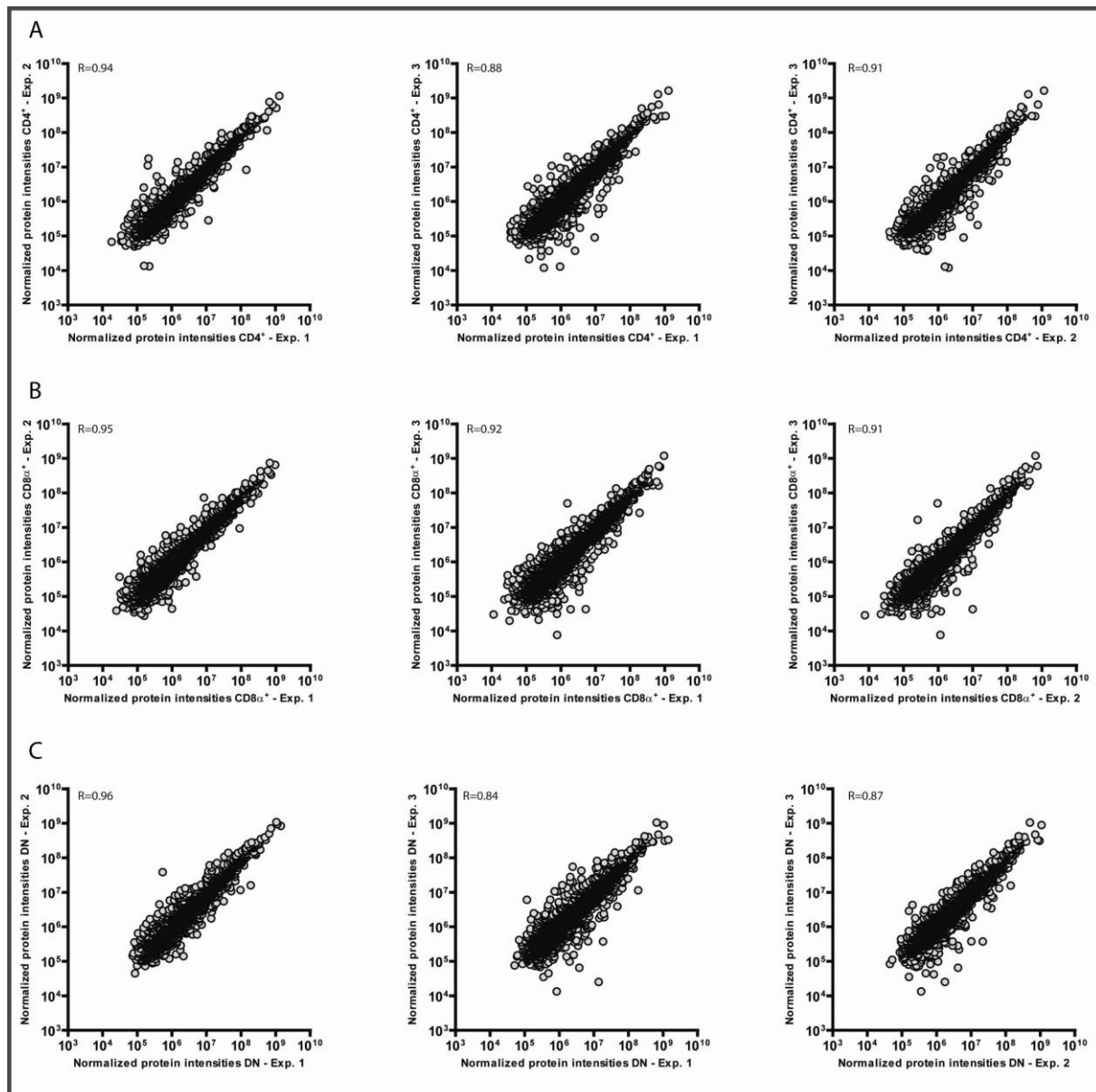
Figure 2-2 Reproducibility of biological and technical replicate measurements of (A) CD4^{+} cDCs, (B) CD8α^{+} cDCs and (C) DN cDCs. Correlation is determined by Pearson coefficient

Expression levels of most proteins were similar and only a relatively small number showed statistically significant differences between any two subsets (p ≤ 0.01) (Figure 2-3). Overall,

differences in protein expression patterns showed that CD4$^+$ and DN cDCs were more closely related to each other than to CD8α^+ cDCs (Figure 2-3) as already suggested by microarray analysis (Edwards et al., 2003a).
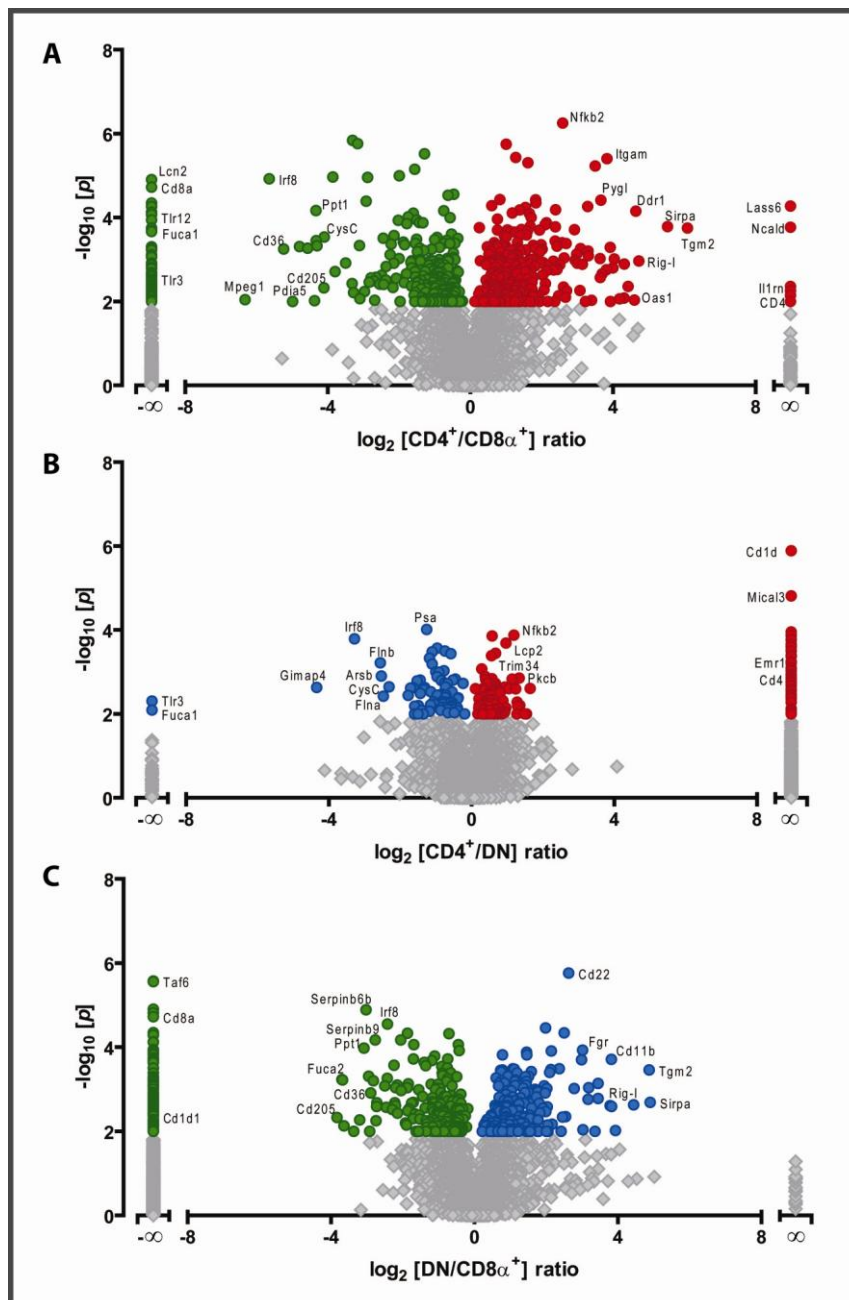
Figure 2-3 Volcano plot of protein expression differences between cDC subsets as a function of statistical significance. Proteins with no detectable signal in one of the subsets were assigned a ratio of infinity. (A) CD4$^+$ vs. CD8α^+ cDCs, (B) CD4$^+$ vs. DN cDCs and (C) DN vs. CD8α^+ cDCs

We then analyzed the correlation between label-free quantitation results and known marker proteins of cDC subsets. All subsets expressed CD11c, the pan-marker of DCs. Markers for other lymphocyte lineages like CD19 for B lymphocytes, CD3 subunits for T lymphocytes or Nk1.1 for NK cells were not detected, indicating that sorted cDC populations were indeed pure and did not contain detectable contaminations from other cell types. The surface

markers CD4 and CD8α, which were used for FACS purification were expressed by the respective population and correctly assigned by our bioinformatic algorithms. Importantly, this was also true for other known surface markers such as DEC-205 and CD36 for CD8α^{+} DC, and CD11b, 33D1 and SIRPα for CD4^{+} and DN cDCs (Table 2-1). Correct assignment of these key surface markers by hypothesis free quantitative label free proteomics demonstrates the robustness of our approach. TLR3, an endosomal TLR, provided a further positive control (Edwards et al., 2003b) (Table S2-1 online).

Table 2-1 Numbers are the median of summed peptide intensities in ion counts per second over three biological replicates.

	CD4^{+} cDCs	CD8α^{+} cDCs	DN cDCs
CD11c	78,828,000	58,823,000	55,484,000
CD8α	0	3,876,600	0
CD205	381,840	6,461,300	443,580
CD36	92,491	3,421,300	445,720
CD4	1,096,000	0	0
Sirpα	6,585,700	139,680	4,044,100
33D1	950,990	0	694,500
CD11b	17,304,000	1,211,600	16,806,000

Subset restricted transcription factors distributed as expected; for example interferon regulatory factor 8 (IRF-8) was specific to CD8α^{+} compared to CD4^{+} DCs, whereas IRF-4 and the NF-κB subunit RelB were much more abundant in CD4^{+} DCs (Table S2-1 online). Interestingly, the class I NF-κB family members NfκB1 and NfκB2 have a similar expression pattern to RelB while RelA and c-Rel have no subtype specificity, suggesting a functional specialization of the NFκB pathway in cDC subtypes, previously only suggested by differential effects on DC subsets in mutant mice lacking members of the NF-κB family (O'Keeffe et al., 2005b; Wu et al., 1998) .

CD97, a member of the EGF-TM7 family of adhesion receptors implicated in leukocyte homing, was four-fold more abundant in CD8α^{+} compared to CD4^{+} cDCs. Flow cytometry with antibodies against CD97 independently confirmed our proteomic finding (Figure 2-4). In contrast, previous microarray data did not classify CD97 as a surface molecule with significant higher expression on CD8α[+] cDC (Dudziak et al., 2007; Edwards et al., 2003a).
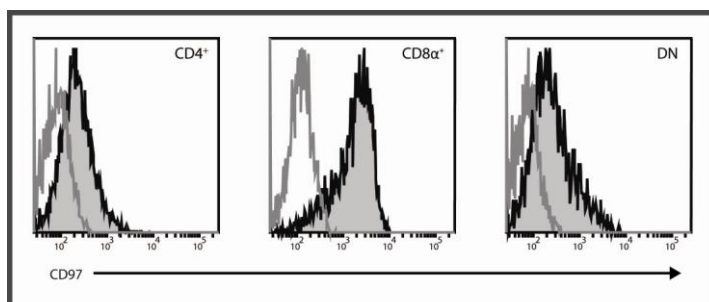
Figure 2-4 Expression of CD97 between cDC subsets measured by FACS

Proteome and transcriptome measurements do not necessarily agree, either due to technical factors or due to additional regulation at the protein level (Bonaldi et al., 2008).

2.3.2   Protein expression reflects different functionality of cDC subsets

Pattern recognition receptors endow DCs and other cells with the ability to sense pathogen associated molecular patterns (Akira et al., 2006) and activate defense programs upon encountering their cognate ligands. Differential expression of individual receptors determines the possible functional response of a cell to a pathogen. We reasoned that differences in protein abundance of individual PRRs might provide us with direct insights into functional differences between cDC subsets. It was previously known that certain TLRs are differentially expressed by cDCs (TLR7 only in CD4$^+$ and DN cDCs; TLR3 mainly in CD8α^+ cDCs) (Table S2-1 online, (Edwards et al., 2003b). Analysis of the expression of other TLRs identified in our analysis revealed that the expression of two uncharacterized members of the TLR family, TLR12 and TLR13 are mainly restricted to CD8α^+ cDCs. On the other hand, members of the NOD-like receptors, NOD1 and IPAF, were much more highly expressed in CD4$^+$ and DN cDCs (Figure 2-5).
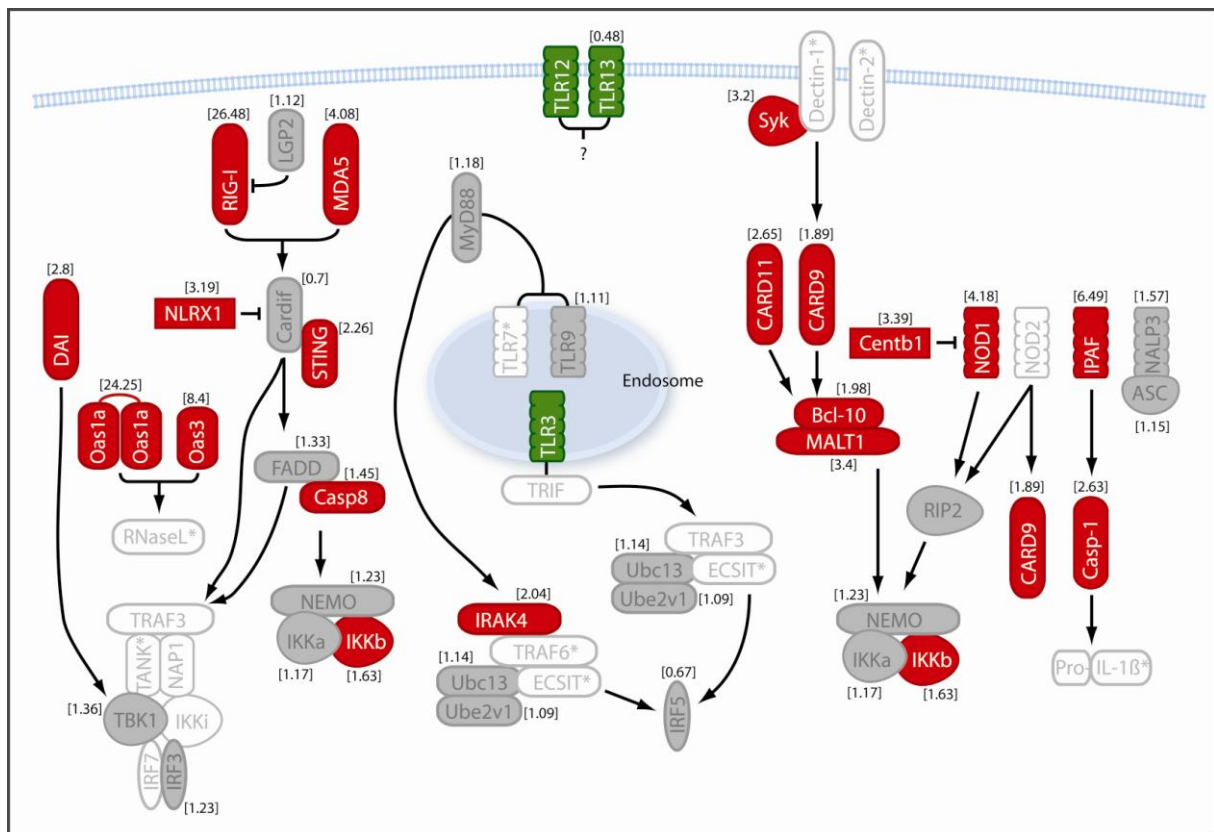
Figure 2-5 Differential expression of pattern recognition receptors between CD4+ and CD8α+ splenic cDCs. Members of pattern recognition receptors are color coded according to statistical significance, with red denoting higher expression in CD4+ cDCs with p ≤ 0.01. Likewise green denotes higher expression in CD8+ DCs. Grey, filled boxes are for proteins with no statistically significant change between subsets (p > 0.01). Unfilled boxes with asterisk are for proteins that have been detected but not quantified, whereas proteins with unfilled boxes have not been detected. Numbers in parentheses are fold changes determined by label-free proteomics

CD8α[+] cDCs are thought to be equipped with antiviral functions due their unique capability to cross-present viral antigens and their ability to produce high amounts of IL-12, which activates antiviral NK cells and T cells (Allan et al., 2003; Belz et al., 2005; Belz et al., 2004; Maldonado-Lopez et al., 1999). However, our data show a higher expression of the viral RNA recognition molecules RIG-I and MDA5 (Kato et al., 2008; Kato et al., 2006) in CD4^{+} and DN DCs (Figure 2-5). These RIG-like helicases (RLHs) signal through interaction with Cardif, which relays the signal to downstream activation of transcription factors and type I IFN response and proinflammatory responses (Meylan et al., 2005). Consistently, NLRX1, a potent regulator of Cardif, is also more highly expressed in CD4^{+} cDCs (Figure 2-5, Table S2-1 online). RIG-I was described to be essential for induction of type I interferon (IFN) upon RNA virus infection of all cDCs (Kato et al., 2005). However, our results suggest that not all cDC subsets are equally equipped to sense RNA viruses. This is further supported by the higher expression in CD4^{+} and DN DCs of OAS1 and OAS3, which are 2',5'-oligoadenylate synthases (OAS) involved in antiviral defense (Silverman, 2007). The restriction of cytoplasmic viral recognition to CD4+ and DN cDCs does not appear to be limited to RNA viruses or RNA intermediates, since we also identified DAI (also known as DLM1 or ZBP1), a cytosolic PRR activated by dsDNA, to be more abundant in CD4^{+} and DN cDCs (Takaoka et al., 2007).

2.3.3 Differential sensing of Sendai virus infection amongst DC subsets

Next, we directly tested the hypothesis from our unbiased quantitative proteomics experiment that cDC subsets differ in their ability to sense viral infection by challenging purified cDC subsets with Sendai virus, a known activator of RIG-I (Kato et al., 2006). Whereas the activation-specific marker CD86 was increased in CD4^{+} and DN cDCs after 18h of viral infection, CD8α^{+} cDCs did not show any upregulation of CD86 (Figure 2-6A).
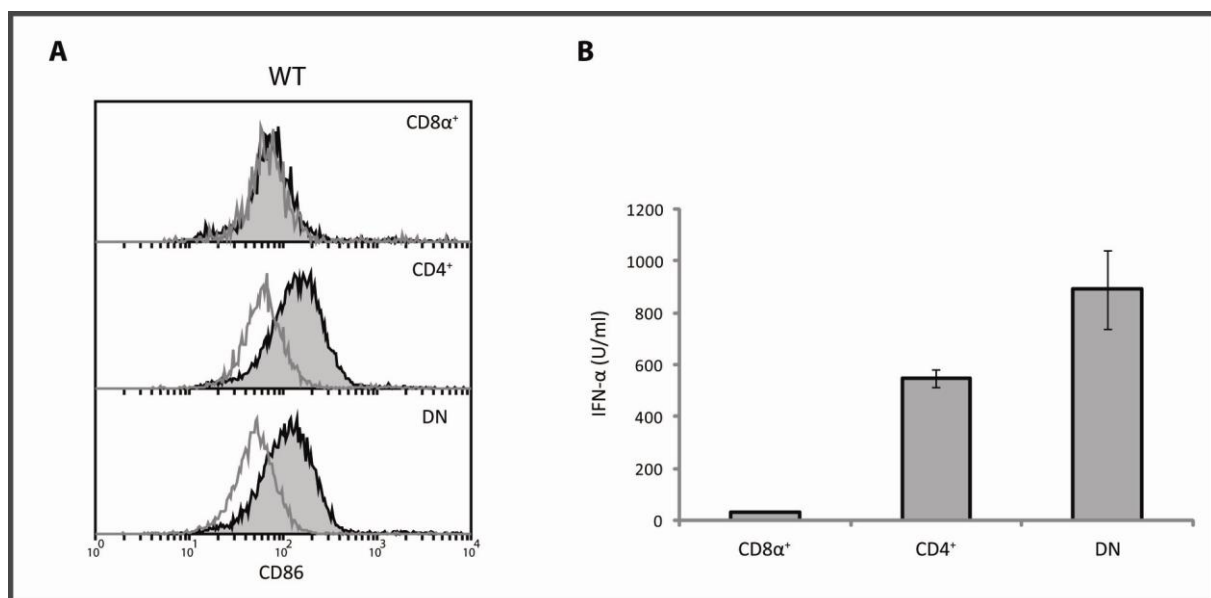

Figure 2-6 (A) Flow cytometry histograms showing expression of CD86 of sorted WT splenic cDC subsets of after incubation with Sendai virus (filled histograms) or without stimulation (open histograms). (B) WT splenic cDC subsets were stimulated with Sendai virus and supernatants were analyzed for IFN-α by ELISA

We measured IFN-α production after viral infection by ELISA and found that - corresponding to the responsiveness seen with maturation - only CD4^{+} cDCs and DN cDCs produced IFN-α (Figure 2-6B). The production of IL-6 and IFN-ß in response to Sendai virus is also restricted to CD4^{+} and DN cDC subsets (data not shown).Thus only CD4^{+} and DN cDCs but not CD8α^{+} cDC respond to direct Sendai virus infection.

In addition to RLHs, DCs can also detect viruses via TLRs. Therefore, it was possible that differences in virus detection were dependent upon differential TLR signaling rather than on the differential expression of RLHs that we detected. We ruled out this possibility with mice lacking MyD88 (Adachi et al., 1998), an adapter protein for most TLR signaling pathways. After viral infection of cDCs from these mice, both CD4^{+} and DN cDCs, but no CD8α^{+} cDCs, upregulated CD86 and produced IFN-α, showing that responsiveness to Sendai virus is functional in the absence of TLR signaling (Figure 2-7**).**
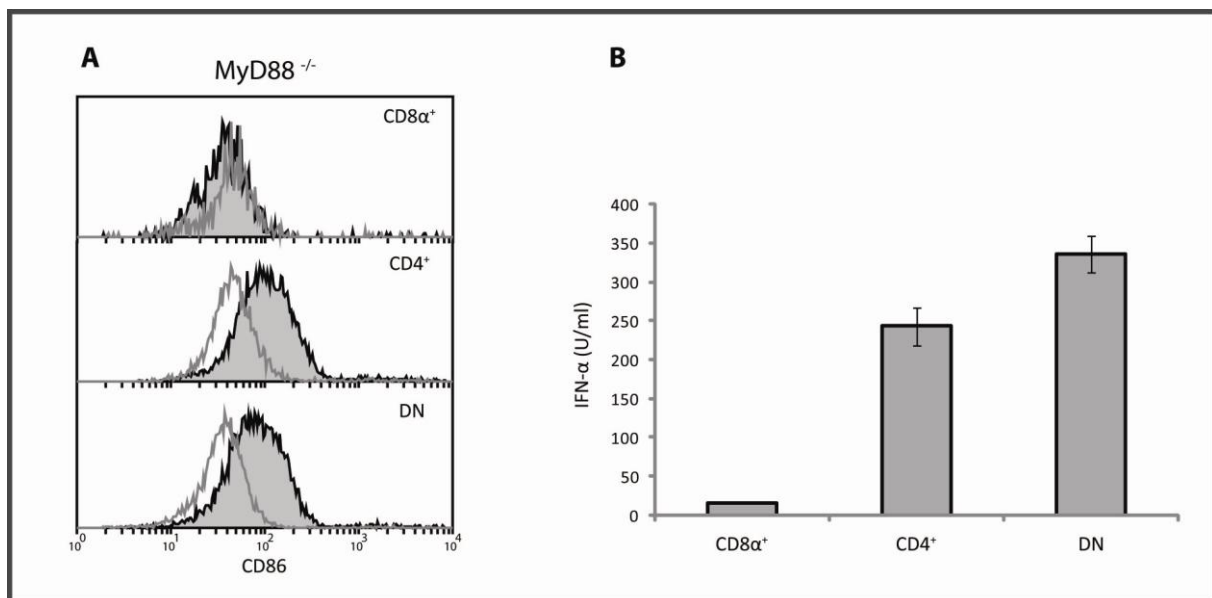
Figure 2-7 (A) Flow cytometry histograms showing expression of CD86 of sorted MyD88^{-/-} splenic cDC subsets of after incubation with Sendai virus (filled histograms) or without stimulation (open histograms). (B) MyD88^{-/-} splenic cDC subsets were stimulated with Sendai virus and supernatants were analyzed for IFN-α by ELISA

To further verify that the RIG-I antiviral pathway is indeed the unique feature enabling CD4^{+} and DN cDCs, but not CD8α^{+} cDCs, to recognize direct viral infection, we tested responses of DCs derived from Cardif^{-/-} mice (Michallet et al., 2008). Without Cardif none of the cDC subsets should be able to recognize RIG-I dependent Sendai virus infection. FL-DC bone marrow cultures from these mice containing equivalents of CD8α^{+} cDCs (eCD8^{+}) and equivalents of both CD4^{+} and DN cDCs (eCD8^{-}) (Naik et al., 2005) were purified by FACS and infected with Sendai virus. Virus infection indeed did not result in any detectable IFN-α from either subset of Cardif^{-/-} mice. Furthermore, eCD8^{-} DCs but no eCD8^{+} DCs of MyD88^{-/-} mice were still able to produce IFN-α (Figure 2-8), showing also in the bone marrow model that this viral recognition is specifically dependent on the RLH pathway but not on the TLR

pathway. FACS purified splenic cDC subsets of Cardif^{-/-} mice gave similar results as the cDC equivalents from FL-cultures (data not shown).
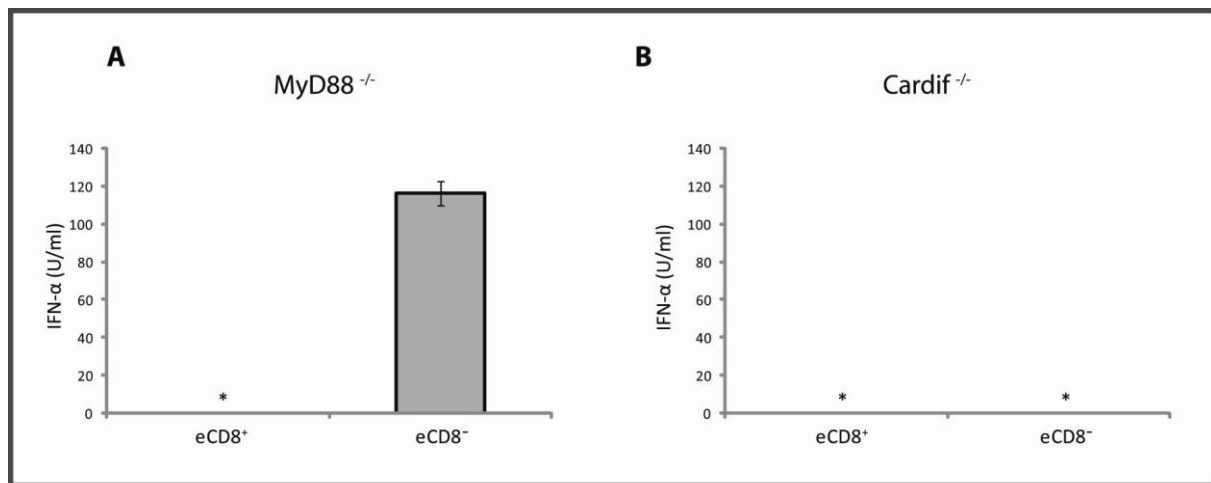
Figure 2-8 FACS purified equivalents of bone marrow derived FL-DC from (A) MyD88 or (B) Cardif deficient mice were stimulated with Sendai virus, and supernatants were analyzed for IFN-α by ELISA

Collectively, these results demonstrate that CD4^{+} and DN cDCs, in contrast to CD8α^{+} cDCs, are uniquely equipped with the RLH pathway to sense viral infection.

2.4   Discussion

Multicellular organisms consist of different cell types that have specialized functions. One of the most striking examples of this principle is the mammalian immune system that consists of many different cell types with a high degree of functional diversity. As most biological processes are carried out by proteins, differences in protein composition should be usable to infer biological functions. In the context of the immune system, different cell types are typically characterized by FACS. While this method is very powerful to highlight differences in protein levels at the single cell level, it alone cannot be used to profile the cellular proteome in an unbiased way. Alternatively, cellular mRNA levels can provide valuable information, but it is generally accepted that proteins as end products of the encoded genes should provide more functional relevance than mRNA expression profiles.

Here we show for the first time, that comprehensive MS-based proteomics combined with newly developed label-free quantitation algorithms can determine the differences in protein abundance for a substantial part of the proteome of steady state cDC subsets *in vivo*.

To our knowledge, our dataset is the most comprehensive quantitative comparison of different *in vivo* cell populations obtained so far. We achieved reliable and reproducible quantitation for more than 5,000 proteins from a few microgram of FACS purified, rare cell types directly isolated from mice. The approach does not involve metabolic labeling and can thus be used to quantify *in vivo* protein levels in all organism including humans. No

additional *in vitro* labeling procedures are required which simplifies the procedure and minimizes biases introduced by differences in sample handling.

The approach was validated by its ability to identified markers known to be expressed in a subset specific manner. Novel subset specific proteins were detected and validated, including CD97 which was not classified as differentially expressed by microarray studies (Dudziak et al., 2007; Edwards et al., 2003a). Collectively, our results demonstrate that label-free quantitation can be used to directly compare levels of thousands of proteins *in vivo.*

Previous functional and microarray data demonstrated selective expression of PRRs amongst cDC subsets. It was shown the endosomal ssRNA recognition receptor TLR7 is exclusively expressed in the $CD4^+$ and DN cDC populations, corresponding with the lack of responsiveness of $CD8\alpha^+$ cDCs to TLR7 ligands (Edwards et al., 2003b). Our proteomic analyses additionally revealed that the orphan TLRs TLR12 and TLR13 were found to be more abundant in $CD8\alpha^+$ cDCs. This finding is of substantial interest since the ligands of these two TLRs are currently unknown, but our data indicate that, at least amongst DC subsets, their detection will be restricted to the response of $CD8\alpha^+$ cDCs. The elucidation of the ligands of these TLRs may lend further insights into the functional capacity of $CD8\alpha^+$ cDCs.

Here we show that RLHs, cytoplasmic RNA detectors, and some key RLH signaling molecules are expressed more abundantly or even uniquely in $CD4^+$ and DN cDCs. Only these cDC subsets produce Type I IFNs and IL-6 and display an activated surface phenotype upon infection with the ssRNA Sendai virus. This viral recognition was specific for the RLH pathway in these cDCs since it was functional in MyD88 mutant mice but abolished in mice lacking the essential RLH signaling molecule Cardif. It is tempting to speculate that the selective absence of ssRNA recognition molecules in the $CD8\alpha^+$ cDCs might play an important role in the biology of these cells. $CD8\alpha^+$ cDCs are well known for their crosspresentation capacity. It has been demonstrated that this ability is abrogated within a short time frame upon stimulation (Wilson et al., 2006). Lack of responsiveness to ssRNA and lack of, or at least delay in $CD8\alpha^+$ cDC activation might be necessary for effective crosspresentation in ssRNA virus infection.

Another important class of cytosolic PRRs are the inflammasome associated NLRs, which are involved in the activation of Caspase 1 and the secretion of proinflammatory cytokines like IL-1 and IL-18 (Kanneganti et al., 2007). We found higher expression of several members of the NLR associated molecules like NOD1, IPAF, CARD9 and CARD11 in $CD4^+$ and DN cDCs, suggesting further possible functional separation amongst DC subsets.

In conclusion, our quantitative proteome study shows the feasibility to quantify rare *in vivo* cell subpopulations at the protein level. The proteomic expression data provided direct insights into the functional segregation of dendritic cell subsets. Direct infection of DC subsets *ex vivo* using Sendai virus confirmed our findings. Moreover, the data produced in this study will provide extensive information for a future detailed comparison of the proteomes of mouse cDC subsets with human cDC subsets. Such a comparison would be a

powerful means for dissecting similarities and differences between the DCs across the species.

3   Novel approaches for label-free quantitation

Abstract

Despite long standing interest in protein quantification without isotopic labels this technology has not yet developed sufficiently to allow accurate and robust proteome-wide quantification. We developed a new intensity normalization procedure that is fully compatible with any peptide or protein separation prior to LC-MS analysis. Protein expression profiles are assembled using the maximum possible information from peptide signals given that the presence of quantifiable peptides varies from sample to sample. On a benchmark dataset with two mixed proteomes we quantify 5,362 proteins and are able to detect differential regulation essentially over the entire protein expression range, with higher precision for abundant proteins. A t-test approach accurately describes significance of individual label-free quantifications. Application of these methods to liver tissue samples shows that technical variability of our method is much smaller than differences in expression patterns between individual littermate mice.

3.1   Introduction

Mass spectrometry based proteomics has become an increasingly powerful technology not only for the identification of large numbers of proteins but also for their quantification (Aebersold and Mann, 2003; Bantscheff et al., 2007; Ong and Mann, 2005). In our laboratory, we have recently employed stable isotope labeling of amino acids in cell culture (SILAC) (Ong et al., 2002) for comprehensive quantification of the yeast proteome in the haploid vs. the diploid state(de Godoy et al., 2008a) and expression changes of several thousand proteins can routinely be measured in more complex eukaryotic cells (Baek et al., 2008; Bonaldi et al., 2008; Graumann et al., 2008; Selbach et al., 2008). Thus proteomics is approaching the depth of other post-genomic technologies such as microarrays (Cox and Mann, 2007). While advances in technological development of high resolution mass spectrometers contributed to these developments (Makarov et al., 2006; Olsen et al., 2005), much of the progress can be attributed to improvements in data analysis (Cox and Mann, 2008).

Despite the success of isotope based methods of quantitative proteomics, label-free quantification is potentially the simplest and most economical method. It would also be ideal for certain types of samples such as clinical material. A vast literature on this topic, reviewed in (Bantscheff et al., 2007; Domon and Aebersold, 2006; Listgarten and Emili, 2005; Mueller et al., 2008), as well as associated software projects (Bellew et al., 2006; Bridges et al., 2007; Jaffe et al., 2006; Johansson et al., 2006; Katajamaa et al., 2006; Kohlbacher et al., 2007; Leptos et al., 2006; Listgarten et al., 2007; May et al., 2007; Mueller et al., 2007; Palagi et al., 2005; Park et al., 2008; Rauch et al., 2006; Roy and Becker, 2007; Smith et al., 2002) already exist. However, reports thus far provide quantitative information for at most a few hundred proteins rather than in-depth proteome coverage. Also, while some researchers report very low coefficients of variation for selected quantified features, many of the reported biomarker proteins in the same studies are not reproducible or show much larger variability, questioning the robustness of these approaches. Furthermore, current label-free methods require measurement of the samples under uniform conditions with strict adherence to standard operating procedures, with minimal fractionation and in tight temporal sequence.

The main advantage of metabolic labeling is its much greater accuracy and robustness, which is mainly due to insensitivity towards irreproducibility in sample processing steps. For instance, any upfront separation of proteins or peptides potentially poses serious problems in a label-free approach, since the partitioning into fractions is prone to change slightly from sample to sample. Chemical labeling (Gygi et al., 1999; Ross et al., 2004) is in principle universally applicable, but since the labels are introduced relatively late in the sample processing it may not be sufficiently accurate. Depending on the label used it can also be uneconomic in many situations.

Two key ingredients in the excellent quantitative accuracy and depth of coverage of isotope based methods achieved with SILAC recently were high peptide mass accuracies and high identification rates. The same algorithmic steps should apply to the label-free case.

Increased identification rate directly improves label-free quantification because it increases the number of data points. While high mass accuracy aids in identification of peptides, it is high mass resolution which is crucial to accurate quantification. At low resolution extracted ion currents (XICs) of peptides are often contaminated by nearby peptide signals and robust deconvolution of intensities is difficult. This has led many researchers to use counts of identified MS/MS spectra as a proxy for the ion intensity (Ishihama et al., 2005a). However, XIC-based methods should clearly be superior to spectral counting given sufficient resolution and optimal algorithms.

Here we solve two of the main problems of label-free protein quantification. We implement 'delayed normalization' which makes label-free quantification fully compatible with any upfront separation. Furthermore, we introduce a novel approach to protein quantification which extracts the maximum ratio information from peptide signals in arbitrary numbers of samples. We also select and benchmark robust statistical tests of quantification accuracy for each of thousands of quantified proteins.

3.2 Experimental Procedures

3.2.1 Benchmark dataset

E.coli K12 strain was grown in standard LB medium, harvested, washed in PBS and lysed in BugBuster (Novagen) according to the manufactures protocol. HeLa S3 cells were grown in standard RPMI 1640 medium supplemented with glutamine, antibiotics and 10% FBS. After washing with PBS cells were lysed in cold modified RIPA buffer (50mM Tris-HCl (pH 7.5), 1mM EDTA, 150mM NaCl, 1% N-octylglycoside, 0.1% sodium deoxycholate, complete protease inhibitor cocktail (Roche)) and incubated for 15min on ice. Lysates were cleared by centrifugation, and after precipitation with chloroform/methanol, proteins were resuspended in 6M urea/2M thiourea/ 10mM HEPES (pH 8.0). Prior to in-solution digestion each 60μg of HeLa S3 lysates were spiked with either 10μg or 30μg of *E.coli* K12 lysates based on protein amount (Bradford).

Both batches containing always the same amount of HeLa S3 lysates but *E.coli* K12 lysates in 1:3 ratio were reduced with dithiothreitol and alkylated with iodoacetamide. Proteins were digested with LysC (Wako Chemicals) for 4 hours, followed by trypsin digestion (Promega) overnight. Protein digestion was stopped by adding 2% trifluroacetic acid. Peptides were separated by isoelectric focusing(Hubner et al., 2008) into 24 fractions on a 3100 OFFGEL Fractionator (Agilent). Each fraction was purified with StageTips and analyzed by liquid chromatography combined with electrospray tandem mass spectrometry on a LTQ Orbitrap (Thermo Fisher) with lock mass calibration (Olsen et al., 2005). The International Protein Index (IPI) version 3.46 human was combined with *E.coli* protein sequences extracted from the NCBI database and used for the Mascot search. MS/MS spectra were filtered to contain

at most six peaks per 100 Dalton intervals. The MS/MS fragment ion tolerance was set to 0.5 Dalton (Cox et al., 2008).

For quantification, intensities can be determined alternatively as the full peak volume or the as the intensity maximum over the retention time profile, using the latter here as default. Likewise, MaxQuant offers a choice of the degree of uniqueness required for peptides to be included for quantification. While offering three alternatives in general – 'all peptides', 'only unique peptides', and 'unique plus razor peptides' (Cox and Mann, 2008) – we choose here the latter version, which is a compromise between the two competing interests of using only peptides that undoubtedly belong to a protein and using as many peptide signals as possible.

3.2.2   Mouse liver samples

Six male sibling C57BL/6 mice were sacrificed by cervical dislocation according to institutional guidelines. Livers were quickly excised and processed as described(Shi et al., 2007). Livers were weighed and homogenized in 50 mM Tris buffer pH 8.0 containing 6M Urea/2M thio-urea. This homogenate was cleared by centrifugation and in-solution digested with LysC (Wako Chemicals) for 4h, followed by trypsin (Promega) overnight. Peptides were purified using StageTips and analyzed by LC-MS/MS as the benchmark data set.

3.2.3   Retention time alignment and identification transfer

To increase the number of peptides that can be used for quantification beyond those that have been sequenced and identified by an MS/MS database search engine, we transfer peptide identifications to unsequenced or unidentified peptides by matching their mass and retention times. A prerequisite for this is that retention times between different LCMS runs are made comparable by alignment. The order in which LCMS runs are aligned is determined by hierarchical clustering, thereby avoiding reliance on a single master run that all other retention times are aligned to. The bottom leaves are mostly connecting LC-MS runs of same or neighboring OFFGEL fractions, since they are most similar. These 'simple cases' are aligned first while moving along the tree structure increasingly dissimilar runs are integrated. The calibration functions that are needed to completely align LCMS runs are usually time-dependent in a non-linear way. Every pair-wise alignment step is performed by two-dimensional Gaussian kernel smoothing of the mass matches between the two runs. Following the ridge of the hill determines the recalibration function. At each tree node the resulting recalibration function is applied to one of the two sub-trees, while the other is left unaltered. The re-calibrations are accumulated for each leaf node along the way to the root.

Unidentified LC-MS features are assigned peptide identifications by matching accurate masses and aligned retention times. The current high mass accuracy on FTICR and Orbitrap instruments is in complex proteomes still insufficient for an unequivocal peptide identification based on the peptide mass alone. Still, when comparing peptides in replicate runs – preferentially of reduced complexity samples – the information contained in peptide

mass and recalibrated retention time is enough to transfer identifications with a sufficiently low FDR. The matching procedure takes into account the upfront separation, in this case isoelectric focusing of peptides into 24 fractions. Identifications are only transferred into adjacent fractions. If, for instance, for a given peptide isotope patterns are found to match by mass and retention time in fractions 6, 7, 8 and 17 the matches in fraction 17 are discarded since they have a much higher probability of being false. The same strategy can be applied to any other upfront peptide or protein separation, like e.g. 1D gel. All matches with retention time difference below 2 minutes are accepted.

3.2.4   Statistical analysis

Principal component analysis (PCA) and hierarchical clustering were done with the TM4 software (Saeed et al., 2003) on the expression matrix filtered for proteins with at least 6 nonzero intensities and with samples brought to equal standard deviation. PCA was performed on mean-centered data and Euclidean distance with z-scored rows and average linkage was used for hierarchical clustering. ANOVA p-values were corrected for multiple hypothesis testing with the Benjamini-Hochberg method and were called significant with 5% FDR. Correlation between Gene Ontology, KEGG and Pfam domains with the ANOVA p-value were tested with a one sided Wilcoxon-Mann-Whitney test and called significant with 5% Benjamini-Hochberg FDR. Expression profiles were averaged over significant categories, z-scored and clustered with Euclidean distance and average linkage.

3.2.5   Data and software access notes

The workflow for label-free quantification is completely integrated into the MaxQuant software (Cox and Mann, 2008). Executables as well as source code of algorithms are available via http://www.maxquant.org upon publication. MaxQuant runs on Windows^{TM} desktop computers and is compatible with XP and Vista. Identified Peptides and Proteins will be uploaded to MAPU 2.0 (proteome.biochem.de), a member of ProteomeCommons. Raw MS data files will be uploaded to Tranche (http://www.proteomecommons.org).

3.3   Results

3.3.1   Creation of a proteome-wide benchmark data set

So far it has been difficult to assess the accuracy of label-free workflows at the proteome scale either because only a few test proteins were spiked in or because the magnitudes of the protein ratio changes were not known. In order to evaluate the coverage and accuracy of our quantification workflow we therefore produced a benchmark dataset by mixing entire and distinguishable proteomes in defined ratios. The combined trypsin-digested lysates of HeLa and *E.coli* cells were separated by isoelectric focusing into 24 fractions as described

(Hubner et al., 2008) and analyzed by LC-MS/MS in three replicates. This was repeated with the same quantity of HeLa, but a three-fold increased amount of *E.coli* lysate. In the resulting six samples all human proteins should have one to one ratios while all *E.coli* proteins should have a ratio of three to one between replicate groups.

The data was processed with the MaxQuant algorithms recently introduced for SILAC (Cox and Mann, 2008), omitting the steps specific to labeling. With peptide and protein false discovery rates (FDR) both set to 1% this resulted in the identification of 6,689 non-redundant proteins; 4,793 of these are human and 1,888 are *E.coli* proteins. The remaining eight protein groups (Cox and Mann, 2008) contained human as well as *E.coli* proteins and were discarded. Average absolute mass deviation over all identifications is 417 ppb. The resulting identification rate of all submitted MS/MS spectra is very high (55.5%). MaxQuant recognized a total of 736,046 quantifiable isotope patterns. Inclusion of low scoring MS/MS hits whose top-scoring peptide sequence had been identified with another MS/MS spectrum increased the number of quantifiable isotope patterns by 14% to 841,517. Transferring identifications by matching masses and recalibrated retention times increased quantifiable isotope patterns more than two-fold.

3.3.2   A novel solution to the normalization problem

A major disadvantage of label-free quantification is that separate processing steps themselves inevitably introduce differences in the fractions to be compared. In principle, correct normalization of each fraction could eliminate this error. However, the total peptide signals, necessary to perform normalization of the LC MS/MS runs of each fraction, are spread over several adjacent runs. Therefore we cannot sum up the peptide signals before we have the normalization coefficients for each fraction. Here we solve this conundrum by delaying normalization until after all peptide signals are added followed by global optimization of the normalization factors for least overall proteome variation.

Formally, we want to determine normalization coefficients N_j which multiply all intensities in the jth LCMS run (j runs from 1 to 144 in our example). The normalization should be done in an 'endogenous' way purely from the obtained data and without the addition of external quantification standards or reliance on a fixed set of 'housekeeping' proteins. Directly adjusting the normalization coefficients N_j for each of the fractions so that the total signal is equalized leads to errors if the fractionation is slightly irreproducible or if the mass spectrometric responses in the jth run are different from average. Therefore, we wish to sum the peptide signals over the fractions in each sample. This, however, already requires the determination of the run specific normalization factors N_j . To solve this problem, we exploit the fact that the majority of the proteome does not change between any two conditions so that their average behavior can be used as a relative standard.

After summing the peptide signals across fractions with as yet unknown N_j factors we determined these factors in a nonlinear optimization model, which minimizes overall

changes for all peptides across all samples (Figure 3-1). For this we define the total intensity of a peptide P in sample A, as

$$I_{P,A}(N) = \sum_k N_{\mathrm{run}(k)} \mathrm{XIC}_k \; ,$$

where the index k runs over all isotope patterns for peptide P in sample A. The quantity

$$H(N) = \sum_{P \in \text{peptides}} \sum_{(A,B) \in \text{sample pairs}} \left| \log \frac{I_{P,A}}{I_{P,B}} \right|^2$$

is the sum of all squared logarithmic fold changes between all samples and summed over all peptides (Figure 3-1).
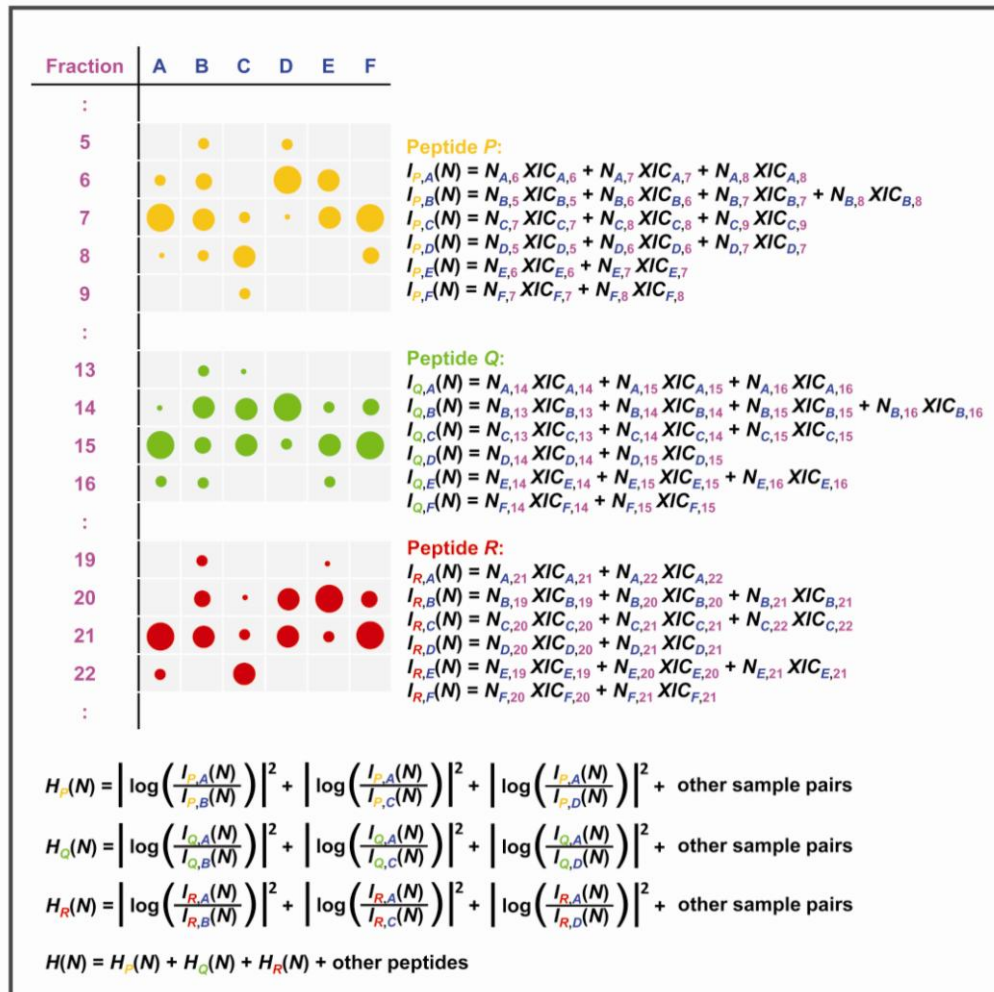

Figure 3-1 Schematic construction of the function H(N) to be minimized in order to determine the normalization coefficients for each LC-MS/MS run. Intensity distributions of three peptides (orange, green and red) over samples and fractions are indicated by the sizes of the circles. H(N) is the sum of the squared logarithmic changes in all samples (A,B, C...) for all peptides (P, Q, R..)

We minimize $H(N)$ numerically with respect to the normalization coefficients N_j by Levenberg-Marquardt optimization (Press et al., 2007) in order to achieve the least possible amount of differential regulation for the bulk of the proteins. This procedure is compatible with any kind of pre-fractionation and also insensitive towards irreproducibility in processing.

3.3.3   Extraction of maximum peptide ratio information

Another principal problem in label-free quantification is the selection of the peptide signals that should contribute to the optimal determination of the protein signal across the samples. A simple solution to this problem is to add up all peptide signals for each protein and then compare protein ratios. However, this solution discards the individual peptide ratios and thus does not extract the maximum possible quantification information. Additionally, it is inaccurate for large ratios because it aggregates the effects of increased peptide ratios and increased peptide numbers, overestimating the change in protein quantity. Instead, ratios deriving from individual peptide signals should be averaged rather than summed up because the XIC ratios for each peptide are already a measurement of the protein ratio.

If all peptides identifying a protein are detected in each of the samples, then protein ratio determination is trivial. However, in practice peptides are often missing in specific samples. One way to nevertheless obtain a signal for each peptide in every sample is to integrate the missing peptide intensities over the mass retention time plane using the integration boundaries from the samples where the peptide has been identified. This procedure has the disadvantage that the noise level effectively substitutes for the signal, underestimating the true ratio (likewise setting these signals to zero will overestimate the ratio). Yet another possibility is to restrict quantification to peptides that have a signal in all samples. While this works well when comparing two samples, it becomes impractical when the number of samples is large: for example requiring a peptide signal to be present in all of 100 patient samples would likely eliminate nearly all peptides from quantification.

We propose a novel method for protein quantification that does not suffer from the problems described above (Figure 3-2). We want to use only common peptides for pair-wise ratio determination without losing scalability for large number of samples. This is achieved for each protein by first calculating its ratio between any two samples using only peptide species (Figure 3-2A, B) which are present in both. Then the pair-wise protein ratio is calculated as follows, taking the pariwise ratio of the protein in sample B and C in the figure as an example: First the intensities of peptides occurring in both samples are employed to calculated peptide ratios. In this case peptide species P2, P3 and P6 are shared (Figure 3-2C). The pairwise protein ratio $\mathbf{r_{CB}}$ (Fig. 2 d) is then defined as the median of the peptide ratios to protect against outliers. We then proceed to determine all pairwise protein ratios; these values grow quadratically with the number of samples. For a valid protein ratio we require a minimal number of peptide ratios. At least two peptide ratios were required in the example in Figure 3-2D.

At this point we have constructed a triangular matrix containing all the pairwise protein ratios between any two samples, which is the maximal possible quantification information. This matrix corresponds to an over-determined system of equations for the underlying protein abundance profile (I_A, I_B, I_C …) across the samples (Figure 3-2E). We perform a least-squares regression analysis to reconstruct the abundance profile optimally satisfying the individual protein ratios in the matrix (Figure 3-2E, F). Finally, this procedure is repeated for all proteins, resulting in an accurate relative abundance estimate for each protein in each sample.
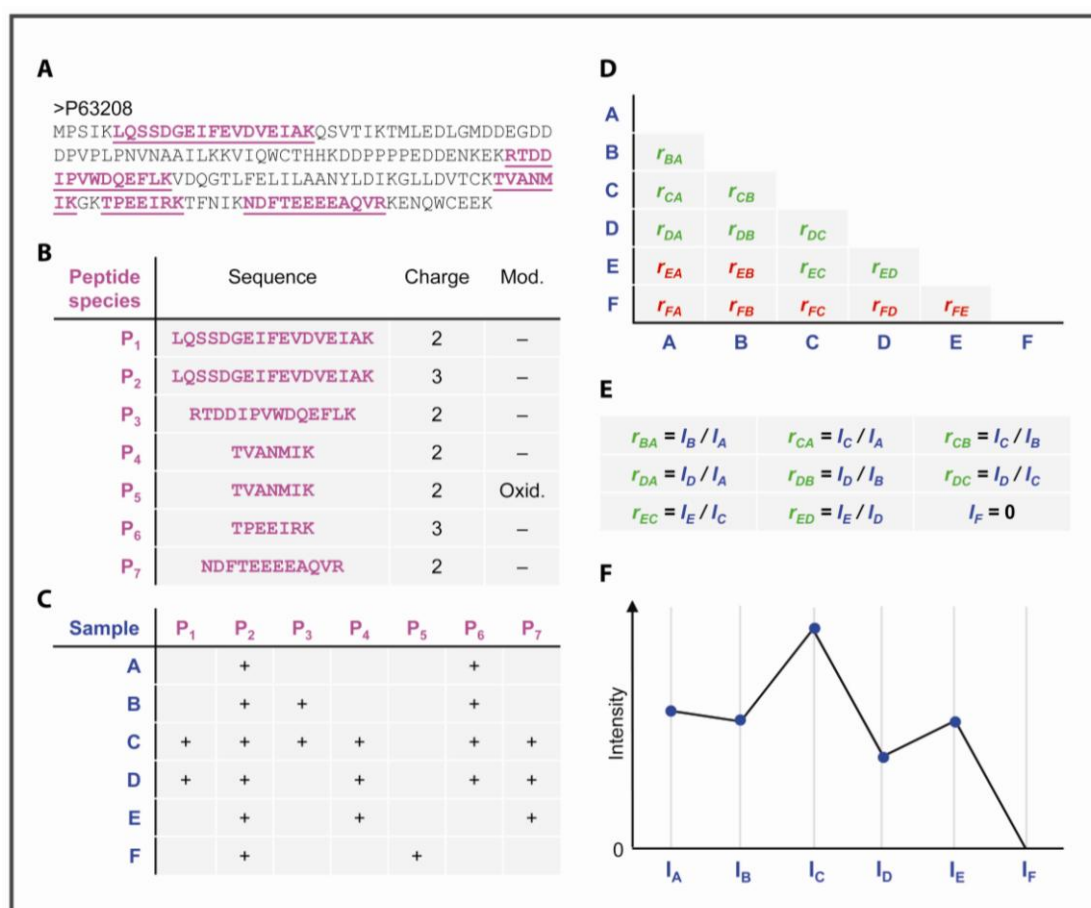
Figure 3-2 Algorithm constructing protein intensity profiles for one protein from its peptide signals. (A) An exemplary protein sequence. Peptides with an XIC-based quantification are indicated in magenta. (B) The five peptide sequences give rise to seven peptide species. For this purpose, a peptide species is a distinct combination of peptide sequence, modification state and charge, each of which has its own occurrence pattern over the different samples (C) Occurrence matrix of peptide species in the six samples. (D) Matrix of pairwise sample protein ratios calculated from the peptide XIC ratios. Valid/invalid ratios are colored in green/red. If a sample has no valid ratio with any other sample – like sample F – the intensity will be set to zero. (E) System of equations that needs to be solved for the protein abundance profile. (F) The resulting protein abundance profile for one protein

3.3.4   Quantification results for the benchmark set

To apply the algorithms to the *E.coli* and HeLa cell mixture, we required a protein to have non-zero intensity in at least three out of the six samples, which is the case for 5,326 proteins in total; 3,701 of human and 1,661 of *E.coli* origin (Figure 3-3A). Ratios are plotted

in Figure 3-3B against the summed peptide intensity, which is a good proxy for the protein abundance (de Godoy et al., 2008a). The human and *E.coli* protein populations are well separated, having very little overlap even at low signal intensity. For highly abundant proteins a fold change far below two can be distinguished from the cloud of 1:1 proteins. Proteins with quantitative changes are separated from non-changing proteins in 94.4 % of the cases (Figure 3-3C), and the remaining proteins are almost never statistically significant by t-test (see below). This result also indicates the robustness of our workflow because one of the 144 LC MS/MS runs failed, but this did not erroneously appear as a regulation of part of the proteome.

A	human	E. coli	all
XICs identified by MS/MS	501,306	340,481	841,787
XICs after MBR*	1,013,696	688,828	1,702,524
Identified peptide sequences	33,996	15,124	49,120
identified proteins (1% FDR)	4,793	1,888	6,681
quantified proteins (≥ 3 nonzero intensities)	3,701	1,661	5,362
- ratio = 0	127	1	128
- ratio = ∞	4	7	11
- 0 < ratio < ∞	3,570	1,653	5,223

*MBR = matching between runs
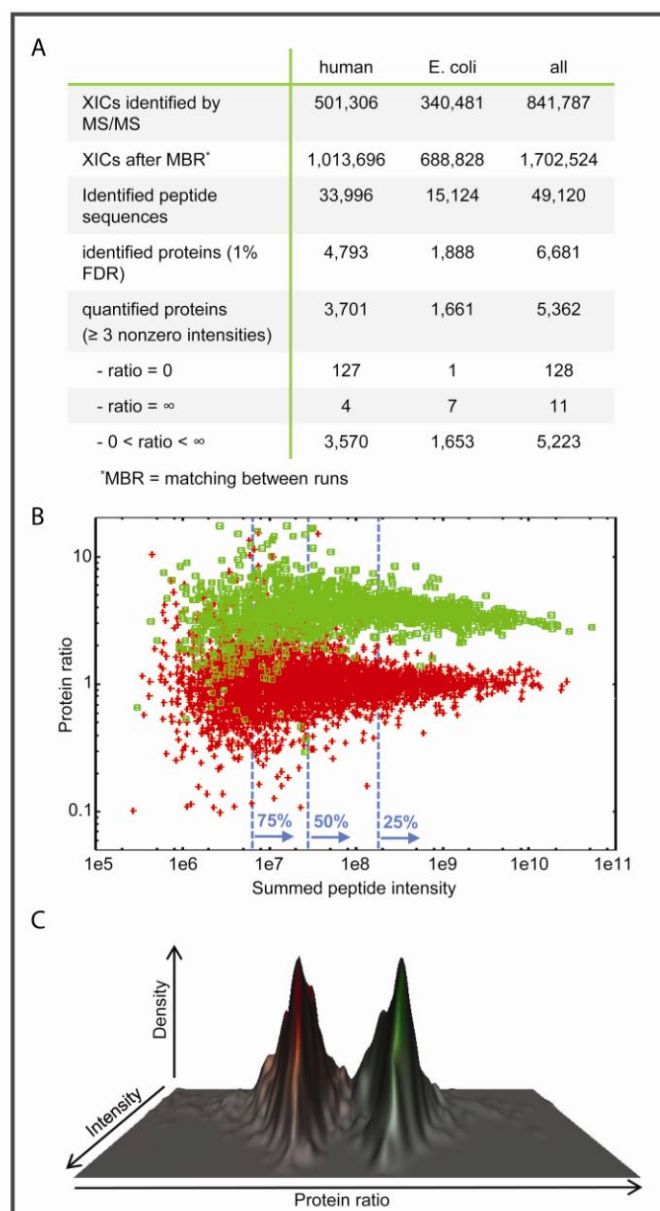
Figure 3-3 Quantification results on the benchmark dataset. (A) Overview of identified and quantified proteins and peptides. (B) Logarithmic plot of protein ratio vs. summed peptide intensity for human (red) and E.coli (green) proteins. The vertical lines indicate the quartiles of the intensity distribution. (C) Three dimensional kernel density visualizing almost complete separation of quantified proteomes. For this comparison, the E.coli distribution (green) was scaled to the HeLa population (red)

How accurate are the label-free protein ratios? To answer this question we divided the intensity distribution into quantiles and determined the 3-σ width of the human proteins in each of them. In the top 25% distribution quantification was accurate within 1.64 fold, in the top 50% intensities 2.01 fold changes could be distinguished with statistical confidence whereas this value was 2.16 for the top 75%. As expected, quantification was less accurate for the low abundance proteins and in the lowest abundance quarter of the proteome the three fold change of the proteomes was marginally sufficient to clearly separate the distributions (3σ fold change = 3.27).

The above analysis on a population level does not provide a statistically sound estimate of the probability that individual proteins are regulated. In fact, Figure 3-3B shows several human proteins that appear to be changing several fold and without further analysis these might have been mistaken as biomarkers in a clinical context. We therefore explored different strategies to retrieve significantly changing proteins based either on simple fold change or on the variance of their quantitative signal: taking the ones with highest apparent fold change (highest ratio of average intensities), with best Wilcoxon-Mann-Whitney p-value, with best standard t-test p-value, and finally with best Welch modified t-test p value. Since we have full knowledge about which proteins are changing (only the *E.coli* ones) we independently know the real false discovery rates and can construct precision-recall curves for each case to assess the performance of our entire quantitative workflow. In Figure 3-4A the resulting four precision-recall curves are shown. Retrieving proteins by ratio (corresponding to a fixed fold change cut-off) is the worst strategy. It has low precision even at small recall values, due to the sensitivity to outlier ratios. When sorting proteins by ratios already the fourth protein is a false positive (Figure 3-4B**)**.
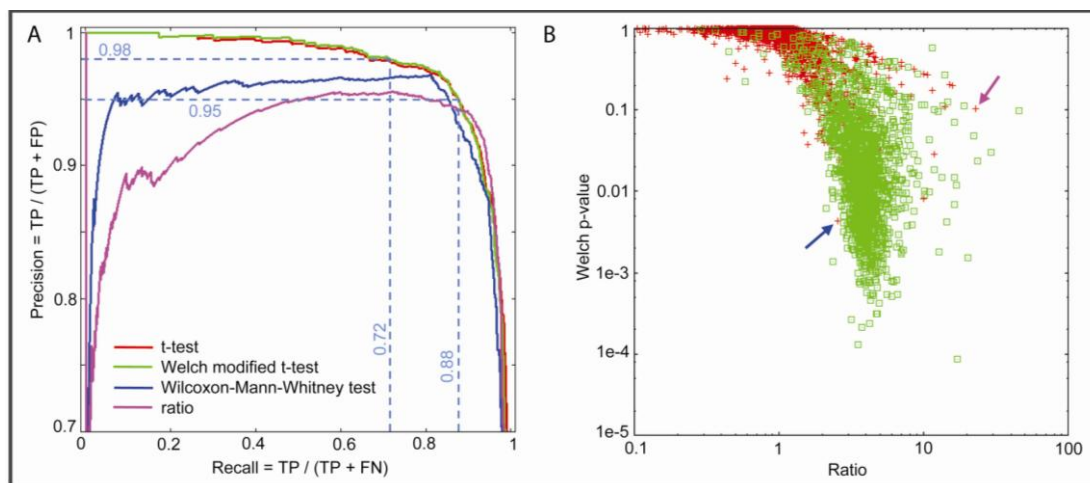
Figure 3-4 Statistical significance of protein regulation. (A) Precision-recall curves based on four different strategies. TP true positives; FP false positives; FN false negatives. (B) The Welch modified t-test p value is plotted logarithmically against the ratio. The vast majority of E.coli proteins (green) have p-values better than 0.05 indicating significant regulation. An extremely small number of human proteins (red) appear to have a large ratio and significant p-value (false positives for quantitation). The arrows indicate that the best strategy is to select significantly regulated proteins by t-test p-value (first false positive after hundreds of correct hits with better p-values; blue arrow) rather than fold change (first false positive after three correct hits with higher fold change; magenta arrow)

The Wilcoxon-Mann-Whitney test performs better but has also problems at low recall. Both versions of the t-test perform significantly better and the Welch modified t-test is slightly better than the standard t-test. At a precision of 0.98 – i.e. 2% false discovery rate (FDR) – 72% of the *E.coli* proteins are recalled. With a FDR of 5% which is often used in similar circumstances almost all (88%) *E.coli* proteins are retrieved with the (Welch modified) t-test.

Finally, we compared the quantification accuracy of our label-free workflow with the SILAC-based procedure normally used in our laboratory. Since we cannot perform a direct SILAC comparison of two entirely different proteomes such as *E.coli* and human, we selected a HeLa SILAC data set also obtained from triplicate analysis of 24 isoelectric focusing fractions. We compared the ratio distributions of the SILAC experiment against the HeLa proteins from this experiment (Figure 3-5). While the quantification accuracy is quite high throughout the proteome for label-free quantification as already described above, the accuracy of the SILAC-based quantification in an experiment of comparable scale and proteome depth the accuracy is considerably higher, by a factor of 4-5 on average. This was expected since label-based quantification allows direct quantitative determination of the peptide ratio within each spectrum and should therefore lead to the best possible accuracy.
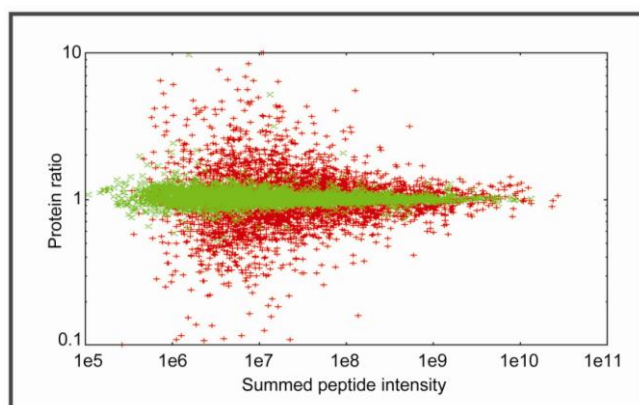
Figure 3-5 Comparison of ratio precision between label free and SILAC data. The points corresponding to human proteins are copied from Figure 3-3B (red). SILAC data (green) is from a comparable dataset on HeLa cells

3.3.5 Label-free expression proteomics of mouse liver

In order to test the performance of our label-free workflow in a typical gene expression context, we dissected the livers from a litter of six genetically identical male mice. In three replicate LC MS/MS runs we identified 2,515 non-redundant proteins at 1% FDR and quantified 1,866 with nonzero intensity in at least three of the 18 samples. Principal component analysis on the full data matrix reveals that in the first two principal components – which together capture 89.9% of the total variance – the difference within technical replicate groups is much smaller than the difference between individual mice (Figure 3-6A). Hierarchical clustering of the entire expression matrix also results in a perfect grouping of technical replicates. ANOVA reveals that more than one third (637) of the proteins show statistically significant inter-mouse variation compared to technical intra-mouse variability.

The two-dimensionally clustered expression matrix of those proteins reveals a grouping into three pairs of similar mice (Figure 3-6B). Their averaged expression profiles were clustered showing the biological processes that are distinguishable between the mice (Figure 3-6C). These turn out to only be metabolic functions, which is consistent with the fact that the mice were genetically identical and treated identically.
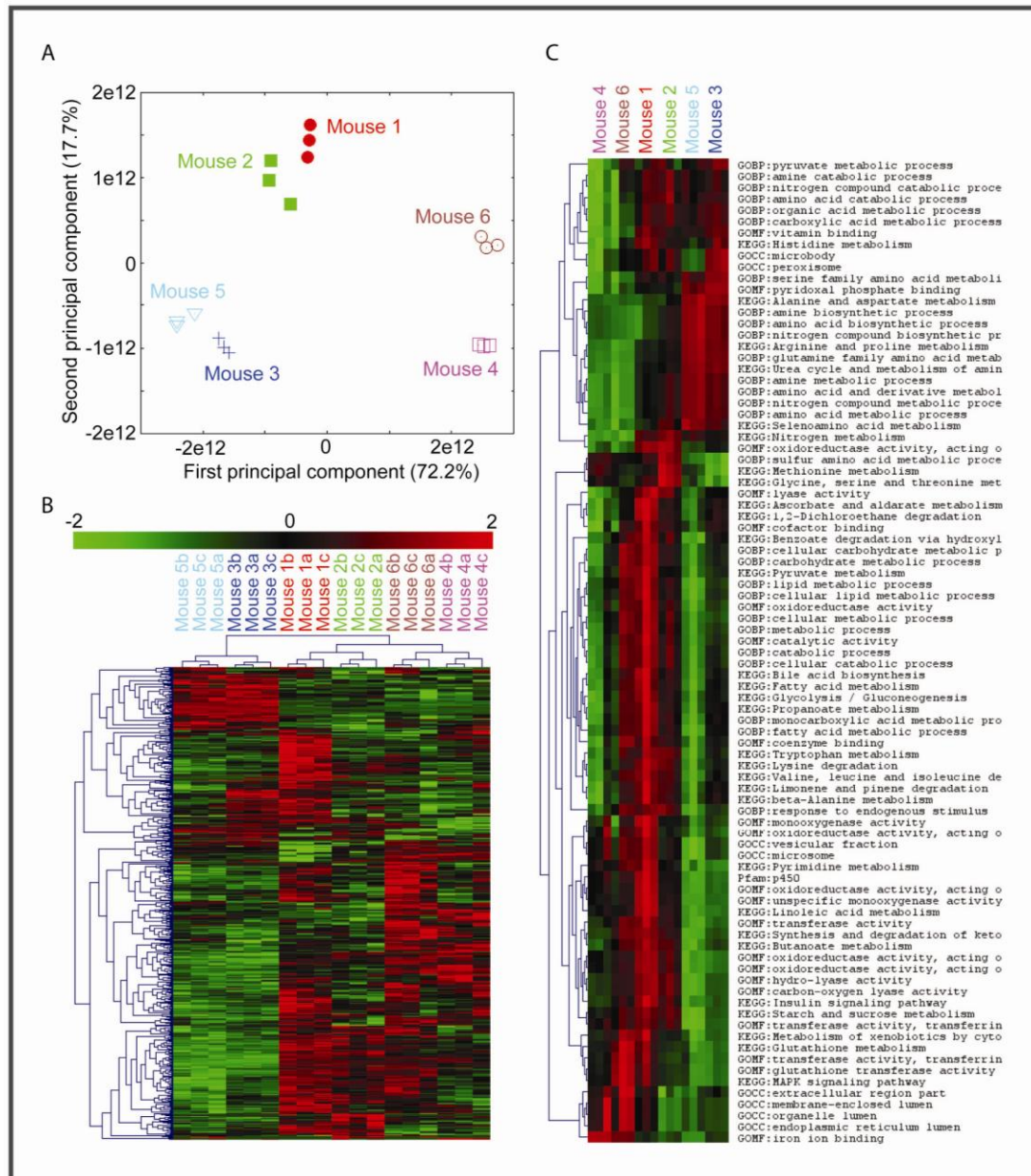
Figure 3-6 Expression proteomics of six mouse liver samples. (A) First two principal components of the mouse liver samples correctly group technical replicates together and different mice apart. (B) Clustered expression matrix of the mouse liver samples on proteins significant in ANOVA likewise correctly clusters the mice. (C) Gene Ontology terms, KEGG pathways and Pfam domains enriched in significant ANOVA proteins together with their clustered averaged expression profiles

3.4   Conclusion and Perspectives

Here we introduced two novel algorithms for quantification without stable isotopes. 'Delayed normalization' efficiently solves the problem of how to compare sample fractions that have been purified in slightly different ways and analyzed with different MS performance. Importantly, delayed normalization does not require selection of arbitrary sets of 'household' genes, which are thought to be unchanging in the experiment. This is in contrast to mRNA measurements, were selection of normalization standards can be a serious experimental design issue. If desired our algorithm can nevertheless be expanded to perform delayed normalization only on selected groups of proteins, i.e. in cases where very wide-spread proteome changes are expected.

The second algorithm allows retrieval of the maximum possible information from peptide ratios across samples, without resorting to arbitrary assignment of the signal when the peptide cannot be detected. The protein ratio is determined as the best estimate satisfying all the pair-wise sample comparisons.

These algorithms performed very well in a mixed proteome experiment, which also allowed us to select the best performing statistical assessment of the significance of protein ratios. Interestingly, for label-free quantification the commonly employed fold change cut-off performs poorly with many proteins appearing to be regulated when they in fact are unchanging. The t-test, in contrast, performed excellently in both precision and recall and should therefore be a suitable tool for biomarker discovery studies.

Among other advantages, our workflow allows label-free comparison of samples measured at separate times. Our laboratory has used this property to measure rare immunological cell populations over the course of more than a year, still leading to accurate quantification as assessed by the correct distribution of cell specific markers and by novel results that turned out to be functionally meaningful (Luber *et al*., submitted).

What will the likely scope of label-free quantification be? As we show here, it is not as accurate as metabolic labeling techniques. However, it should already become the method of choice if isotope labeling is not possible and or if relatively large changes are anticipated. In future, instrumental advances will in effect elevate the majority of the proteome into the accuracy range now typical of the most abundant proteins. In conclusion, we predict an essential role for label-free quantification not only in clinical but also in other areas of proteomics.

4 The SILAC mouse

Abstract

Stable isotope labeling by amino acids in cell culture (SILAC) has become a versatile tool for quantitative, mass spectrometry (MS)-based proteomics. Here we completely label mice with a diet containing either the natural or the $^{13}C_6$-substituted version of lysine. Mice were labeled over four generations with the heavy diet without affecting development, growth or behavior. MS analysis of incorporation levels allowed determining incorporation rates of proteins from blood cells and organs. The F2 generation was completely labeled in all organs tested. SILAC analysis from various organs lacking expression of β1 integrin, β-Parvin or the integrin tail binding protein Kindlin-3 confirmed their absence and disclosed a structural defect of the red blood cell membrane skeleton in Kindlin-3-deficient erythrocytes. The SILAC-mouse approach is a versatile tool to quantitatively compare proteomes from knockout mice and thereby determine protein functions under complex in vivo conditions.

4.1   Introduction

The administration of radioactive or stable isotope tracers to animals is a well established technique to investigate the rate of protein synthesis and protein degradation (Wolfe and Chinkes, 2005). This technology has been used for many decades (Schoenheimer and Rittenberg, 1935). The infusion of stable isotopes (^{13}C or ^{15}N) as tracer combined with measurements of ^{13}CO$_2$ or ^{15}N in urinary urea or ammonia is a broadly used technique to explore the amino acid flux in metabolic pathways (Bier, 1997; Dietz et al., 1982). Extensive incorporation of ^{13}C or ^{15}N stable isotopes does not result in discernable health effects of the treated animals (Doherty and Beynon, 2006; Gregg et al., 1973).

Mass spectrometry (MS) is not inherently quantitative and relative protein expression changes are instead most accurately measured by comparison of the natural form of a peptide with its stable isotope analog (Ong and Mann, 2005). In recent years, ^{15}N labeling has been applied to microorganisms such as yeast (Oda et al., 1999; Pratt et al., 2002), C. elegans and Drosophila (Krijgsveld et al., 2003). Even a rat has been partially (Wu et al., 2004) or completely ^{15}N labeled (McClatchy et al., 2007). In addition, non-saturated labeling of a chicken, using the essential amino acid valine, allows the MS-based analysis of protein turnover rates in vivo (Doherty et al., 2005).

Our laboratory has previously described the stable isotope labeling by amino acids in cell culture (SILAC) (Mann, 2006; Ong et al., 2002), which has unique advantages for quantitative and functional proteomics because of its inherent accuracy of quantitation and the ease of interpretation of MS results (Blagoev et al., 2004; Kratchmarova et al., 2005). In a SILAC experiment two cell populations are generated, one in a medium that contains the natural amino acid (i.e. ^{12}C$_6$-lysine) and the other in a medium that contains the heavy isotope substituted version (i.e. ^{13}C$_6$-lysine). This allows direct comparison of protein expression levels by mixing the non-labeled 'light' and labeled 'heavy' cell populations (Cox and Mann, 2007). Each peptide appears as a pair in MS analysis with a difference in mass of 6 Da and the relative peak intensities reflect the abundance ratios. To date SILAC-labeling has been limited to cell culture or microorganisms. To extent this powerful technique to higher organisms, Oda and co-workers have SILAC labeled the Neuro 2A cell line to serve as internal standard for quantitation of a subset of peptides of the mouse brain proteome (Ishihama et al., 2005b).

In the present paper we report the development of a mouse SILAC diet that leads to complete labeling of the F2 generation. We used in vivo SILAC quantitation to analyze newly synthesized proteins from plasma and tissue samples in vivo. Furthermore, we validated our in vivo quantitation system by comparing the proteomes from platelets, heart and erythrocytes from β1 integrin, β-parvin and Kindlin-3-deficient mice, respectively.

Integrins are heterodimeric transmembrane proteins, consist of α and β subunits, are ubiquitously expressed and perform cell-cell and cell-matrix adhesion functions. Association of the corresponding α and β subunits is required for their stability and transport to the

plasma membrane, as single subunits are not stable and are rapidly degraded. Integrin-mediated cell adhesion triggers intracellular signaling pathways (outside-in signaling) that control migration, proliferation, survival and differentiation of cells. Prior to ligand binding integrins require an energy-dependent activation step, which is triggered within the cell (inside-out signaling) and characterized by a profound conformational change in both integrin subunits. Although the mechanism(s) underlying integrin activation are far from understood it is believed that the binding of the FERM domain-containing adaptor proteins, talin and Kindlin to the integrin β cytoplasmic domains represents the last step in the activation pathway (Calderwood, 2004; Moser et al., 2008)

Upon activation and ligand binding integrins recruit and assemble a multiprotein complex at the site of cell adhesion that fulfils two major tasks: it connects the ECM with the actin cytoskeleton and it alters the fluxes of many intracellular signalling pathways. A preformed complex consisting of the three proteins, ILK, PINCH and Parvin, represents an important component of the integrin adhesion complex (Legate et al., 2006). Parvins are a family of three proteins, α-, β- and γ-parvin, that directly bind to ILK, F-actin and other actin associated proteins thereby linking the adhesion complex to the actin cytoskeleton and controlling actin dynamics.

Kindlins have recently been identified within the integrin mediated cell adhesion complex and represent a further family of ILK binding proteins (Montanez et al., 2007). They consist of three members (Kindlin1-3) and are named after the gene mutated in Kindler syndrome, an autosomal recessive skin blister disease in humans. Kindlin-3 expression is restricted to hematopoietic cells with highest levels in megakaryocytes (Ussar et al., 2006). Inactivation of the Kindlin-3 gene in mice results in severe anaemia, which is thought to be due to a bleeding defect caused by impaired activation of platelet integrins, defects in platelet aggregation and thrombus formation (Moser et al., 2008).

To screen for potential defects in other cellular compartments of the hematopoietic system in Kindlin-3-defcient mice we compared their proteome with those from control mice. In the course of these studies, we discovered a deficit of structural proteins in the plasma membrane of Kindlin-3-deficient erythrocytes, which contributes to the severe anaemia seen in Kindlin-3-deficient mice.

4.2   Experimental Procedures

4.2.1   Materials and reagents

$^{13}C_6$-Lysine (98 atom % ^{13}C) was from Silantes, Martinsried, Germany. Chemicals for the 'in solution' and 'in gel' digests were purchased from Sigma-Aldrich, LysC was obtained from WAKO. Wild-type mice were obtained from an in house C57Bl/6 colony.

4.2.2   Knockout mice

Transgenic mice expressing the Cre recombinase under the control of the Mx1 promotor
(Kuhn et al., 1995) were mated with mice carrying a floxed β1 integrin gene (Brakebusch et
al., 2000). To ensure extensive down regulation of the β1 integrin on platelets pI:pC
(Amersham) injected intraperitoneally 3 times in a 2-day interval with a concentration of
250µg pI:pC per mouse.

Kindlin-3 deficient mice were generated as described in (Moser et al., 2008). A detailed
description of the β-parvin gene inactivation will be published elsewhere (Thievessen and
Fässler).

4.2.3   Food preparation, weight gain, and food consumption

A customized lysine free mouse diet (Harlan-Tekland, TD.99386) was combined with the
heavy L-^{13}C$_6$-lysine and the natural isotope L-lysine (Sigma) to a final concentration of 1%. To
obtain a homogenous distribution of the amino acid, the powder was vigorously mixed with
a blender for 5 min. For the preparation of food pellets, approximately 10g of the mixture
were filled into an in-house manufactured cylinder with an inner diameter of 1.5 cm and
length of 10 cm. Food was compressed with an exactly fitting pestle for 1 min. Pellets were
taken out and dried over night at room temperature. After drying, the pellets were cut into
smaller pieces.

The lysine content was checked as described (Moore et al., 1958). Although the hydrolysis
with subsequent chromatography does not allow exact determination of the amino acid
contents, the supplemented lysine amount was comparable to that in the customized diet
containing the natural lysine isotope.

For testing weight gain and food consumption one group (n= 3 females) was fed with a
regular mouse diet, one group (n=3 females) was fed with the customized lysine free diet
supplemented with natural lysine (Sigma), and one animal with the diet containing the heavy
isotope for lysine. All animals were fed ad libitum with access to water.

Food consumption was measured daily for 10 days during breeding and weaning periods.
Label percentage was calculated as the mean of heavy labeled peptide signal divided by the
sum of light and heavy signal.

4.2.4   Sample preparation

Blood samples; mice were anesthetized with isofluran and 20 µl blood was taken from the
retro-orbitral plexus. Blood samples were incubated with heparin (20 U/ml) and after
centrifugation the supernatant was frozen in liquid nitrogen and stored at -80°C. Tissue
harvest; after sacrificing animals by cervical dislocation, tissues were dissected, washed in
phosphate buffered saline (PBS; pH 7.4), and frozen in liquid nitrogen. For protein isolation,

tissues were homogenized in a buffer containing 1% NP-40, 0.1% sodium deoxycholate, 150 mM NaCl, 1 mM EDTA, 50 mM Tris pH 7.5 and protease inhibitors (Complete tablets, Roche).The lysates were centrifuged at 14,000 x g to pellet cellular debris. A Bradford assay was performed to determine protein concentrations of the supernatants.

Mitochondria isolation; liver tissue was quickly washed in water, then three times in 250 mM sucrose, 10 mM Tris-HCl, 0.1 mM EGTA (pH 7.4) supplemented with protease inhibitors (Roche). Crude mitochondria were isolated as described previously (Forner et al., 2006) and purified on a 30% Percoll density centrifugation gradient.

Platelets were isolated by differential centrifugations steps as described in (Moebius et al., 2005). Epithelial cell isolation from gut; small intestine was cut open and washed with PBS. The small intestine was transferred to dissociation buffer (130mM NaCl, 10mM EDTA, 10mM Hepes pH 7.4, 10% FCS and 1mM DTT) and incubated for 45 minutes on a rotor at 37°C. The rest of the intestine was removed and the epithelial clumps were collected by centrifugation at 800 rpm for 5' and PBS washed.

For B cell isolation spleen was cut into small fragments and digested with collagenase and DNase followed by the addition of EDTA. Subsequently, cells were incubated with anti-CD45R, anti-CD3, and anti-CD49b (BD PharMingen). B cells were selected as cells that stained positive for CD45R (B220, (Coffman, 1982)) and negative for both anti-CD3 and anti-CD49b and then sorted using a FACS Aria system (Becton Dickinson).

4.2.5   Mass spectrometry

For protein separation samples were load on a NuPAGE 4%-12% Bis-Tris gel (Invitrogen). After staining of the gel with the Colloidal Blue Staining Kit (Invitrogen) evenly sized gel pieces were excised from the gel and processed for enhanced liquid chromatography-mass spectrometry (GeLC-MS).

For blood analysis, Coomassie stained gel lanes were cut into eight pieces. To determine incorporation ratios we analyzed three gel pieces per lane from heart, gut epithelia, liver, red blood, and platelets samples

The gel pieces were subjected to in gel reduction and alkylation, followed by LysC digestion as previously described (Andersen et al., 2005; Shevchenko et al., 1996). Finally, peptides were extracted twice by adding an equal volume of 30% acetonitrile/0.3% trifluoraceticacid (TFA) in water to digest the mixture followed by a final extraction with 100% acetonitrile. Extracts were evaporated in a speedvac to remove acetonitrile and subsequently acidified with 0.5% TFA. Samples were desalted and concentrated with StageTips and resuspended in 5 µl of 0.5% acetic acid/ 1% TFA (Rappsilber et al., 2003). In solution digestion of proteins were performed as described in (Ong and Mann, 2006).

Reverse phase nano-LC-MS/MS was done using an Agilent 1100/1200 nanoflow LC system (Agilent technologies) using a cooled thermostated 96-well autosampler. The LC system was coupled to a 7-Tesla LTQ-FT or LTQ Orbitrap instrument (Thermo Fisher Scientific) equipped with a nanoeletrospray source (Proxeon). Chromatographic separation of peptides was performed in a 10 cm long 8 μm tip opening/75 μm inner diameter capillary needle (Proxeon). The column was custom-made with methanol slurry of reverse-phase ReproSil-Pur C18-AQ 3-μm resin (Dr. Maisch GmbH). The LysC digested peptide mixtures were autosampled at a flowrate of 0.5 μl /min and then eluted with a linear gradient at a flow rate 0.25 μl / min. The mass spectrometers were operated in the data-dependent mode to automatically measure MS and MS/MS. LTQ-FT full scan MS spectra (from m/z 300 to 1,600) were acquired with a resolution R = 100,000 at m/z 400 (after accumulation to a target value of 3,000,000 in the linear ion trap). The five most intense ions were sequentially isolated and fragmented in the linear ion trap using collisionally induced dissociation at a target value of 10,000 (Olsen et al., 2004).

Raw data files were converted to Mascot generic format files with in house software (Raw2MSM) and Mascot (version 2.0) was used for database search and protein identification. The following search parameters were used in all MASCOT searches: LysC digest, no missed cleavage, carbamidomethylation of cysteine was set as a fixed modification and oxidation of methionines, and L-lysine-6 were allowed as variable modifications. The maximum allowed mass deviation for MS scans was 10 ppm and 0.5 Da for MS/MS scans, respectively. Only proteins that had at least two peptides with ion scores >20 were considered for identification and quantitation. MSQuant (Schulze and Mann, 2004) was used to verify and quantify the resulting SILAC-peptide pairs. All proteomic results were deposited in the publicly accessible MAPU database (Zhang et al., 2007). A target decoy database approach was used to identify false positive peptides and to set threshold criteria such that < 1% false positives were included in the peptide list. After mass recalibration using MSQuant, the average absolute mass error of all peptides was better than three ppm.

Samples from all mouse mutants were analyzed by the in house developed software MaxQuant (Cox and Mann, 2007; Graumann et al., 2007). Briefly, MaxQuant performs a peak list, SILAC- and XIC-based quantitation, false positive rates (Gingras et al., 2007), and peptide identification based on Mascot search results. All data were searched against the Mouse International Protein Index protein sequence database (IPI, version 3.24) (Kersey et al., 2004). Fold-change for ghost proteins was determined from the gel slice corresponding to the expected migration of the full length protein.

4.2.6   Blood cell analyses

Hematocrit was measured from peripheral blood with a hematology analyzer (Nihon Kohden).For "ghost" preparation, erythrocytes were washed twice in 0.9% NaCl, 10mM sodium phosphate buffer, pH7.0 before hypotonic lysis were performed in 0,25% NaCl,

10mM sodium phosphate buffer, ph7.0. Lysis was performed in several rounds in hypotonic buffer until the pellet became white.

4.2.7   Flow cytometry

Flow cytometric lacZ staining of hematopoietic cells were performed on Ter119 positive bone marrow cells that have been incubated with the fluorescent β-galactosidase substrate FDG (fluorescein di-β-D-galactopyranoside) (Sigma) as described (Montanez et al., 2007). Flow cytometry was carried out on a Becton Dickinson FACSCalibur.

4.3   Results

4.3.1   Heavy SILAC-diet has no influence on weight gain and fertility

We prepared a SILAC diet by mixing $^{13}C_6$-lysine or $^{12}C_6$-lysine into a customized lysine-free mouse diet to a final concentration of 1% (Figure 4-1A) according to standard mouse nutritional requirements (Benevenga et al., 1995). The amino acid content was subsequently checked by hydrolysis and cation exchange chromatography (Figure S1 online). We first tested whether the diet permits normal weight gain by feeding mice with a regular or the SILAC diet (with $^{12}C_6$-lysine or $^{13}C_6$-lysine). During an observation period of four weeks all animals showed the same food consumption and a similar increase in body weight of about 17% (Figure S2A,B online), normal fertility and motor activity irrespective of the diet consumed. Furthermore, we SILAC-labeled mice over four generations (see below), indicating that the labeling is compatible with normal development and physiology. Thus we conclude that SILAC-labeling with a $^{13}C_6$-substituted essential amino acid does not lead to obvious discernable health effects in mice (Figure 4-1B).

4.3.2   SILAC incorporation rates differ in blood, liver and gut epithelium

To track $^{13}C_6$-lysine incorporation into the proteome over time, we sampled blood each week for four weeks. Serum proteins were separated on 1D gels in triplicate, in-gel digested and analyzed by high resolution MS. The average relative standard deviation of all quantified proteins was about 20% (Figure 4-1C), an accuracy similar to previous SILAC quantitation experiments (Blagoev et al., 2004; Ong et al., 2003).

As an example of different incorporation levels, SILAC peptide pairs of three serum proteins and one red blood cell protein are shown in Figure 4-1C. For serum albumin we observed a SILAC-ratio of 1:3.2 indicating that at least 74% of the protein had been newly synthesized during the first week of feeding. Because proteins can be synthesized from dietary amino acids as well as from amino acids derived by protein catabolism, this value is a lower limit for the true turnover (Beynon and Pratt, 2005). After four weeks the three serum proteins were

labeled to 90%. In contrast, hemoglobin was only labeled to 57% after four weeks (Figure 4-1C), due to the 60 days half-life of mouse erythrocytes (Berlin et al., 1959).
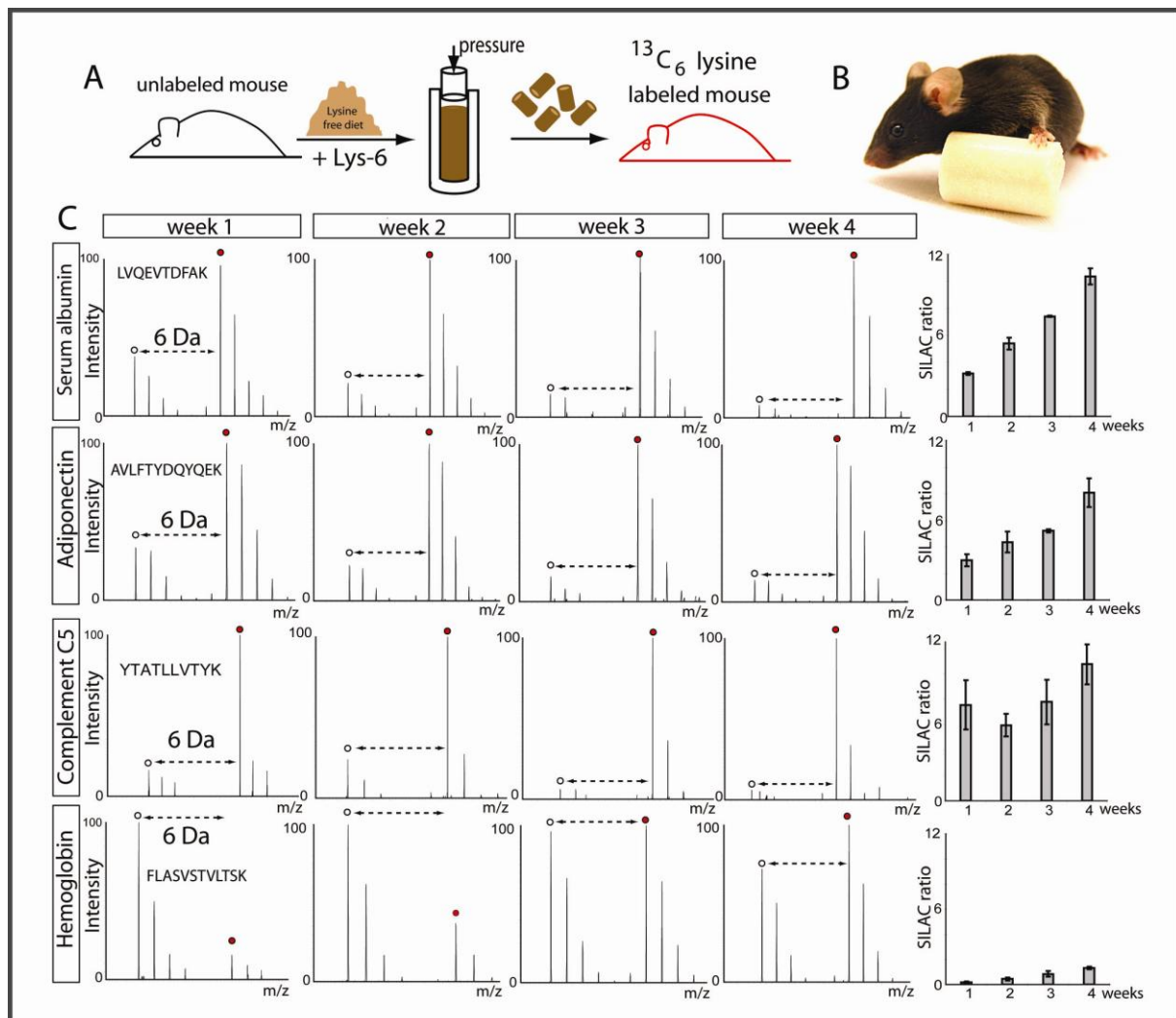
Figure 4-1 SILAC labeling and incorporation rates of blood proteins. (A) Mice are SILAC labeled by feeding a pelleted lysine-free diet supplemented with normal or heavy lysine. (B) Mice on a SILAC diet cannot be visually distinguished from mice with anormal, commercial diet. (C) Mass spectra showing SILAC pairs of a representative peptide for four blood proteins. The right hand side shows lysine-6 incorporation over four weeks as average measurement of triplicates

Next, we measured the labeling efficiencies of a number of organs after four weeks of feeding with the SILAC diet. Proteins from heart showed an average protein ratio of 4.4 (Figure 4-2A, Table S2 online), much lower than the serum proteins. Furthermore, the distribution of SILAC-ratios was relatively broad, reflecting the different incorporation rates of individual cell types and the 'contamination' of serum proteins in non-perfused samples. For example, serum albumin has a similarly high incorporation rate in blood (ratio 9) and heart (ratio 10; Figure 4-1C and Figure 4-2A). In contrast to heart tissue, in which most cells are quiescent, the intestinal epithelium regenerates within a few days (Radtke and Clevers, 2005). Disaggregating the epithelium from the digestive tube resulted in a more homogeneous cell pool consisting of only a few cell types. As a consequence we observed a

high SILAC-ratio of 9.1+/- 2.1 reflecting a labeling efficiency of more than 90 % (Figure 4-2B), which is fully consistent with the high proliferation rate of this tissue. For example, villin-1, a marker for epithelial cells from the digestive system, showed a SILAC ratio of 10.
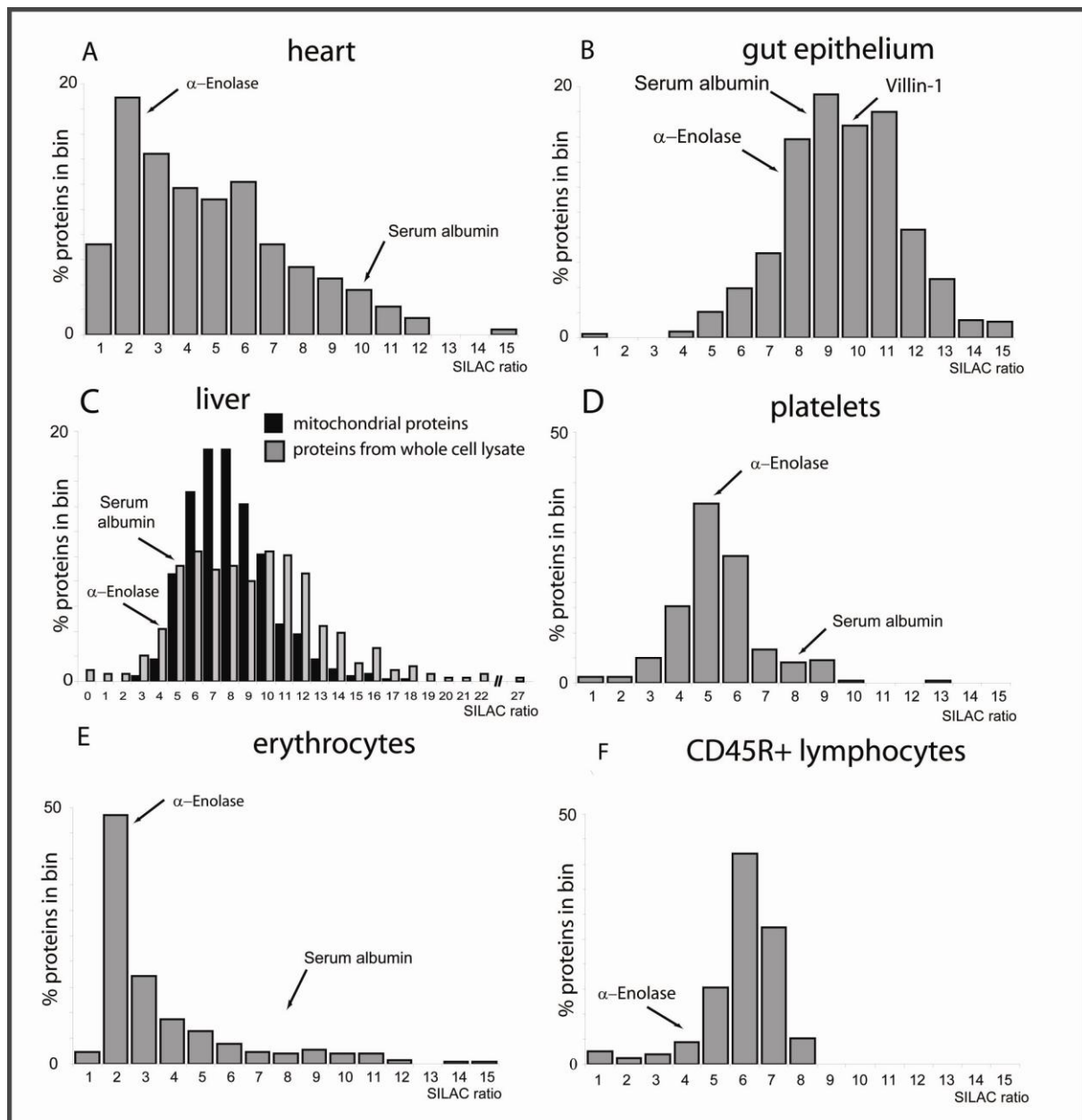
Figure 4-2 SILAC label incorporation into different cell types and tissues after 4 weeks. The panels show the relative number of proteins with the specified ratios for each proteome investigated. (A) heart tissue, (B) gut epithelium, (C) incorporation into whole liver (grey bars) is compared with incorporation into liver mitochondria (black bars), (D) platelets, (E) erythrocytes, (F) CD45R-positive B-lymphocytes from spleen

Liver has a number of different physiological roles, including metabolic functions and the production of major blood proteins. Accordingly we observed a wide distribution of SILAC incorporation ratios among liver proteins. Hepatocytes are the predominant liver cell type, and they are very rich in mitochondria. To demonstrate that in vivo SILAC ratios can be measured with subcellular resolution we isolated mitochondria from liver cells (Forner et al., 2006) and compared their labeling ratios to whole cell lysates from the same sample (Figure

4-2C, black bars). Interestingly, proteins from mitochondria showed an average SILAC-ratio of 8.6+/-2.4. This shows that the incorporation rates of an organelle are more narrowly distributed and distinguishable from that of a whole tissue.

We next investigated several cell types of the hematopoietic system. Platelets are cell fragments which are constantly released by megakaryocytes into the blood stream. They have a half live of approximately 7-9 days. We isolated platelets from a SILAC mouse after four weeks of labeling and measured incorporation levels of 86% from 241 quantified proteins (Figure 4-2D). In contrast, serum albumin, which was also measured within the platelet sample due to serum contamination, has a much higher incorporation level compared to platelet proteins. Analysis of the red blood cell proteome revealed a significantly lower $^{13}C_6$-lysine incorporation of 75% (Figure 4-2E). Thus, consideration of SILAC incorporation rates could aid in determining the origin of the same proteins from different cellular pools via their different dynamic incorporation rates.

To combine SILAC-mouse analysis with cell sorting to obtain an accurately defined cell population, we separated CD45R-positive B-lymphocytes from spleen by FACS (Figure 4-2F, Figure S3 online). An in solution protein digest was performed from lysates of $1x10^6$ spleen cells (Table S2F online). The distribution of measured ratios was 5.4+/-1.3 demonstrating that FACS-sorted populations of interest can readily be investigated in the SILAC-mouse.

Taken together, our results indicate that feeding mice with a SILAC diet is a suitable approach to label proteins in vivo and to follow their metabolic incorporation in any organ.

4.3.3   Complete SILAC-based labeling of F2 mice

Although the label efficiency was relatively high in many tissues, we found that extending the labeling time did not lead to complete labeling. This is likely due to the recycling of internal amino acid sources (Doherty et al., 2005).
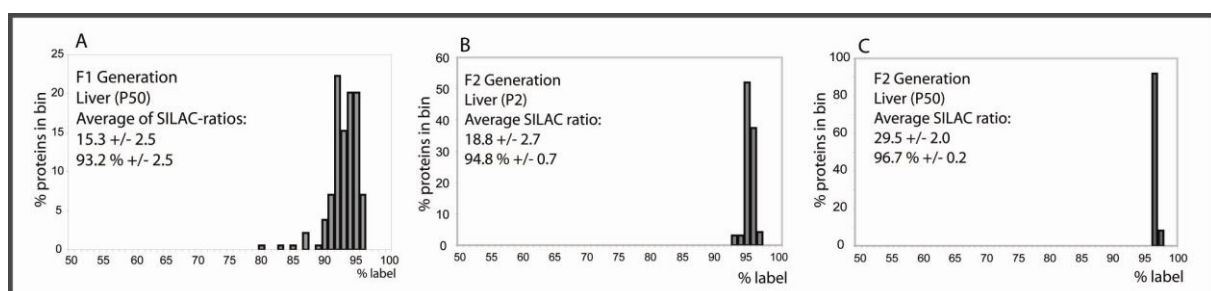
Figure 4-3 Complete labeling of the F2 generation. (A) Label efficiency of the liver of a two days old mouse of the F1 generation. (B) Histograms of liver proteins with the specified percent incorporation at P2 and (C) at P50 of the F2 generation. The averages of the SILAC ratios and the corresponding percent of the SILAC labeling are displayed in the histogram. The analysis encompasses about 100 proteins

Since labeling rates above 95% are required to perform comparative and quantitative proteomics by MS we started feeding our mice over several generations with the heavy diet.

Importantly, the consumption of the heavy diet did not affect litter size. The F1 to F4 offspring developed normally, gained weight within the normal weight gain chart and showed normal mating behavior. Furthermore, newborn animals of the F1 generation were almost completely labeled and reached about 93 % in blood, brain and liver (Figure 4-3 and Figure S4 online). To obtain fully labeled animals to serve as internal standards and to investigate if SILAC-labeling could be performed for many generations, we bred F2, F3 and F4 mice. These mice contained virtually no unlabeled peptides (Figure 4-3B,C, Figure 5A, Table S3 online).

4.3.4   Proteome of β1 integrin-deficient platelets

For validation of our in vivo quantitative proteomics approach we analyzed and compared protein lysates from β1 integrin deficient and control platelets (Nieswandt et al., 2001). We generated β1 integrin-deficient platelets by intercrossing β1 floxed mice ($\beta1^{fl/fl}$) with a transgenic mouse expressing an Mx1 promoter-driven, interferon inducible Cre (Mx1-Cre) (Brakebusch et al., 2000; Kuhn et al., 1995). We treated ($\beta1^{fl/fl}$; Mx1-Cre) mice with synthetic double-stranded RNA (polyinosinic-polycytidylic acid, pI:pC) which triggers endogenous interferon production and subsequent Mx1-Cre activity. This leads to deletion of the β1 integrin gene in all hematopoietic cells including megakaryocytes. To monitor the knockout efficiency of β1 integrin, we compared platelets from labeled wild-type animals with platelet populations from three groups of mice: (i) non-labeled wild-type platelets, (ii) platelets from non-labeled, non pI-pC-induced $\beta1^{fl/fl}$; Mx1-Cre mice, and (iii) platelets from non-labeled, pI-pC-induced $\beta1^{fl/fl}$; Mx1-Cre mice (Figure 4-4). All mice were backcrossed on a C57BL/6 background to reduce genetic variability.

We quantified about 645 proteins in these platelets and as expected, protein ratios of labeled and non-labeled wild-type platelets were tightly distributed with an overall ratio of 1:1. The quantitative MS analysis revealed complete loss of β1 integrin in platelets from pI-pC-induced $\beta1^{fl/fl}$; Mx1-Cre mice (Figure 4-4F). The proteins with the next highest ratios were the dimerization partners of the β1 integrin subunit, strikingly confirming the sensitivity and reliability of our SILAC mouse labeling system (Figure 4-4I). In a boxplot analysis β1, α2 and α6 integrins were all more than ten interquartile ranges away from the median (Table S4 and Figure S5A online).The complete loss of both α subunits can be explained by the formation of a stable integrin heterodimer during the synthesis and transport of the complexed integrin subunits to the plasma membrane. Without the correct β integrin subunit the α subunit is rapidly degraded (Hynes, 2002). In contrast, the loss of β1 integrin has no impact on the expression of other integrins, such as the major platelet integrin αIIbβ3.

In addition, several other proteins in β1 integrin-deficient platelets were outliers in the boxplot (Table S4, Figure S5A online). However, a second independent experiment did not

verify these proteins as significantly downregulated. (Figure S5C). In contrast, the β1 integrin dimerization partners, α2 and α6 integrins were again strongly reduced (Figure S5C).

Interestingly the analysis of platelets from non-induced β1$^{fl/fl}$ Mx1-Cre mice also revealed a slight down regulation of the β1, α2, and α6 integrin levels compared to labeled wild-type platelets (Figure 4-4J). This effect is due to the natural, endogenous α/β interferon production in the bone marrow causing a low Mx1 promoter activity (Kuhn et al., 1995). The detection of this 'leak' impressively underscores the sensitivity of our quantitative proteomics approach.
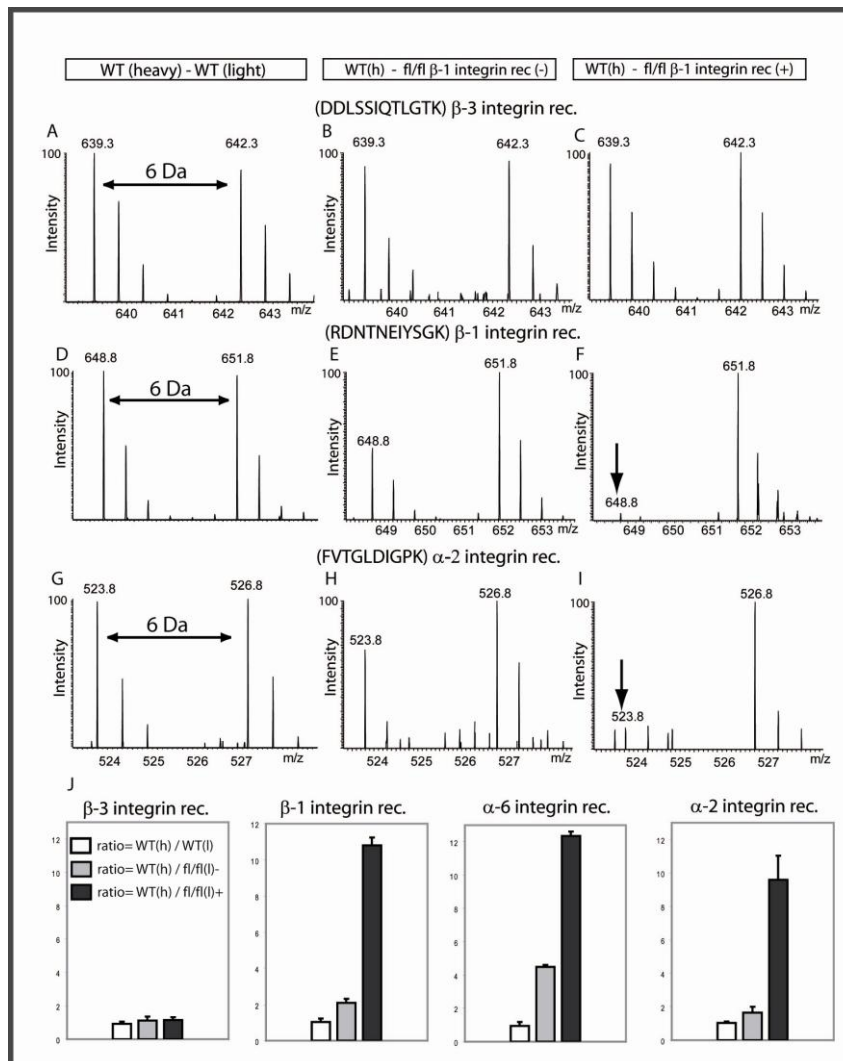
Figure 4-4 Analysis of β1 integrin knockout platelets. (A, D, G) Platelets from SILAC labeled wild-type mice were mixed with platelets from a non-labeled wild-type control mouse. Comparison of the wild-type SILAC mouse with the non-induced, β1fl/fl; Mx1-Cre mice (B, E, H) and with pI-pC induced β1fl/fl; Mx1-Cre (C, F, I). The slight decrease of β1 integrin in E is due to Cre activity induced by low endogenous interferon expression. The arrows in (F) and (I) label the reduced peak intensity of β1 and α2 integrin. (J) Summary of quantified SILAC-ratios for β3, β1, α2 and α6 integrin subunits. White bars represent the ratio between the labeled wild-type wt(heavy) animal and non-labeled wild-type animal, grey bars represents SILAC-ratio of wt(h) and non-induced, β1fl/fl, and black bar shows the SILAC-ratio between wt(h) and induced β1fl/fl; Mx1-Cre. The error bars show the variability of the measured ratios.

4.3.5   β-Parvin deficiency in heart is compensated by α-Parvin induction

We next wanted to confirm the applicability of our in vivo SILAC approach to analyze the proteomes from knockout mice in a solid organ. To this end we compared the proteomes from hearts of β-Parvin deficient mice with control littermates. As a heavy standard we used heart lysates from two weeks old mice of the F4 generation which showed an overall 97.7% incorporation of 13C-lysine (Figure 4-5A). To test our quantitation system we mixed "heavy" and "light" protein lysates from wild-type hearts in ratios of 1:1, 1:2, and 1:4. As shown in (Figure 4-5B), mixing of protein lysates from different heart samples gave rise to SILAC ratios that accurately reflected the lysate mixture.
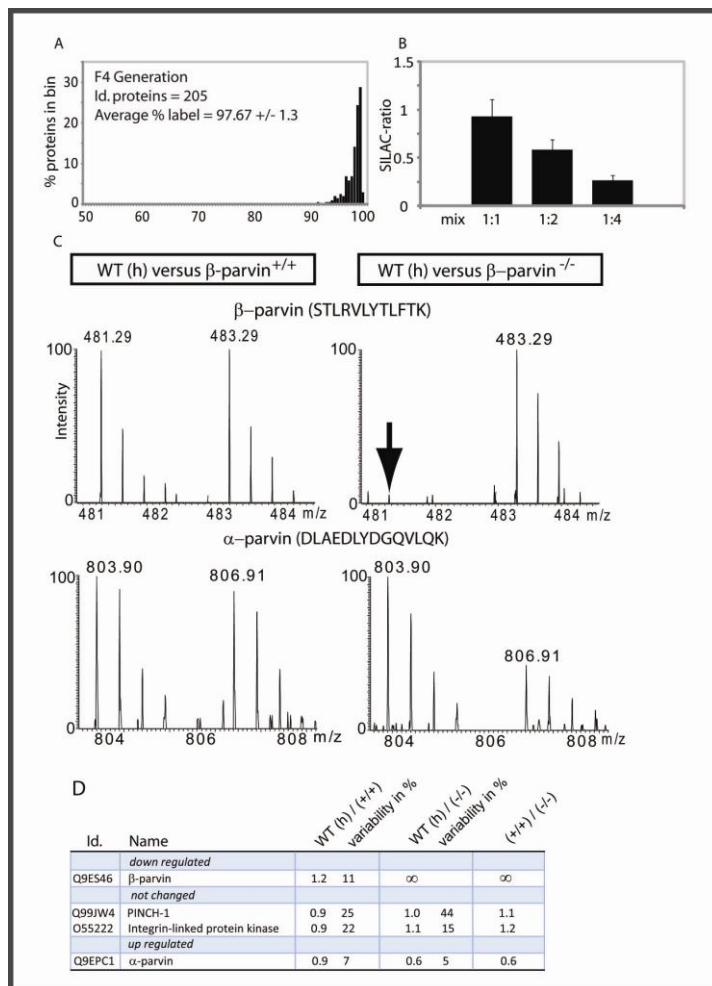
Figure 4-5 Analysis of heart tissue from β-Parvin knockout mice. (A) $^{13}C_6$ lysine incorporation of heart tissue from mice of the F4 generation shows a label efficiency of 97.7% (B) Heart tissue from labeled and non-labeled animals were mixed 1:1, 1:2, and 1:4. The measured SILAC ratios after in solution digestion were: 0.93+/-0.17 for 1:1 mix, 0.58+/-0.10 for 1:2 mix, and 0.26+/-0.05 for 1:4 mix). Approximately 300 SILAC protein ratios were used for the quantification. (C) Heart tissue from SILAC labeled wild-type mice were mixed with non-labeled β-parvin (+/+) and β-parvin (-/-) hearts. Arrow indicates the complete absence β-parvin. (D) SILAC-ratios of selected proteins

β-Parvin represents the dominant Parvin isoform of the heart, since α-Parvin is only weakly present and γ-Parvin is absent from heart. β-Parvin deficient mice were generated by homologous recombination of a targeting vector in embryonic stem (ES) cells, which lacks

exon 2 and 3 of the β-Parvin gene (Thievessen and Fässler, will be described elsewhere). β-Parvin deficient mice were viable, fertile and did not show any overt phenotype indicating that β-Parvin is not essential for mouse development and organ formation. Mass spectrometric measurements of whole protein lysates from β-Parvin deficient and control hearts of 2 weeks old animals showed a complete absence of β-Parvin in knockout animals (Figure 4-5C,D). Out of 1205 proteins only 4 proteins showed two-fold decrease in their abundance compared to wild-type hearts (Table S5 online). Interestingly, lack of β-Parvin had no dramatic consequence on the level of ILK and PINCH-1, which are the two other components of the ILK/Pinch/Parvin complex. The twofold increase of α-Parvin in β-Parvin deficient hearts suggests that the absence of an obvious phenotype is due to compensatory up regulation of α-Parvin (Figure 4-5C).

4.3.6   Kindlin-3 deficiency disrupts the red blood cell membrane skeleton

Kindlin-3-deficient mice die at birth and suffer from severe bleeding, anaemia and pale skin colour (Figure 4-7A,B) (Moser et al., 2008). To further validate the power of in vivo SILAC and to obtain novel insights into Kindlin-3 function, we performed quantitative proteomics of platelets and erythrocytes from Kindlin-3$^{-/-}$ mice.

Platelet analysis identified Kindlin-3 as the protein with the highest fold-change of more than 1200 platelet proteins (Table S6 online, Figure S6A online). Interestingly, the levels of integrin αIIb and β3 subunits were normal suggesting that the reduced surface levels found by FACS (Moser et al., 2008) were due to an impaired integrin trafficking in the absence of Kindlin-3 (Figure S6B online).

We have previously reported that Kindlin-3 (also known as 'unc-related protein 2') is present in red blood cells (Pasini et al., 2006). This was confirmed by different SILAC incorporation levels in platelets (incorporation rate of 6.0) compared to erythrocytes (incorporation rate 2.1) measured after the initial four weeks labeling period (Figure 4-2, Figure S7A,B online). Furthermore, Kindlin-3 gene activity in Ter119-positive Kindlin-3-heterozygous erythroblasts was further corroborated by measuring Kindlin-3 promoter driven β-galactosidase reporter gene activity with FACS (Figure S7C online).

To investigate whether loss of Kindlin-3 affects erythroid cells we determined and quantitatively compared the proteomes from wild-type, Kindlin-3$^{+/-}$ and Kindlin-3$^{-/-}$ erythrocytes (Figure 4-6, Table S7 online). Mass spectrometry confirmed a 50% reduction of Kindlin-3 in heterozygous and a complete absence of Kindlin-3 in Kindlin-3$^{-/-}$ erythrocytes (Figure 4-6A). Out of 881 proteins identified in all three proteomes, more than 50 were two-fold increased in Kindlin-3$^{-/-}$ erythrocytes and only a few revealed a more than two-fold reduction. Interestingly, a large proportion of the up-regulated proteins were annotated to be nuclear (Table S7 online).

Blood smears from Kindlin-3$^{-/-}$ embryos and P3 animals showed a strong reduction of cells when compared to wild-type controls and, in concordance with this proteomic finding, many more nucleated erythroblasts (Figure 4-7B,C). In addition, the size and shape of Kindlin-3$^{-/-}$ erythrocytes were markedly irregular.
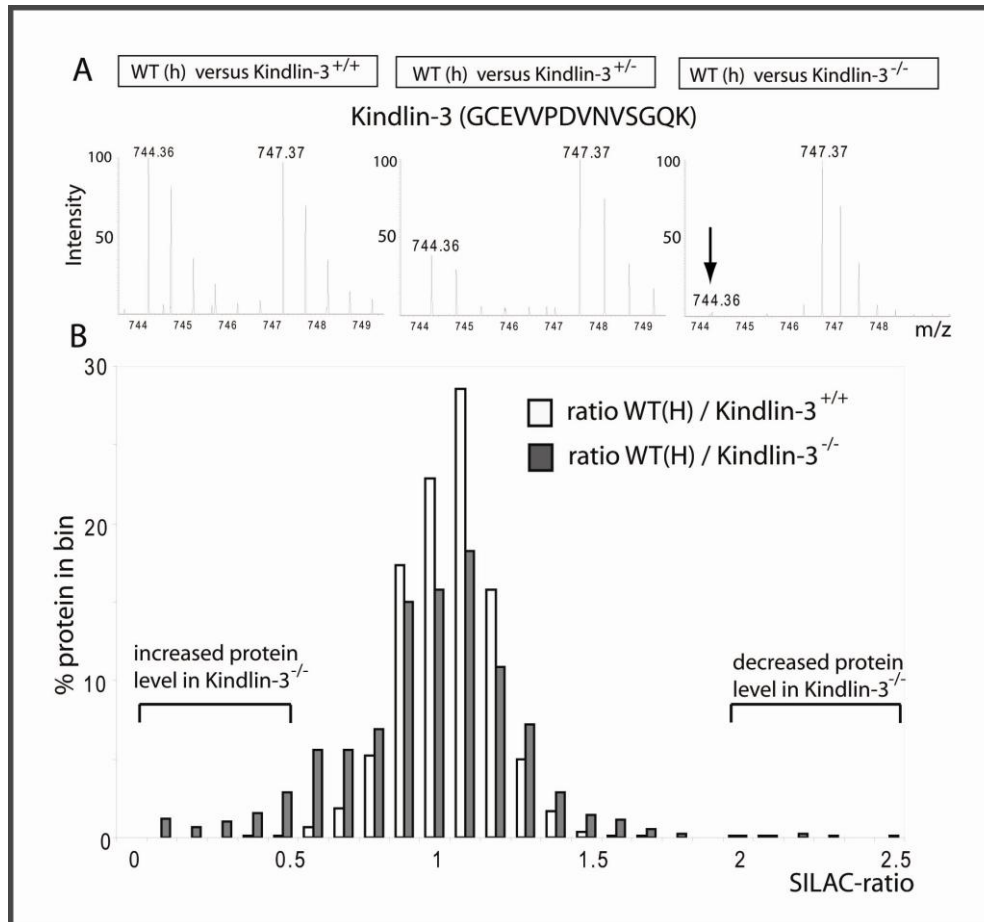
Figure 4-6 Quantitative proteomics of erythrocytes from Kindlin-3-/- mice. (A) Mass spectra of a Kindlin-3 peptide SILAC pair in Kindlin-3+/+, Kindlin-3+/-, and Kindlin-3-/- erythrocytes. (B) Histogram of SILAC ratios of wild-type (white bars) and Kindlin-3-/- erythrocytes (grey bars). The measured ratios were grouped into ratio-bins and the y axis shows the relative number of detected ratios per bin

Scanning electron microscopy showed abnormally shaped erythrocytes with striking membrane invaginations and protuberances (Figure 4-7D). Red blood cell membrane abnormalities are often caused by mutations within membrane skeleton proteins and the absence of key components can have drastic consequences on the stability of the red cell membrane (Delaunay, 1995). To obtain an explanation for the structural defects we quantitatively compared the membrane skeleton proteins from total erythrocytes by SILAC-based MS. The levels of the most prominent skeleton proteins (e.g. α/β spectrin, ankyrin, band 3, band 4.1, band 4.2 and actin) did not significantly differ between wild-type and Kindlin-3$^{-/-}$ mice.

Next we determined whether these proteins have formed a stable meshwork which is connected with the erythrocyte membrane. To address this question, we isolated the erythrocyte membranes (so called red blood cell 'ghosts') from wild-type and Kindlin-3$^{-/-}$

mice and compared them to ghosts from SILAC-labeled control animals (Figure 4-7E). Quantitative SILAC-based analysis revealed an almost complete absence of ankyrin-1, band 4.1, adducin-2, and dematin (Figure 4-7F right rows, Table S8 online) while other membrane skeleton proteins like α/β spectrin and band-3 were not changed.

MW in kDa	Name	total erythrocytes					membrane fraction				
		ratio 1 WT(H) / +/+	variability in %	ratio 2 WT(H) / -/-	variability in %	ratio (+/+)/(-/-)	ratio 1 WT(H) / +/+	variability in %	ratio 2 WT(H) / -/-	variability in %	ratio (+/+)/(-/-)
76	Kindlin-3	1.0	11	∞		∞	1.3	18	∞		∞
279	Spectrin α	1.0	12	1.0	6	1.0	0.9	27	1.0	25	1.0
268	Spectrin β	0.9	12	1.0	10	1.1	3.0	25	3.6	7	1.2
204	Ankyrin-1	1.1	15	1.3	9	1.1	0.9	26	24.6	3	27.9
103	Band 3	0.8	8	1.2	6	1.5	1.2	13	0.9	8	0.8
96	Band 4.1	0.8	7	1.4	7	1.7	0.9	39	13.0	9	13.9
81	Adducin 2	0.9	13	1.3	9	1.5	0.7	29	12.6	5	17.0
77	Band 4.2	0.8	9	1.1	162	1.5	0.7	25	1.0	58	1.5
45	Dematin	0.8	8	1.8	17	2.2	0.9	49	24.8	3	29.0
42	Actin 1	0.8	9	0.5	21	0.6	1.0	19	0.9	43	0.9
31	Band 7	0.8	3	1.4	8	1.8	0.6	25	2.0	19	3.4
10	Glycophorin C	0.9	12	1.4		1.6	0.8	0.2	1.0	13	1.3

Figure 4-7 Kindlin-3-deficient erythrocytes show disrupt membrane skeleton. (A) Kindlin-3 knockout mice are anemic. (B) Decreased hematocrit in Kindlin-3^{-/-} mutants at embryonic day 15 and P3. (C) Blood smears from E15 embryos and P3 wild-type and Kindlin-3^{-/-} mice reveal less erythrocytes and an increased number of nucleated erythroblasts. (D) Scanning electron microscopy of wildtype and Kindlin-3^{-/-} erythrocytes. Scale bar represents 1μm. (E) "Ghost"-lysates from wild-type, heterozygous and Kindlin-3^{-/-} mice were stained by Coomassie blue after SDS-PAGE. Arrows indicate absence of proteins within the membraneskeleton fraction of Kindlin-3^{-/-} erythrocytes.(F) SILAC-ratio comparison of total erythrocytes (left rows) and the membrane fraction (right row).

Together these findings show that Kindlin-3 is required for the assembly of a subset of proteins within the red blood cell membrane skeleton. Furthermore, the proteomic, morphological and functional data provide a clear explanation for the anemia that leads to post-natal lethality.

4.4   Discussion

So far quantitative gene expression comparisons in higher organisms have been restricted to RNA analyses by gene chip approaches. These methods have many advantages, for example ready accessibility and the fact that in principle almost all genes can be analyzed on one chip. However, because of post-transcriptional regulation as well as regulated protein degradation these data do not necessarily predict changes in protein levels within cells or tissues. Furthermore, there are specific cell populations, such as the platelets and erythrocytes investigated here, that are devoid of mRNA and therefore out of reach for these techniques.

Here we show that SILAC, a versatile and successful method for quantitative proteomics in cell culture based systems or microorganisms, can be extended to a mammalian model systems. Mice can be SILAC-labeled without any obvious effect on growth, behavior or fertility. SILAC food preparation is straightforward and not particularly expensive when considering other resources required for the generation and maintenance of knockout animals. We chose $^{13}C_6$-lysine labeling as lysine is not converted into other amino acids. This makes endoprotease Lys-C the preferred choice as the proteolytic enzyme. Another interesting enzyme for SILAC-mice is Lys-N, which has recently been described as an efficient enzyme for proteomics and de-novo peptide sequencing (Taouatas et al., 2008). Organs derived from SILAC mice can serve as standards for a large number of subsequent experiments, in which wild-type and knockout mice are compared. Importantly, cell types such as intestinal epithelium that are difficult to study ex vivo can be analyzed by the in vivo SILAC approach. Moreover, the SILAC mouse can serve as a reference model at any biological scale, from the whole organ through specific cell types down to intracellular compartments or single proteins of interest. As an example, we used SILAC mice to successfully study the mitochondrial proteome, which can be extended to investigations in relevant organs from metabolic or neurodegenerative disease models. In studies where a large number of mice is required – such as in toxicology – labeled organ tissue could be stored used as internal standard for each measurement. A labeled SILAC-mouse liver, for example, yields sufficient internal standard for more than a thousand measurements. Although not shown here, phospho-peptides can also be enriched from SILAC mice and serve as a standard for functional and time-resolved phosphoproteomics (Olsen et al., 2006).

We analyzed the proteomes of cells from three independent knockout mice. In all analyses the complete absence of the targeted genes was immediately revealed by the SILAC technique. Furthermore, heterozygous Kindlin-3 animals present the expected two-fold reduction from wild-type levels, emphasizing the quantitative nature of our proteomic

technology. This may be particularly useful in quantifying knockdown efficiencies in transgenic RNAi mice. The sensitivity of the SILAC-based quantitation system became remarkably obvious by an observation from the β1 integrin inactivation in platelets. Deletion of the β1 integrin gene in hematopoietic cells is achieved by the induction of the Mx1-Cre transgene through the injection of pI-pC into β1 integrin floxed animals. Even without induction of Cre the low expression levels of naturally expressed α/β-interferon activated the Mx1-promoter and trigger β1 integrin deletion in a few cells. Even this slight difference in total β1 integrin expression proved sufficient for detection by the SILAC method.

Our proteomic data on platelets of β1-integrin mice showed that although integrins control a number of different signaling pathways, the lack of the β1 integrin has no consequences on the levels of other proteins in platelets apart from its dimerization partners α2 and α6 integrins. This may be due to the fact that in resting platelets integrins are inactive and signaling into the cell is only induced upon stimulation via molecules like thrombin or collagen (Ruggeri, 2002). Further studies using the SILAC-mouse system could focus on activation of signaling cascades during platelet aggregation using phosphoproteomics.

To test the SILAC-based analysis in a solid organ system, we compared the proteomes from heart of β-parvin deficient mice with control littermates. The complexity of a tissue, formed by different cell types, poses no limitation for the quantitative analysis by mass spectrometry. The interpretation of results, however, is more challenging because changes in protein levels may result from non cell autonomous defects caused for example by altered cell-cell communication rather than cell autonomous defects.

To study the molecular cause of the anemia observed in Kindlin-3 mutants, we analyzed the consequences of this deletion on the proteome of platelets and erythrocytes. Recently, we characterized Kindlin-3 as an essential factor for the activation of platelet integrins (Moser et al., 2008). Kindlin-3 directly binds to the cytoplasmic tails of both β1 and β3 integrin subunits. Its expression is restricted to cells of the hematopoietic system (Ussar et al., 2006). Our SILAC based analysis of Kindlin-3 deficient erythrocytes revealed an increased amount of nuclear proteins prompting us to investigate consequences of the knockout on this cell type. Consistent with the proteomic results, we found an increased number of nucleated erythroblasts in blood smears. Furthermore, Kindlin-3 deficient erythrocytes are irregular in size and shape. The structural defects of the red blood cell membrane skeleton suggested an additional function of Kindlin-3. With the help of the SILAC method we quantitatively compared the membrane skeleton proteins of control and Kindlin-3 deficient erythrocytes and revealed a critical role of Kindlin-3 in the formation or stabilization of this structure. The inner surface of the red blood cell membrane is laminated by a protein network that is linked to transmembrane proteins. In humans and mice mutations in genes encoding ankyrin, band 3, spectrin and protein 4.1 or protein 4.2 cause hereditary spherocytosis or poikilocytosis often accompanied with hemolytic anemias (Delaunay, 1995; Peters et al., 1998; Rybicki et al., 1995; Shi et al., 1999; Southgate et al., 1996). The dramatic reduction of ankyrin-1, protein 4.1 and dematin in membrane preparations from Kindlin-3 deficient erythrocytes

explains the severe malformations. Thus, loss of Kindlin-3 affects erythropoiesis by disrupting the assembly of structural components within the red blood cell membrane skeleton.

In summary, a direct combination of the SILAC technology for quantitative proteomics with the large number of powerful mouse models generated by the community is now possible. We have demonstrated here how proteomics can be combined with several of the powerful technologies already used in this endeavor. We are confident that this technology will help to elucidate disease processes and guide novel intervention strategies.

5   Concluding remarks

The research described herein had the aim of using MS-based quantitative proteomics for the characterization of *in vivo* cells. Proteomics has proven its applicability in a variety of cell culture models for phenotyping of cell lines, for the deciphering of signal transduction pathways after certain stimuli and for the determination of binding partners. The next step was to apply this technology *in vivo*. However, this is not a trivial task: Primary cells have to be isolated in a laborious way from tissues, which in general leads to only to a few million cells of high purity. This is roughly the equivalent of just one 15-centimeter cell culture dish of HeLa cells, the most used cell line in many laboratories. Further challenges arise due to the lack of robust quantitation methods like the SILAC approach for experiments involving many mice or human material. Taken together, these challenges hampered the in depth analysis of *in vivo* cells using MS-based quantitative proteomics.

In this thesis, I have shown that quantitative proteomics is applicable to the analysis of rare *in vivo* cell populations and that it can provide direct insights into specific functions of closely related cell types. The development of novel label-free quantitation algorithms allowed accurate and robust proteome wide quantitation, as shown on the benchmark dataset with two mixed proteomes of human and *E.coli* proteins. This quantitation method without stable isotopes is not as accurate as metabolic labeling strategies, but certainly the method of choice if isotope labeling is not possible as in the case of the comparative analysis of *in vivo* cells.

I have further applied this method to conventional dendritic cell subsets, rare populations of important orchestrators of the immune system. Isolation procedures of pooled spleens from 32 mice yielded only $5x10^6$ CD4$^+$ and $2.5x10^6$ of both CD8α^+ and DN cDC subsets, making proteomic analysis extremely challenging. However using our optimized proteomics workflow together with newly developed label-free quantitation algorithms, we were able to determine the proteome of cDC subsets to a depth of 5780 proteins, requiring just 20-25 µg of sample. This shows the applicability of our developed method for the quantitative analysis of rare cell populations. My large-scale proteomic dataset showed strikingly different expression of pattern recognition receptors, like the RIG-like helicases RIG-I and MDA5, between DC subsets, which prompted us to make functional predictions about these closely related cell types. *Ex vivo* infection of cDC subsets with Sendai virus confirmed our proteomic finding and defined a novel important role of CD4$^+$ and DN cDCs in viral infections.

The third project of my thesis, in which I have been involved, was the generation of the SILAC mouse. An inarguable advantage of the SILAC approach is its precise quantitation

capability. However, so far SILAC has been limited to cultured cell lines. We described the extension of the SILAC technology to the *in vivo* mouse model. Using a special SILAC diet containing only $^{13}C_6$-lysine enabled us to label the entire mouse, including all tissues such as gut, liver or cell populations like B-lymphocytes. The labeled tissues or cell population can now be used as internal standards for studying the phenotype of any mouse model under any experimental conditions, making the SILAC mouse to a very useful tool for drug development.

In conclusion, the approaches described in my thesis opens the field of MS-based proteomics for accurate and robust quantitation of *in vivo* samples with the possibility for direct functional conclusions.

6   References

Adachi, O., Kawai, T., Takeda, K., Matsumoto, M., Tsutsui, H., Sakagami, M., Nakanishi, K., and Akira, S. (1998). Targeted disruption of the MyD88 gene results in loss of IL-1- and IL-18-mediated function. Immunity *9*, 143-150.

Aebersold, R., and Mann, M. (2003). Mass spectrometry-based proteomics. Nature *422*, 198-207.

Agger, R., Witmer-Pack, M., Romani, N., Stossel, H., Swiggard, W.J., Metlay, J.P., Storozynsky, E., Freimuth, P., and Steinman, R.M. (1992). Two populations of splenic dendritic cells detected with M342, a new monoclonal to an intracellular antigen of interdigitating dendritic cells and some B lymphocytes. Journal of leukocyte biology *52*, 34-42.

Akira, S., Uematsu, S., and Takeuchi, O. (2006). Pathogen recognition and innate immunity. Cell *124*, 783-801.

Alexopoulou, L., Holt, A.C., Medzhitov, R., and Flavell, R.A. (2001). Recognition of double-stranded RNA and activation of NF-kappaB by Toll-like receptor 3. Nature *413*, 732-738.

Allan, R.S., Smith, C.M., Belz, G.T., van Lint, A.L., Wakim, L.M., Heath, W.R., and Carbone, F.R. (2003). Epidermal viral immunity induced by CD8alpha+ dendritic cells but not by Langerhans cells. Science (New York, N.Y *301*, 1925-1928.

Andersen, J.S., Lam, Y.W., Leung, A.K., Ong, S.E., Lyon, C.E., Lamond, A.I., and Mann, M. (2005). Nucleolar proteome dynamics. Nature *433*, 77-83.

Baek, D., Villen, J., Shin, C., Camargo, F.D., Gygi, S.P., and Bartel, D.P. (2008). The impact of microRNAs on protein output. Nature *455*, 64-71.

Banchereau, J., Briere, F., Caux, C., Davoust, J., Lebecque, S., Liu, Y.J., Pulendran, B., and Palucka, K. (2000). Immunobiology of dendritic cells. Annual review of immunology *18*, 767-811.

Banchereau, J., and Steinman, R.M. (1998). Dendritic cells and the control of immunity. Nature *392*, 245-252.

Bantscheff, M., Schirle, M., Sweetman, G., Rick, J., and Kuster, B. (2007). Quantitative mass spectrometry in proteomics: a critical review. Anal Bioanal Chem *389*, 1017-1031.

Barchet, W., Blasius, A., Cella, M., and Colonna, M. (2005a). Plasmacytoid dendritic cells: in search of their niche in immune responses. Immunol Res *32*, 75-83.

Barchet, W., Cella, M., and Colonna, M. (2005b). Plasmacytoid dendritic cells--virus experts of innate immunity. Semin Immunol *17*, 253-261.

Bauer, S., Kirschning, C.J., Hacker, H., Redecke, V., Hausmann, S., Akira, S., Wagner, H., and Lipford, G.B. (2001). Human TLR9 confers responsiveness to bacterial DNA via species-specific CpG motif recognition. Proc Natl Acad Sci U S A *98*, 9237-9242.

Bellew, M., Coram, M., Fitzgibbon, M., Igra, M., Randolph, T., Wang, P., May, D., Eng, J., Fang, R., Lin, C.*, et al.* (2006). A suite of algorithms for the comprehensive analysis of

complex protein mixtures using high-resolution LC-MS. Bioinformatics (Oxford, England) *22*, 1902-1909.

Belz, G., Mount, A., and Masson, F. (2009). Dendritic cells in viral infections. Handbook of experimental pharmacology, 51-77.

Belz, G.T., Shortman, K., Bevan, M.J., and Heath, W.R. (2005). CD8alpha+ dendritic cells selectively present MHC class I-restricted noncytolytic viral and intracellular bacterial antigens in vivo. J Immunol *175*, 196-200.

Belz, G.T., Smith, C.M., Eichner, D., Shortman, K., Karupiah, G., Carbone, F.R., and Heath, W.R. (2004). Cutting edge: conventional CD8 alpha+ dendritic cells are generally involved in priming CTL immunity to viruses. J Immunol *172*, 1996-2000.

Benevenga, N.J., Calvert, C., Eckhert, C.D., Fahey, G.C., Greger, J.L., Keen, C.L., Knapka, J.J., Magalhaes, H., and Oftedal, O.T. (1995). Nutrient Requirements of the Mouse. In Nutrient Requirements of Laboratory Animals (Washington, D.C.: NATIONAL ACADEMY PRESS), p. 192.

Berlin, N.I., Waldmann, T.A., and Weissman, S.M. (1959). Life span of red blood cell. Physiol Rev *39*, 577-616.

Beutler, B., Jiang, Z., Georgel, P., Crozat, K., Croker, B., Rutschmann, S., Du, X., and Hoebe, K. (2006). Genetic analysis of host resistance: Toll-like receptor signaling and immunity at large. Annual review of immunology *24*, 353-389.

Beynon, R.J., and Pratt, J.M. (2005). Metabolic labeling of proteins for proteomics. Mol Cell Proteomics *4*, 857-872.

Bier, D.M. (1997). Stable isotopes in biosciences, their measurement and models for amino acid metabolism. European journal of pediatrics *156 Suppl 1*, S2-8.

Binder, R.J., Han, D.K., and Srivastava, P.K. (2000). CD91: a receptor for heat shock protein gp96. Nature immunology *1*, 151-155.

Blagoev, B., Ong, S.E., Kratchmarova, I., and Mann, M. (2004). Temporal analysis of phosphotyrosine-dependent signaling networks by quantitative proteomics. Nat Biotechnol *22*, 1139-1145.

Bonaldi, T., Straub, T., Cox, J., Kumar, C., Becker, P.B., and Mann, M. (2008). Combined use of RNAi and quantitative proteomics to study gene function in Drosophila. Mol Cell *31*, 762-772.

Boyden, E.D., and Dietrich, W.F. (2006). Nalp1b controls mouse macrophage susceptibility to anthrax lethal toxin. Nature genetics *38*, 240-244.

Brakebusch, C., Grose, R., Quondamatteo, F., Ramirez, A., Jorcano, J.L., Pirro, A., Svensson, M., Herken, R., Sasaki, T., Timpl, R.*, et al.* (2000). Skin and hair follicle integrity is crucially dependent on beta 1 integrin expression on keratinocytes. Embo J *19*, 3990-4003.

Brasel, K., De Smedt, T., Smith, J.L., and Maliszewski, C.R. (2000). Generation of murine dendritic cells from flt3-ligand-supplemented bone marrow cultures. Blood *96*, 3029-3039.

Brawand, P., Fitzpatrick, D.R., Greenfield, B.W., Brasel, K., Maliszewski, C.R., and De Smedt, T. (2002). Murine plasmacytoid pre-dendritic cells generated from Flt3 ligand-supplemented bone marrow cultures are immature APCs. J Immunol *169*, 6711-6719.

Bridges, S.M., Magee, G.B., Wang, N., Williams, W.P., Burgess, S.C., and Nanduri, B. (2007). ProtQuant: a tool for the label-free quantification of MudPIT proteomics data. BMC bioinformatics *8 Suppl 7*, S24.

Brocker, T. (1997). Survival of mature CD4 T lymphocytes is dependent on major histocompatibility complex class II-expressing dendritic cells. The Journal of experimental medicine *186*, 1223-1232.

Burzyn, D., Rassa, J.C., Kim, D., Nepomnaschy, I., Ross, S.R., and Piazzon, I. (2004). Toll-like receptor 4-dependent activation of dendritic cells by a retrovirus. J Virol *78*, 576-584.

Calderwood, D.A. (2004). Integrin activation. Journal of cell science *117*, 657-666.

Carter, R.W., Thompson, C., Reid, D.M., Wong, S.Y., and Tough, D.F. (2006). Preferential induction of CD4+ T cell responses through in vivo targeting of antigen to dendritic cell-associated C-type lectin-1. J Immunol *177*, 2276-2284.

Cassel, S.L., Eisenbarth, S.C., Iyer, S.S., Sadler, J.J., Colegio, O.R., Tephly, L.A., Carter, A.B., Rothman, P.B., Flavell, R.A., and Sutterwala, F.S. (2008). The Nalp3 inflammasome is essential for the development of silicosis. Proceedings of the National Academy of Sciences of the United States of America *105*, 9035-9040.

Cella, M., Engering, A., Pinet, V., Pieters, J., and Lanzavecchia, A. (1997). Inflammatory stimuli induce accumulation of MHC class II complexes on dendritic cells. Nature *388*, 782-787.

Cella, M., Salio, M., Sakakibara, Y., Langen, H., Julkunen, I., and Lanzavecchia, A. (1999). Maturation, activation, and protection of dendritic cells induced by double-stranded RNA. The Journal of experimental medicine *189*, 821-829.

Chamaillard, M., Hashimoto, M., Horie, Y., Masumoto, J., Qiu, S., Saab, L., Ogura, Y., Kawasaki, A., Fukase, K., Kusumoto, S.*, et al.* (2003). An essential role for NOD1 in host recognition of bacterial peptidoglycan containing diaminopimelic acid. Nature immunology *4*, 702-707.

Cheers, C., Haigh, A.M., Kelso, A., Metcalf, D., Stanley, E.R., and Young, A.M. (1988). Production of colony-stimulating factors (CSFs) during infection: separate determinations of macrophage-, granulocyte-, granulocyte-macrophage-, and multi-CSFs. Infect Immun *56*, 247-251.

Chen, W., Masterman, K.A., Basta, S., Haeryfar, S.M., Dimopoulos, N., Knowles, B., Bennink, J.R., and Yewdell, J.W. (2004). Cross-priming of CD8+ T cells by viral and tumor antigens is a robust phenomenon. Eur J Immunol *34*, 194-199.

Ciavarra, R.P., Stephens, A., Nagy, S., Sekellick, M., and Steel, C. (2006). Evaluation of immunological paradigms in a virus model: are dendritic cells critical for antiviral immunity and viral clearance? J Immunol *177*, 492-500.

Coffman, R.L. (1982). Surface antigen expression and immunoglobulin gene rearrangement during mouse pre-B cell development. Immunol Rev *69*, 5-23.

Cox, J., Hubner, N.C., and Mann, M. (2008). How Much Peptide Sequence Information Is Contained in Ion Trap Tandem Mass Spectra? J Am Soc Mass Spectrom.

Cox, J., Luber, C.A., Nagaraj, N., and Mann, M. (submitted and attached). Delayed normalization and maximal peptide ratio pairing for proteome-wide label-free quantification.

Cox, J., and Mann, M. (2007). Is proteomics the new genomics? Cell *130*, 395-398.

Cox, J., and Mann, M. (2008). MaxQuant enables high peptide identification rates, individualized p.p.b.-range mass accuracies and proteome-wide protein quantification. Nature biotechnology *26*, 1367-1372.

Cravatt, B.F., Simon, G.M., and Yates, J.R., 3rd (2007). The biological impact of mass-spectrometry-based proteomics. Nature *450*, 991-1000.

Dangl, J.L., and McDowell, J.M. (2006). Two modes of pathogen recognition by plants. Proceedings of the National Academy of Sciences of the United States of America *103*, 8575-8576.

de Godoy, L.M., Olsen, J.V., Cox, J., Nielsen, M.L., Hubner, N.C., Frohlich, F., Walther, T.C., and Mann, M. (2008a). Comprehensive mass-spectrometry-based proteome quantification of haploid versus diploid yeast. Nature.

de Godoy, L.M., Olsen, J.V., Cox, J., Nielsen, M.L., Hubner, N.C., Frohlich, F., Walther, T.C., and Mann, M. (2008b). Comprehensive mass-spectrometry-based proteome quantification of haploid versus diploid yeast. Nature *455*, 1251-1254.

De Smedt, T., Pajak, B., Muraille, E., Lespagnard, L., Heinen, E., De Baetselier, P., Urbain, J., Leo, O., and Moser, M. (1996). Regulation of dendritic cell numbers and maturation by lipopolysaccharide in vivo. The Journal of experimental medicine *184*, 1413-1424.

Delaunay, J. (1995). Genetic disorders of the red cell membranes. FEBS Lett *369*, 34-37.

den Haan, J.M., Lehar, S.M., and Bevan, M.J. (2000). CD8(+) but not CD8(-) dendritic cells cross-prime cytotoxic T cells in vivo. The Journal of experimental medicine *192*, 1685-1696.

Diebold, S.S., Kaisho, T., Hemmi, H., Akira, S., and Reis e Sousa, C. (2004). Innate antiviral responses by means of TLR7-mediated recognition of single-stranded RNA. Science *303*, 1529-1531.

Dietz, W.H., Jr., Wolfe, M.H., and Wolfe, R.R. (1982). A method for the rapid determination of protein turnover. Metabolism: clinical and experimental *31*, 749-754.

Doherty, M.K., and Beynon, R.J. (2006). Protein turnover on the scale of the proteome. Expert Rev Proteomics *3*, 97-110.

Doherty, M.K., Whitehead, C., McCormack, H., Gaskell, S.J., and Beynon, R.J. (2005). Proteome dynamics in complex organisms: using stable isotopes to monitor individual protein turnover rates. Proteomics *5*, 522-533.

Domon, B., and Aebersold, R. (2006). Mass spectrometry and protein analysis. Science (New York, N.Y *312*, 212-217.

Dostert, C., Petrilli, V., Van Bruggen, R., Steele, C., Mossman, B.T., and Tschopp, J. (2008). Innate immune activation through Nalp3 inflammasome sensing of asbestos and silica. Science (New York, N.Y *320*, 674-677.

Dubois, B., and Caux, C. (2005). Critical role of ITIM-bearing FcgammaR on DCs in the capture and presentation of native antigen to B cells. Immunity *23*, 463-464.

Dudziak, D., Kamphorst, A.O., Heidkamp, G.F., Buchholz, V.R., Trumpfheller, C., Yamazaki, S., Cheong, C., Liu, K., Lee, H.W., Park, C.G., *et al.* (2007). Differential antigen processing by dendritic cell subsets in vivo. Science (New York, N.Y *315*, 107-111.

Duncan, J.A., Bergstralh, D.T., Wang, Y., Willingham, S.B., Ye, Z., Zimmermann, A.G., and Ting, J.P. (2007). Cryopyrin/NALP3 binds ATP/dATP, is an ATPase, and requires ATP binding to mediate inflammatory signaling. Proceedings of the National Academy of Sciences of the United States of America *104*, 8041-8046.

Edelmann, K.H., Richardson-Burns, S., Alexopoulou, L., Tyler, K.L., Flavell, R.A., and Oldstone, M.B. (2004). Does Toll-like receptor 3 play a biological role in virus infections? Virology *322*, 231-238.

Edman, P. (1970). Sequence determination. Molecular biology, biochemistry, and biophysics *8*, 211-255.

Edwards, A.D., Chaussabel, D., Tomlinson, S., Schulz, O., Sher, A., and Reis e Sousa, C. (2003a). Relationships among murine CD11c(high) dendritic cell subsets as revealed by baseline gene expression patterns. J Immunol *171*, 47-60.

Edwards, A.D., Diebold, S.S., Slack, E.M., Tomizawa, H., Hemmi, H., Kaisho, T., Akira, S., and Reis e Sousa, C. (2003b). Toll-like receptor expression in murine DC subsets: lack of TLR7 expression by CD8 alpha+ DC correlates with unresponsiveness to imidazoquinolines. European journal of immunology *33*, 827-833.

Fenn, J.B. (2003). Electrospray wings for molecular elephants (Nobel lecture). Angewandte Chemie (International ed *42*, 3871-3894.

Fischer, M., and Ehlers, M. (2008). Toll-like receptors in autoimmunity. Annals of the New York Academy of Sciences *1143*, 21-34.

Forner, F., Foster, L.J., Campanaro, S., Valle, G., and Mann, M. (2006). Quantitative proteomic comparison of rat mitochondria from muscle, heart, and liver. Mol Cell Proteomics *5*, 608-619.

Franchi, L., Amer, A., Body-Malapel, M., Kanneganti, T.D., Ozoren, N., Jagirdar, R., Inohara, N., Vandenabeele, P., Bertin, J., Coyle, A*., et al.* (2006). Cytosolic flagellin requires Ipaf for activation of caspase-1 and interleukin 1beta in salmonella-infected macrophages. Nature immunology *7*, 576-582.

Fuchsberger, M., Hochrein, H., and O'Keeffe, M. (2005). Activation of plasmacytoid dendritic cells. Immunology and cell biology *83*, 571-577.

Geissmann, F., Jung, S., and Littman, D.R. (2003). Blood monocytes consist of two principal subsets with distinct migratory properties. Immunity *19*, 71-82.

Gingras, A.C., Gstaiger, M., Raught, B., and Aebersold, R. (2007). Analysis of protein complexes using mass spectrometry. Nature reviews *8*, 645-654.

Gitlin, L., Barchet, W., Gilfillan, S., Cella, M., Beutler, B., Flavell, R.A., Diamond, M.S., and Colonna, M. (2006). Essential role of mda-5 in type I IFN responses to polyriboinosinic:polyribocytidylic acid and encephalomyocarditis picornavirus. Proc Natl Acad Sci U S A *103*, 8459-8464.

Graumann, J., Hubner, N.C., Kim, J.B., Ko, K., Moser, M., Kumar, C., Cox, J., Schoeler, H., and Mann, M. (2007). SILAC-labeling and proteome quantitation of mouse embryonic stem cells to a depth of 5111 proteins. Mol Cell Proteomics.

Graumann, J., Hubner, N.C., Kim, J.B., Ko, K., Moser, M., Kumar, C., Cox, J., Scholer, H., and Mann, M. (2008). Stable isotope labeling by amino acids in cell culture (SILAC) and proteome quantitation of mouse embryonic stem cells to a depth of 5,111 proteins. Mol Cell Proteomics *7*, 672-683.

Gregg, C.T., Hutson, J.Y., Prine, J.R., Ott, D.G., and Furchner, J.E. (1973). Substantial replacement of mammalian body carbon with carbon-13. Life Sci *13*, 775-782.

Groothuis, T.A., and Neefjes, J. (2005). The many roads to cross-presentation. The Journal of experimental medicine *202*, 1313-1318.

Gygi, S.P., Rist, B., Gerber, S.A., Turecek, F., Gelb, M.H., and Aebersold, R. (1999). Quantitative analysis of complex protein mixtures using isotope-coded affinity tags. Nature biotechnology *17*, 994-999.

Haas, T., Metzger, J., Schmitz, F., Heit, A., Muller, T., Latz, E., and Wagner, H. (2008). The DNA sugar backbone 2' deoxyribose determines toll-like receptor 9 activation. Immunity *28*, 315-323.

Hammad, H., de Vries, V.C., Maldonado-Lopez, R., Moser, M., Maliszewski, C., Hoogsteden, H.C., and Lambrecht, B.N. (2004). Differential capacity of CD8+ alpha or CD8- alpha dendritic cell subsets to prime for eosinophilic airway inflammation in the T-helper type 2-prone milieu of the lung. Clin Exp Allergy *34*, 1834-1840.

Hanson, P.I., and Whiteheart, S.W. (2005). AAA+ proteins: have engine, will work. Nat Rev Mol Cell Biol *6*, 519-529.

Hasegawa, M., Yang, K., Hashimoto, M., Park, J.H., Kim, Y.G., Fujimoto, Y., Nunez, G., Fukase, K., and Inohara, N. (2006). Differential release and distribution of Nod1 and Nod2 immunostimulatory molecules among bacterial species and environments. The Journal of biological chemistry *281*, 29054-29063.

Hawiger, D., Inaba, K., Dorsett, Y., Guo, M., Mahnke, K., Rivera, M., Ravetch, J.V., Steinman, R.M., and Nussenzweig, M.C. (2001). Dendritic cells induce peripheral T cell unresponsiveness under steady state conditions in vivo. The Journal of experimental medicine *194*, 769-779.

Heath, W.R., Belz, G.T., Behrens, G.M., Smith, C.M., Forehan, S.P., Parish, I.A., Davey, G.M., Wilson, N.S., Carbone, F.R., and Villadangos, J.A. (2004). Cross-presentation, dendritic cell subsets, and the generation of immunity to cellular antigens. Immunological reviews *199*, 9-26.

Heath, W.R., and Carbone, F.R. (2001). Cross-presentation, dendritic cells, tolerance and immunity. Annu Rev Immunol *19*, 47-64.

Heil, F., Hemmi, H., Hochrein, H., Ampenberger, F., Kirschning, C., Akira, S., Lipford, G., Wagner, H., and Bauer, S. (2004). Species-specific recognition of single-stranded RNA via toll-like receptor 7 and 8. Science (New York, N.Y *303*, 1526-1529.

Hemmi, H., Takeuchi, O., Kawai, T., Kaisho, T., Sato, S., Sanjo, H., Matsumoto, M., Hoshino, K., Wagner, H., Takeda, K., and Akira, S. (2000). A Toll-like receptor recognizes bacterial DNA. Nature *408*, 740-745.

Hochrein, H., and O'Keeffe, M. (2008). Dendritic cell subsets and toll-like receptors. Handbook of experimental pharmacology, 153-179.

Hochrein, H., Schlatter, B., O'Keeffe, M., Wagner, C., Schmitz, F., Schiemann, M., Bauer, S., Suter, M., and Wagner, H. (2004). Herpes simplex virus type-1 induces IFN-alpha production via Toll-like receptor 9-dependent and -independent pathways. Proceedings of the National Academy of Sciences of the United States of America *101*, 11416-11421.

Hochrein, H., Shortman, K., Vremec, D., Scott, B., Hertzog, P., and O'Keeffe, M. (2001). Differential production of IL-12, IFN-alpha, and IFN-gamma by mouse dendritic cell subsets. J Immunol *166*, 5448-5455.

Hornung, V., Bauernfeind, F., Halle, A., Samstad, E.O., Kono, H., Rock, K.L., Fitzgerald, K.A., and Latz, E. (2008). Silica crystals and aluminum salts activate the NALP3 inflammasome through phagosomal destabilization. Nature immunology *9*, 847-856.

Hornung, V., Ellegast, J., Kim, S., Brzozka, K., Jung, A., Kato, H., Poeck, H., Akira, S., Conzelmann, K.K., Schlee, M.*, et al.* (2006). 5'-Triphosphate RNA is the ligand for RIG-I. Science *314*, 994-997.

Hoshino, K., Takeuchi, O., Kawai, T., Sanjo, H., Ogawa, T., Takeda, Y., Takeda, K., and Akira, S. (1999). Cutting edge: Toll-like receptor 4 (TLR4)-deficient mice are hyporesponsive to lipopolysaccharide: evidence for TLR4 as the Lps gene product. J Immunol *162*, 3749-3752.

Hu, Q., Noll, R.J., Li, H., Makarov, A., Hardman, M., and Graham Cooks, R. (2005). The Orbitrap: a new mass spectrometer. J Mass Spectrom *40*, 430-443.

Hubner, N.C., Ren, S., and Mann, M. (2008). Peptide separation with immobilized pI strips is an attractive alternative to in-gel protein digestion for proteome analysis. Proteomics.

Hugot, J.P., Chamaillard, M., Zouali, H., Lesage, S., Cezard, J.P., Belaiche, J., Almer, S., Tysk, C., O'Morain, C.A., Gassull, M.*, et al.* (2001). Association of NOD2 leucine-rich repeat variants with susceptibility to Crohn's disease. Nature *411*, 599-603.

Hynes, R.O. (2002). Integrins: bidirectional, allosteric signaling machines. Cell *110*, 673-687.

Inaba, K., Inaba, M., Romani, N., Aya, H., Deguchi, M., Ikehara, S., Muramatsu, S., and Steinman, R.M. (1992). Generation of large numbers of dendritic cells from mouse bone marrow cultures supplemented with granulocyte/macrophage colony-stimulating factor. The Journal of experimental medicine *176*, 1693-1702.

Inohara, N., and Nunez, G. (2003). NODs: intracellular proteins involved in inflammation and apoptosis. Nature reviews *3*, 371-382.

Ishihama, Y., Oda, Y., Tabata, T., Sato, T., Nagasu, T., Rappsilber, J., and Mann, M. (2005a). Exponentially modified protein abundance index (emPAI) for estimation of absolute protein amount in proteomics by the number of sequenced peptides per protein. Mol Cell Proteomics *4*, 1265-1272.

Ishihama, Y., Sato, T., Tabata, T., Miyamoto, N., Sagane, K., Nagasu, T., and Oda, Y. (2005b). Quantitative mouse brain proteomics using culture-derived isotope tags as internal standards. Nat Biotechnol *23*, 617-621.

Jaffe, J.D., Mani, D.R., Leptos, K.C., Church, G.M., Gillette, M.A., and Carr, S.A. (2006). PEPPeR, a platform for experimental proteomic pattern recognition. Mol Cell Proteomics *5*, 1927-1941.

Janeway, C.A., Jr. (1989). Approaching the asymptote? Evolution and revolution in immunology. Cold Spring Harb Symp Quant Biol *54 Pt 1*, 1-13.

Janeway, C.A., Jr., and Medzhitov, R. (2002). Innate immune recognition. Annual review of immunology *20*, 197-216.

Jiang, W., Swiggard, W.J., Heufler, C., Peng, M., Mirza, A., Steinman, R.M., and Nussenzweig, M.C. (1995). The receptor DEC-205 expressed by dendritic cells and thymic epithelial cells is involved in antigen processing. Nature *375*, 151-155.

Johansson, C., Samskog, J., Sundstrom, L., Wadensten, H., Bjorkesten, L., and Flensburg, J. (2006). Differential expression analysis of Escherichia coli proteins using a novel software for relative quantitation of LC-MS/MS data. Proteomics *6*, 4475-4485.

Jonckheere, J.A., Thienpont, L.M., De Leenheer, A.P., De Backer, P., Debackere, M., and Belpaire, F.M. (1980). Selected ion monitoring assay for bromhexine in biological fluids. Biomedical mass spectrometry *7*, 582-587.

Jung, S., Unutmaz, D., Wong, P., Sano, G., De los Santos, K., Sparwasser, T., Wu, S., Vuthoori, S., Ko, K., Zavala, F.*, et al.* (2002). In vivo depletion of CD11c(+) dendritic cells abrogates priming of CD8(+) T cells by exogenous cell-associated antigens. Immunity *17*, 211-220.

Kagi, D., Ledermann, B., Burki, K., Hengartner, H., and Zinkernagel, R.M. (1994). CD8+ T cell-mediated protection against an intracellular bacterium by perforin-dependent cytotoxicity. European journal of immunology *24*, 3068-3072.

Kanneganti, T.D., Lamkanfi, M., and Nunez, G. (2007). Intracellular NOD-like receptors in host defense and disease. Immunity *27*, 549-559.

Katajamaa, M., Miettinen, J., and Oresic, M. (2006). MZmine: toolbox for processing and visualization of mass spectrometry based molecular profile data. Bioinformatics (Oxford, England) *22*, 634-636.

Kato, H., Sato, S., Yoneyama, M., Yamamoto, M., Uematsu, S., Matsui, K., Tsujimura, T., Takeda, K., Fujita, T., Takeuchi, O., and Akira, S. (2005). Cell type-specific involvement of RIG-I in antiviral response. Immunity *23*, 19-28.

Kato, H., Takeuchi, O., Mikamo-Satoh, E., Hirai, R., Kawai, T., Matsushita, K., Hiiragi, A., Dermody, T.S., Fujita, T., and Akira, S. (2008). Length-dependent recognition of double-stranded ribonucleic acids by retinoic acid-inducible gene-I and melanoma differentiation-associated gene 5. The Journal of experimental medicine *205*, 1601-1610.

Kato, H., Takeuchi, O., Sato, S., Yoneyama, M., Yamamoto, M., Matsui, K., Uematsu, S., Jung, A., Kawai, T., Ishii, K.J.*, et al.* (2006). Differential roles of MDA5 and RIG-I helicases in the recognition of RNA viruses. Nature *441*, 101-105.

Kawai, T., and Akira, S. (2008). Toll-like receptor and RIG-I-like receptor signaling. Annals of the New York Academy of Sciences *1143*, 1-20.

Kersey, P.J., Duarte, J., Williams, A., Karavidopoulou, Y., Birney, E., and Apweiler, R. (2004). The International Protein Index: an integrated database for proteomics experiments. Proteomics *4*, 1985-1988.

Kobayashi, K., Inohara, N., Hernandez, L.D., Galan, J.E., Nunez, G., Janeway, C.A., Medzhitov, R., and Flavell, R.A. (2002). RICK/Rip2/CARDIAK mediates signalling for receptors of the innate and adaptive immune systems. Nature *416*, 194-199.

Kohlbacher, O., Reinert, K., Gropl, C., Lange, E., Pfeifer, N., Schulz-Trieglaff, O., and Sturm, M. (2007). TOPP--the OpenMS proteomics pipeline. Bioinformatics (Oxford, England) *23*, e191-197.

Kratchmarova, I., Blagoev, B., Haack-Sorensen, M., Kassem, M., and Mann, M. (2005). Mechanism of divergent growth factor effects in mesenchymal stem cell differentiation. Science *308*, 1472-1477.

Krijgsveld, J., Ketting, R.F., Mahmoudi, T., Johansen, J., Artal-Sanz, M., Verrijzer, C.P., Plasterk, R.H., and Heck, A.J. (2003). Metabolic labeling of C. elegans and D. melanogaster for quantitative proteomics. Nat Biotechnol *21*, 927-931.

Krug, A., Rothenfusser, S., Hornung, V., Jahrsdorfer, B., Blackwell, S., Ballas, Z.K., Endres, S., Krieg, A.M., and Hartmann, G. (2001). Identification of CpG oligonucleotide sequences with high induction of IFN-alpha/beta in plasmacytoid dendritic cells. Eur J Immunol *31*, 2154-2163.

Kruger, M., Moser, M., Ussar, S., Thievessen, I., Luber, C.A., Forner, F., Schmidt, S., Zanivan, S., Fassler, R., and Mann, M. (2008). SILAC mouse for quantitative proteomics uncovers kindlin-3 as an essential factor for red blood cell function. Cell *134*, 353-364.

Kuhn, R., Schwenk, F., Aguet, M., and Rajewsky, K. (1995). Inducible gene targeting in mice. Science *269*, 1427-1429.

Kurt-Jones, E.A., Popova, L., Kwinn, L., Haynes, L.M., Jones, L.P., Tripp, R.A., Walsh, E.E., Freeman, M.W., Golenbock, D.T., Anderson, L.J., and Finberg, R.W. (2000). Pattern recognition receptors TLR4 and CD14 mediate response to respiratory syncytial virus. Nat Immunol *1*, 398-401.

Legate, K.R., Montanez, E., Kudlacek, O., and Fassler, R. (2006). ILK, PINCH and parvin: the tIPP of integrin signalling. Nature reviews *7*, 20-31.

Lemaitre, B., Nicolas, E., Michaut, L., Reichhart, J.M., and Hoffmann, J.A. (1996). The dorsoventral regulatory gene cassette spatzle/Toll/cactus controls the potent antifungal response in Drosophila adults. Cell *86*, 973-983.

Leptos, K.C., Sarracino, D.A., Jaffe, J.D., Krastins, B., and Church, G.M. (2006). MapQuant: open-source software for large-scale protein quantification. Proteomics *6*, 1770-1782.

Lin, M.L., Zhan, Y., Villadangos, J.A., and Lew, A.M. (2008). The cell biology of cross-presentation and the role of dendritic cell subsets. Immunol Cell Biol *86*, 353-362.

Listgarten, J., and Emili, A. (2005). Statistical and computational methods for comparative proteomic profiling using liquid chromatography-tandem mass spectrometry. Mol Cell Proteomics *4*, 419-434.

Listgarten, J., Neal, R.M., Roweis, S.T., Wong, P., and Emili, A. (2007). Difference detection in LC-MS data for protein biomarker discovery. Bioinformatics (Oxford, England) *23*, e198-204.

Liu, Y.J. (2005). IPC: professional type 1 interferon-producing cells and plasmacytoid dendritic cell precursors. Annu Rev Immunol *23*, 275-306.

Lopez-Bravo, M., and Ardavin, C. (2008). In vivo induction of immune responses to pathogens by conventional dendritic cells. Immunity *29*, 343-351.

Lutz, M.B., Kukutsch, N., Ogilvie, A.L., Rossner, S., Koch, F., Romani, N., and Schuler, G. (1999). An advanced culture method for generating large quantities of highly pure dendritic cells from mouse bone marrow. J Immunol Methods *223*, 77-92.

Makarov, A., Denisov, E., Kholomeev, A., Balschun, W., Lange, O., Strupat, K., and Horning, S. (2006). Performance evaluation of a hybrid linear ion trap/orbitrap mass spectrometer. Analytical chemistry *78*, 2113-2120.

Maldonado-Lopez, R., De Smedt, T., Michel, P., Godfroid, J., Pajak, B., Heirman, C., Thielemans, K., Leo, O., Urbain, J., and Moser, M. (1999). CD8alpha+ and CD8alpha-subclasses of dendritic cells direct the development of distinct T helper cells in vivo. The Journal of experimental medicine *189*, 587-592.

Mann, M. (2006). Functional and quantitative proteomics using SILAC. Nat Rev Mol Cell Biol *7*, 952-958.

Mann, M. (2008). Can proteomics retire the western blot? Journal of proteome research *7*, 3065.

Maraskovsky, E., Brasel, K., Teepe, M., Roux, E.R., Lyman, S.D., Shortman, K., and McKenna, H.J. (1996). Dramatic increase in the numbers of functionally mature dendritic cells in Flt3 ligand-treated mice: multiple dendritic cell subpopulations identified. The Journal of experimental medicine *184*, 1953-1962.

Mariathasan, S., Newton, K., Monack, D.M., Vucic, D., French, D.M., Lee, W.P., Roose-Girma, M., Erickson, S., and Dixit, V.M. (2004). Differential activation of the inflammasome by caspase-1 adaptors ASC and Ipaf. Nature *430*, 213-218.

Mariathasan, S., Weiss, D.S., Newton, K., McBride, J., O'Rourke, K., Roose-Girma, M., Lee, W.P., Weinrauch, Y., Monack, D.M., and Dixit, V.M. (2006). Cryopyrin activates the inflammasome in response to toxins and ATP. Nature *440*, 228-232.

Matzinger, P. (2001). Introduction to the series. Danger model of immunity. Scandinavian journal of immunology *54*, 2-3.

May, D., Fitzgibbon, M., Liu, Y., Holzman, T., Eng, J., Kemp, C.J., Whiteaker, J., Paulovich, A., and McIntosh, M. (2007). A platform for accurate mass and time analyses of mass spectrometry data. Journal of proteome research *6*, 2685-2694.

McClatchy, D.B., Dong, M.Q., Wu, C.C., Venable, J.D., and Yates, J.R., 3rd (2007). (15)N Metabolic Labeling of Mammalian Tissue with Slow Protein Turnover. J Proteome Res.

McKenna, H.J., Stocking, K.L., Miller, R.E., Brasel, K., De Smedt, T., Maraskovsky, E., Maliszewski, C.R., Lynch, D.H., Smith, J., Pulendran, B.*, et al.* (2000). Mice lacking flt3 ligand have deficient hematopoiesis affecting hematopoietic progenitor cells, dendritic cells, and natural killer cells. Blood *95*, 3489-3497.

Medzhitov, R., and Janeway, C., Jr. (2000). The Toll receptor family and microbial recognition. Trends in microbiology *8*, 452-456.

Medzhitov, R., Preston-Hurlburt, P., and Janeway, C.A., Jr. (1997). A human homologue of the Drosophila Toll protein signals activation of adaptive immunity. Nature *388*, 394-397.

Mellman, I., and Steinman, R.M. (2001). Dendritic cells: specialized and regulated antigen processing machines. Cell *106*, 255-258.

Metcalf, D. (1988). Mechanisms contributing to the sex difference in levels of granulocyte-macrophage colony-stimulating factor in the urine of GM-CSF transgenic mice. Exp Hematol *16*, 794-800.

Metlay, J.P., Witmer-Pack, M.D., Agger, R., Crowley, M.T., Lawless, D., and Steinman, R.M. (1990). The distinct leukocyte integrins of mouse spleen dendritic cells as identified with new hamster monoclonal antibodies. The Journal of experimental medicine *171*, 1753-1771.

Meylan, E., Curran, J., Hofmann, K., Moradpour, D., Binder, M., Bartenschlager, R., and Tschopp, J. (2005). Cardif is an adaptor protein in the RIG-I antiviral pathway and is targeted by hepatitis C virus. Nature *437*, 1167-1172.

Miao, E.A., Alpuche-Aranda, C.M., Dors, M., Clark, A.E., Bader, M.W., Miller, S.I., and Aderem, A. (2006). Cytoplasmic flagellin activates caspase-1 and secretion of interleukin 1beta via Ipaf. Nature immunology *7*, 569-575.

Miceli-Richard, C., Lesage, S., Rybojad, M., Prieur, A.M., Manouvrier-Hanu, S., Hafner, R., Chamaillard, M., Zouali, H., Thomas, G., and Hugot, J.P. (2001). CARD15 mutations in Blau syndrome. Nature genetics *29*, 19-20.

Michallet, M.C., Meylan, E., Ermolaeva, M.A., Vazquez, J., Rebsamen, M., Curran, J., Poeck, H., Bscheider, M., Hartmann, G., Konig, M.*, et al.* (2008). TRADD protein is an essential component of the RIG-like helicase antiviral pathway. Immunity *28*, 651-661.

Moebius, J., Zahedi, R.P., Lewandrowski, U., Berger, C., Walter, U., and Sickmann, A. (2005). The human platelet membrane proteome reveals several new potential membrane proteins. Mol Cell Proteomics *4*, 1754-1761.

Montanez, E., Piwko-Czuchra, A., Bauer, M., Li, S., Yurchenco, P., and Fassler, R. (2007). Analysis of integrin functions in peri-implantation embryos, hematopoietic system, and skin. Methods Enzymol *426*, 239-289.

Moore, S., Spackman, D.H., and Stein, W.H. (1958). Automatic recording apparatus for use in the chromatography of amino acids. Fed Proc *17*, 1107-1115.

Moser, M., Nieswandt, B., Ussar, S., Pozgajova, M., and Fässler, R. (2008). Kindlin-3 is essential for integrin activation and platelet aggregation. Nature Medicine *14*, doi:10.1038/nm1722.

Mueller, L.N., Brusniak, M.Y., Mani, D.R., and Aebersold, R. (2008). An assessment of software solutions for the analysis of mass spectrometry based quantitative proteomics data. Journal of proteome research *7*, 51-61.

Mueller, L.N., Rinner, O., Schmidt, A., Letarte, S., Bodenmiller, B., Brusniak, M.Y., Vitek, O., Aebersold, R., and Muller, M. (2007). SuperHirn - a novel tool for high resolution LC-MS-based peptide/protein profiling. Proteomics *7*, 3470-3480.

Muranski, P., Chmielowski, B., and Ignatowicz, L. (2000). Mature CD4+ T cells perceive a positively selecting class II MHC/peptide complex in the periphery. J Immunol *164*, 3087-3094.

Naik, S.H., Proietto, A.I., Wilson, N.S., Dakic, A., Schnorrer, P., Fuchsberger, M., Lahoud, M.H., O'Keeffe, M., Shao, Q.X., Chen, W.F.*, et al.* (2005). Cutting edge: generation of splenic CD8+ and CD8- dendritic cell equivalents in Fms-like tyrosine kinase 3 ligand bone marrow cultures. J Immunol *174*, 6592-6597.

Nieswandt, B., Brakebusch, C., Bergmeier, W., Schulte, V., Bouvard, D., Mokhtari-Nejad, R., Lindhout, T., Heemskerk, J.W., Zirngibl, H., and Fassler, R. (2001). Glycoprotein VI but not alpha2beta1 integrin is essential for platelet interaction with collagen. Embo J *20*, 2120-2130.

O'Keeffe, M., Brodnicki, T.C., Fancke, B., Vremec, D., Morahan, G., Maraskovsky, E., Steptoe, R., Harrison, L.C., and Shortman, K. (2005a). Fms-like tyrosine kinase 3 ligand administration overcomes a genetically determined dendritic cell deficiency in NOD mice and protects against diabetes development. Int Immunol *17*, 307-314.

O'Keeffe, M., Grumont, R.J., Hochrein, H., Fuchsberger, M., Gugasyan, R., Vremec, D., Shortman, K., and Gerondakis, S. (2005b). Distinct roles for the NF-kappaB1 and c-Rel transcription factors in the differentiation and survival of plasmacytoid and conventional dendritic cells activated by TLR-9 signals. Blood *106*, 3457-3464.

O'Keeffe, M., Hochrein, H., Vremec, D., Caminschi, I., Miller, J.L., Anders, E.M., Wu, L., Lahoud, M.H., Henri, S., Scott, B.*, et al.* (2002a). Mouse plasmacytoid cells: long-lived cells, heterogeneous in surface phenotype and function, that differentiate into CD8(+) dendritic cells only after microbial stimulus. The Journal of experimental medicine *196*, 1307-1319.

O'Keeffe, M., Hochrein, H., Vremec, D., Pooley, J., Evans, R., Woulfe, S., and Shortman, K. (2002b). Effects of administration of progenipoietin 1, Flt-3 ligand, granulocyte colony-stimulating factor, and pegylated granulocyte-macrophage colony-stimulating factor on dendritic cell subsets in mice. Blood *99*, 2122-2130.

O'Keeffe, M., Hochrein, H., Vremec, D., Scott, B., Hertzog, P., Tatarczuch, L., and Shortman, K. (2003). Dendritic cell precursor populations of mouse blood: identification of the murine homologues of human blood plasmacytoid pre-DC2 and CD11c+ DC1 precursors. Blood *101*, 1453-1459.

O'Rourke, A.M., and Mescher, M.F. (1992). Cytotoxic T-lymphocyte activation involves a cascade of signalling and adhesion events. Nature *358*, 253-255.

Oda, Y., Huang, K., Cross, F.R., Cowburn, D., and Chait, B.T. (1999). Accurate quantitation of protein expression and site-specific phosphorylation. Proc Natl Acad Sci U S A *96*, 6591-6596.

Ogura, Y., Bonen, D.K., Inohara, N., Nicolae, D.L., Chen, F.F., Ramos, R., Britton, H., Moran, T., Karaliuskas, R., Duerr, R.H.*, et al.* (2001). A frameshift mutation in NOD2 associated with susceptibility to Crohn's disease. Nature *411*, 603-606.

Olsen, J.V., Blagoev, B., Gnad, F., Macek, B., Kumar, C., Mortensen, P., and Mann, M. (2006). Global, in vivo, and site-specific phosphorylation dynamics in signaling networks. Cell *127*, 635-648.

Olsen, J.V., de Godoy, L.M., Li, G., Macek, B., Mortensen, P., Pesch, R., Makarov, A., Lange, O., Horning, S., and Mann, M. (2005). Parts per million mass accuracy on an Orbitrap mass spectrometer via lock mass injection into a C-trap. Mol Cell Proteomics *4*, 2010-2021.

Olsen, J.V., Ong, S.E., and Mann, M. (2004). Trypsin cleaves exclusively C-terminal to arginine and lysine residues. Mol Cell Proteomics *3*, 608-614.

Ong, S.E., Blagoev, B., Kratchmarova, I., Kristensen, D.B., Steen, H., Pandey, A., and Mann, M. (2002). Stable isotope labeling by amino acids in cell culture, SILAC, as a simple and accurate approach to expression proteomics. Mol Cell Proteomics *1*, 376-386.

Ong, S.E., Kratchmarova, I., and Mann, M. (2003). Properties of 13C-substituted arginine in stable isotope labeling by amino acids in cell culture (SILAC). J Proteome Res *2*, 173-181.

Ong, S.E., and Mann, M. (2005). Mass spectrometry-based proteomics turns quantitative. Nature chemical biology *1*, 252-262.

Ong, S.E., and Mann, M. (2006). A practical recipe for stable isotope labeling by amino acids in cell culture (SILAC). Nat Protoc *1*, 2650-2660.

Ozinsky, A., Underhill, D.M., Fontenot, J.D., Hajjar, A.M., Smith, K.D., Wilson, C.B., Schroeder, L., and Aderem, A. (2000). The repertoire for pattern recognition of pathogens by the innate immune system is defined by cooperation between toll-like receptors. Proc Natl Acad Sci U S A *97*, 13766-13771.

Palagi, P.M., Walther, D., Quadroni, M., Catherinet, S., Burgess, J., Zimmermann-Ivol, C.G., Sanchez, J.C., Binz, P.A., Hochstrasser, D.F., and Appel, R.D. (2005). MSight: an image analysis software for liquid chromatography-mass spectrometry. Proteomics *5*, 2381-2384.

Panchaud, A., Affolter, M., Moreillon, P., and Kussmann, M. (2008). Experimental and computational approaches to quantitative proteomics: status quo and outlook. Journal of proteomics *71*, 19-33.

Park, S.K., Venable, J.D., Xu, T., and Yates, J.R., 3rd (2008). A quantitative analysis software tool for mass spectrometry-based proteomics. Nature methods *5*, 319-322.

Parker, D.C. (1993). T cell-dependent B cell activation. Annual review of immunology *11*, 331-360.

Pasini, E.M., Kirkegaard, M., Mortensen, P., Lutz, H.U., Thomas, A.W., and Mann, M. (2006). In-depth analysis of the membrane and cytosolic proteome of red blood cells. Blood *108*, 791-801.

Peters, L.L., Weier, H.U., Walensky, L.D., Snyder, S.H., Parra, M., Mohandas, N., and Conboy, J.G. (1998). Four paralogous protein 4.1 genes map to distinct chromosomes in mouse and human. Genomics *54*, 348-350.

Pichlmair, A., Schulz, O., Tan, C.P., Naslund, T.I., Liljestrom, P., Weber, F., and Reis e Sousa, C. (2006). RIG-I-mediated antiviral responses to single-stranded RNA bearing 5'-phosphates. Science *314*, 997-1001.

Pierre, P., Turley, S.J., Gatti, E., Hull, M., Meltzer, J., Mirza, A., Inaba, K., Steinman, R.M., and Mellman, I. (1997). Developmental regulation of MHC class II transport in mouse dendritic cells. Nature *388*, 787-792.

Poltorak, A., He, X., Smirnova, I., Liu, M.Y., Van Huffel, C., Du, X., Birdwell, D., Alejos, E., Silva, M., Galanos, C.*, et al.* (1998). Defective LPS signaling in C3H/HeJ and C57BL/10ScCr mice: mutations in Tlr4 gene. Science *282*, 2085-2088.

Pooley, J.L., Heath, W.R., and Shortman, K. (2001). Cutting edge: intravenous soluble antigen is presented to CD4 T cells by CD8- dendritic cells, but cross-presented to CD8 T cells by CD8+ dendritic cells. J Immunol *166*, 5327-5330.

Pratt, J.M., Robertson, D.H., Gaskell, S.J., Riba-Garcia, I., Hubbard, S.J., Sidhu, K., Oliver, S.G., Butler, P., Hayes, A., Petty, J., and Beynon, R.J. (2002). Stable isotope labelling in vivo as an aid to protein identification in peptide mass fingerprinting. Proteomics *2*, 157-163.

Press, W.H., Teukolsky, S.H., Vetterling, W.T., and Flannery, B.P. (2007). Numerical Recipes: The Art of Scientific Computing, Third Edition (Cambridge University Press).

Proietto, A.I., O'Keeffe, M., Gartlan, K., Wright, M.D., Shortman, K., Wu, L., and Lahoud, M.H. (2004). Differential production of inflammatory chemokines by murine dendritic cell subsets. Immunobiology *209*, 163-172.

Radtke, F., and Clevers, H. (2005). Self-renewal and cancer of the gut: two sides of a coin. Science *307*, 1904-1909.

Rakoff-Nahoum, S., and Medzhitov, R. (2009). Toll-like receptors and cancer. Nat Rev Cancer *9*, 57-63.

Rappsilber, J., Ishihama, Y., and Mann, M. (2003). Stop and go extraction tips for matrix-assisted laser desorption/ionization, nanoelectrospray, and LC/MS sample pretreatment in proteomics. Analytical chemistry *75*, 663-670.

Rappsilber, J., Ryder, U., Lamond, A.I., and Mann, M. (2002). Large-scale proteomic analysis of the human spliceosome. Genome research *12*, 1231-1245.

Rauch, A., Bellew, M., Eng, J., Fitzgibbon, M., Holzman, T., Hussey, P., Igra, M., Maclean, B., Lin, C.W., Detter, A.*, et al.* (2006). Computational Proteomics Analysis System (CPAS): an extensible, open-source analytic system for evaluating and publishing proteomic data and high throughput biological experiments. Journal of proteome research *5*, 112-121.

Reis e Sousa, C., Hieny, S., Scharton-Kersten, T., Jankovic, D., Charest, H., Germain, R.N., and Sher, A. (1997). In vivo microbial stimulation induces rapid CD40 ligand-independent production of interleukin 12 by dendritic cells and their redistribution to T cell areas. The Journal of experimental medicine *186*, 1819-1829.

Reis e Sousa, C., Stahl, P.D., and Austyn, J.M. (1993). Phagocytosis of antigens by Langerhans cells in vitro. The Journal of experimental medicine *178*, 509-519.

Rescigno, M., Granucci, F., Citterio, S., Foti, M., and Ricciardi-Castagnoli, P. (1999). Coordinated events during bacteria-induced DC maturation. Immunology today *20*, 200-203.

Ross, P.L., Huang, Y.N., Marchese, J.N., Williamson, B., Parker, K., Hattan, S., Khainovski, N., Pillai, S., Dey, S., Daniels, S.*, et al.* (2004). Multiplexed protein quantitation in Saccharomyces cerevisiae using amine-reactive isobaric tagging reagents. Mol Cell Proteomics *3*, 1154-1169.

Rothenfusser, S., Goutagny, N., DiPerna, G., Gong, M., Monks, B.G., Schoenemeyer, A., Yamamoto, M., Akira, S., and Fitzgerald, K.A. (2005). The RNA helicase Lgp2 inhibits TLR-independent sensing of viral replication by retinoic acid-inducible gene-I. J Immunol *175*, 5260-5268.

Roy, S.M., and Becker, C.H. (2007). Quantification of proteins and metabolites by mass spectrometry without isotopic labeling. Methods in molecular biology (Clifton, N.J *359*, 87-105.

Ruggeri, Z.M. (2002). Platelets in atherothrombosis. Nat Med *8*, 1227-1234.

Rybicki, A.C., Musto, S., and Schwartz, R.S. (1995). Decreased content of protein 4.2 in ankyrin-deficient normoblastosis (nb/nb) mouse red blood cells: evidence for ankyrin enhancement of protein 4.2 membrane binding. Blood *86*, 3583-3589.

Saeed, A.I., Sharov, V., White, J., Li, J., Liang, W., Bhagabati, N., Braisted, J., Klapa, M., Currier, T., Thiagarajan, M*., et al.* (2003). TM4: a free, open-source system for microarray data management and analysis. BioTechniques *34*, 374-378.

Saito, T., Hirai, R., Loo, Y.M., Owen, D., Johnson, C.L., Sinha, S.C., Akira, S., Fujita, T., and Gale, M., Jr. (2007). Regulation of innate antiviral defenses through a shared repressor domain in RIG-I and LGP2. Proc Natl Acad Sci U S A *104*, 582-587.

Saito, T., Owen, D.M., Jiang, F., Marcotrigiano, J., and Gale, M., Jr. (2008). Innate immunity induced by composition-dependent RIG-I recognition of hepatitis C virus RNA. Nature *454*, 523-527.

Sallusto, F., and Lanzavecchia, A. (1994). Efficient presentation of soluble antigen by cultured human dendritic cells is maintained by granulocyte/macrophage colony-stimulating factor plus interleukin 4 and downregulated by tumor necrosis factor alpha. The Journal of experimental medicine *179*, 1109-1118.

Schiess, R., Mueller, L.N., Schmidt, A., Mueller, M., Wollscheid, B., and Aebersold, R. (2008). Analysis of cell surface proteome changes via label-free, quantitative mass spectrometry. Mol Cell Proteomics.

Schnorrer, P., Behrens, G.M., Wilson, N.S., Pooley, J.L., Smith, C.M., El-Sukkari, D., Davey, G., Kupresanin, F., Li, M., Maraskovsky, E*., et al.* (2006). The dominant role of CD8+ dendritic cells in cross-presentation is not dictated by antigen capture. Proc Natl Acad Sci U S A *103*, 10729-10734.

Schoenheimer, R., and Rittenberg, D. (1935). Deuterium as an indicator in the study of intermediary metabolism. Science *82*, 156-157.

Schuler, G., and Steinman, R.M. (1985). Murine epidermal Langerhans cells mature into potent immunostimulatory dendritic cells in vitro. The Journal of experimental medicine *161*, 526-546.

Schulz, O., Diebold, S.S., Chen, M., Naslund, T.I., Nolte, M.A., Alexopoulou, L., Azuma, Y.T., Flavell, R.A., Liljestrom, P., and Reis e Sousa, C. (2005). Toll-like receptor 3 promotes cross-priming to virus-infected cells. Nature *433*, 887-892.

Schulze, W.X., and Mann, M. (2004). A novel proteomic screen for peptide-protein interactions. J Biol Chem *279*, 10756-10764.

Selbach, M., Schwanhausser, B., Thierfelder, N., Fang, Z., Khanin, R., and Rajewsky, N. (2008). Widespread changes in protein synthesis induced by microRNAs. Nature *455*, 58-63.

Serbina, N.V., Salazar-Mather, T.P., Biron, C.A., Kuziel, W.A., and Pamer, E.G. (2003). TNF/iNOS-producing dendritic cells mediate innate immune defense against bacterial infection. Immunity *19*, 59-70.

Shevchenko, A., Wilm, M., Vorm, O., and Mann, M. (1996). Mass spectrometric sequencing of proteins silver-stained polyacrylamide gels. Anal Chem *68*, 850-858.

Shi, R., Kumar, C., Zougman, A., Zhang, Y., Podtelejnikov, A., Cox, J., Wisniewski, J.R., and Mann, M. (2007). Analysis of the mouse liver proteome using advanced mass spectrometry. Journal of proteome research *6*, 2963-2972.

Shi, Z.T., Afzal, V., Coller, B., Patel, D., Chasis, J.A., Parra, M., Lee, G., Paszty, C., Stevens, M., Walensky, L.*, et al.* (1999). Protein 4.1R-deficient mice are viable but have erythroid membrane skeleton abnormalities. J Clin Invest *103*, 331-340.

Shimazu, R., Akashi, S., Ogata, H., Nagai, Y., Fukudome, K., Miyake, K., and Kimoto, M. (1999). MD-2, a molecule that confers lipopolysaccharide responsiveness on Toll-like receptor 4. The Journal of experimental medicine *189*, 1777-1782.

Shortman, K., and Naik, S.H. (2007). Steady-state and inflammatory dendritic-cell development. Nature reviews *7*, 19-30.

Silverman, R.H. (2007). Viral encounters with 2',5'-oligoadenylate synthetase and RNase L during the interferon antiviral response. Journal of virology *81*, 12720-12729.

Smith, R.D., Anderson, G.A., Lipton, M.S., Pasa-Tolic, L., Shen, Y., Conrads, T.P., Veenstra, T.D., and Udseth, H.R. (2002). An accurate mass tag strategy for quantitative and high-throughput proteome measurements. Proteomics *2*, 513-523.

Southgate, C.D., Chishti, A.H., Mitchell, B., Yi, S.J., and Palek, J. (1996). Targeted disruption of the murine erythroid band 3 gene results in spherocytosis and severe haemolytic anaemia despite a normal membrane skeleton. Nat Genet *14*, 227-230.

Squier, M.K., and Cohen, J.J. (1994). Cell-mediated cytotoxic mechanisms. Current opinion in immunology *6*, 447-452.

Starr, T.K., Jameson, S.C., and Hogquist, K.A. (2003). Positive and negative selection of T cells. Annu Rev Immunol *21*, 139-176.

Steinman, R.M. (2007). Lasker Basic Medical Research Award. Dendritic cells: versatile controllers of the immune system. Nature medicine *13*, 1155-1159.

Steinman, R.M., and Banchereau, J. (2007). Taking dendritic cells into medicine. Nature *449*, 419-426.

Steinman, R.M., and Nussenzweig, M.C. (2002). Avoiding horror autotoxicus: the importance of dendritic cells in peripheral T cell tolerance. Proceedings of the National Academy of Sciences of the United States of America *99*, 351-358.

Stetson, D.B., and Medzhitov, R. (2006). Type I interferons in host defense. Immunity *25*, 373-381.

Stockinger, B. (1999). T lymphocyte tolerance: from thymic deletion to peripheral control mechanisms. Advances in immunology *71*, 229-265.

Svensson, M., Stockinger, B., and Wick, M.J. (1997). Bone marrow-derived dendritic cells can process bacteria for MHC-I and MHC-II presentation to T cells. J Immunol *158*, 4229-4236.

Takaoka, A., Wang, Z., Choi, M.K., Yanai, H., Negishi, H., Ban, T., Lu, Y., Miyagishi, M., Kodama, T., Honda, K.*, et al.* (2007). DAI (DLM-1/ZBP1) is a cytosolic DNA sensor and an activator of innate immune response. Nature *448*, 501-505.

Takeda, K., Kaisho, T., and Akira, S. (2003). Toll-like receptors. Annu Rev Immunol *21*, 335-376.

Takeuchi, O., Hoshino, K., and Akira, S. (2000). Cutting edge: TLR2-deficient and MyD88-deficient mice are highly susceptible to Staphylococcus aureus infection. J Immunol *165*, 5392-5396.

Tamura, T., Tailor, P., Yamaoka, K., Kong, H.J., Tsujimura, H., O'Shea, J.J., Singh, H., and Ozato, K. (2005). IFN regulatory factor-4 and -8 govern dendritic cell subset development and their functional diversity. J Immunol *174*, 2573-2581.

Taouatas, N., Drugan, M.M., Heck, A.J., and Mohammed, S. (2008). Straightforward ladder sequencing of peptides using a Lys-N metalloendopeptidase. Nat Methods.

Ussar, S., Wang, H.V., Linder, S., Fassler, R., and Moser, M. (2006). The Kindlins: subcellular localization and expression during murine development. Exp Cell Res *312*, 3142-3151.

Veerman, A.J., and van Ewijk, W. (1975). White pulp compartments in the spleen of rats and mice. A light and electron microscopic study of lymphoid and non-lymphoid celltypes in T- and B-areas. Cell Tissue Res *156*, 417-441.

Villadangos, J.A., and Schnorrer, P. (2007). Intrinsic and cooperative antigen-presenting functions of dendritic-cell subsets in vivo. Nat Rev Immunol *7*, 543-555.

Villadangos, J.A., and Young, L. (2008). Antigen-presentation properties of plasmacytoid dendritic cells. Immunity *29*, 352-361.

Vremec, D., Lieschke, G.J., Dunn, A.R., Robb, L., Metcalf, D., and Shortman, K. (1997). The influence of granulocyte/macrophage colony-stimulating factor on dendritic cell levels in mouse lymphoid organs. Eur J Immunol *27*, 40-44.

Vremec, D., O'Keeffe, M., Hochrein, H., Fuchsberger, M., Caminschi, I., Lahoud, M., and Shortman, K. (2007). Production of interferons by dendritic cells, plasmacytoid cells, natural killer cells, and interferon-producing killer dendritic cells. Blood *109*, 1165-1173.

Vremec, D., Pooley, J., Hochrein, H., Wu, L., and Shortman, K. (2000). CD4 and CD8 expression by dendritic cell subtypes in mouse thymus and spleen. J Immunol *164*, 2978-2986.

Vremec, D., and Shortman, K. (2008). The isolation and identification of murine dendritic cell populations from lymphoid tissues and their production in culture. Methods Mol Biol *415*, 163-178.

Vremec, D., Zorbas, M., Scollay, R., Saunders, D.J., Ardavin, C.F., Wu, L., and Shortman, K. (1992). The surface phenotype of dendritic cells purified from mouse thymus and spleen: investigation of the CD8 expression by a subpopulation of dendritic cells. The Journal of experimental medicine *176*, 47-58.

Wang, T., Town, T., Alexopoulou, L., Anderson, J.F., Fikrig, E., and Flavell, R.A. (2004). Toll-like receptor 3 mediates West Nile virus entry into the brain causing lethal encephalitis. Nat Med *10*, 1366-1373.

Wilkins, M.R., Sanchez, J.C., Gooley, A.A., Appel, R.D., Humphery-Smith, I., Hochstrasser, D.F., and Williams, K.L. (1996). Progress with proteome projects: why all proteins expressed by a genome should be identified and how to do it. Biotechnology & genetic engineering reviews *13*, 19-50.

Wilson, N.S., Behrens, G.M., Lundie, R.J., Smith, C.M., Waithman, J., Young, L., Forehan, S.P., Mount, A., Steptoe, R.J., Shortman, K.D*., et al.* (2006). Systemic activation of dendritic cells

by Toll-like receptor ligands or malaria infection impairs cross-presentation and antiviral immunity. Nature immunology *7*, 165-172.

Wilson, N.S., El-Sukkari, D., Belz, G.T., Smith, C.M., Steptoe, R.J., Heath, W.R., Shortman, K., and Villadangos, J.A. (2003). Most lymphoid organ dendritic cell types are phenotypically and functionally immature. Blood *102*, 2187-2194.

Wilson, N.S., El-Sukkari, D., and Villadangos, J.A. (2004). Dendritic cells constitutively present self antigens in their immature state in vivo and regulate antigen presentation by controlling the rates of MHC class II synthesis and endocytosis. Blood *103*, 2187-2195.

Wilson, N.S., Young, L.J., Kupresanin, F., Naik, S.H., Vremec, D., Heath, W.R., Akira, S., Shortman, K., Boyle, J., Maraskovsky, E.*, et al.* (2008). Normal proportion and expression of maturation markers in migratory dendritic cells in the absence of germs or Toll-like receptor signaling. Immunol Cell Biol *86*, 200-205.

Wolfe, R.R., and Chinkes, D.L. (2005). Isotope tracers in metabolic research (New Jersey: Wiley-LISS).

Wu, C.C., MacCoss, M.J., Howell, K.E., Matthews, D.E., and Yates, J.R., 3rd (2004). Metabolic labeling of mammalian organisms with stable isotopes for quantitative proteomic analysis. Anal Chem *76*, 4951-4959.

Wu, L., D'Amico, A., Winkel, K.D., Suter, M., Lo, D., and Shortman, K. (1998). RelB is essential for the development of myeloid-related CD8alpha- dendritic cells but not of lymphoid-related CD8alpha+ dendritic cells. Immunity *9*, 839-847.

Wykes, M., Pombo, A., Jenkins, C., and MacPherson, G.G. (1998). Dendritic cells interact directly with naive B lymphocytes to transfer antigen and initiate class switching in a primary T-dependent response. J Immunol *161*, 1313-1319.

Xagorari, A., and Chlichlia, K. (2008). Toll-like receptors and viruses: induction of innate antiviral immune responses. Open Microbiol J *2*, 49-59.

Xu, D., Suenaga, N., Edelmann, M.J., Fridman, R., Muschel, R.J., and Kessler, B.M. (2008). Novel MMP-9 substrates in cancer cells revealed by a label-free quantitative proteomics approach. Mol Cell Proteomics *7*, 2215-2228.

Xu, Y., Zhan, Y., Lew, A.M., Naik, S.H., and Kershaw, M.H. (2007). Differential development of murine dendritic cells by GM-CSF versus Flt3 ligand has implications for inflammation and trafficking. J Immunol *179*, 7577-7584.

Yang, G.X., Lian, Z.X., Kikuchi, K., Liu, Y.J., Ansari, A.A., Ikehara, S., and Gershwin, M.E. (2005). CD4- plasmacytoid dendritic cells (pDCs) migrate in lymph nodes by CpG inoculation and represent a potent functional subset of pDCs. J Immunol *174*, 3197-3203.

Ye, Z., Lich, J.D., Moore, C.B., Duncan, J.A., Williams, K.L., and Ting, J.P. (2008). ATP binding by monarch-1/NLRP12 is critical for its inhibitory function. Molecular and cellular biology *28*, 1841-1850.

Yoneyama, M., and Fujita, T. (2007). Function of RIG-I-like receptors in antiviral innate immunity. J Biol Chem *282*, 15315-15318.

Yoneyama, M., Kikuchi, M., Matsumoto, K., Imaizumi, T., Miyagishi, M., Taira, K., Foy, E., Loo, Y.M., Gale, M., Jr., Akira, S.*, et al.* (2005). Shared and unique functions of the DExD/H-box helicases RIG-I, MDA5, and LGP2 in antiviral innate immunity. J Immunol *175*, 2851-2858.

Young, L.J., Wilson, N.S., Schnorrer, P., Proietto, A., ten Broeke, T., Matsuki, Y., Mount, A.M., Belz, G.T., O'Keeffe, M., Ohmura-Hoshino, M.*, et al.* (2008). Differential MHC class II

synthesis and ubiquitination confers distinct antigen-presenting properties on conventional and plasmacytoid dendritic cells. Nat Immunol *9*, 1244-1252.

Zhang, Y., Zhang, Y., Adachi, J., Olsen, J.V., Shi, R., de Souza, G., Pasini, E., Foster, L.J., Macek, B., Zougman, A.*, et al.* (2007). MAPU: Max-Planck Unified database of organellar, cellular, tissue and body fluid proteomes. Nucleic Acids Res *35*, D771-779.

Zinkernagel, R.M. (2003). On natural and artificial vaccinations. Annual review of immunology *21*, 515-546.

Zinkernagel, R.M., and Doherty, P.C. (1974). Restriction of in vitro T cell-mediated cytotoxicity in lymphocytic choriomeningitis within a syngeneic or semiallogeneic system. Nature *248*, 701-702.

Acknowledgements

First of all to my boss Matthias Mann for his generous support and the opportunity to learn cutting edge mass spectrometry from a visionary leader in the field. In particular, I want to thank Matthias for understanding the PhD candidate specific problems and his willingness to do something against it: "Mangelfachzulage". For supporting all my scientific trips: Vienna (NIBR), Edinburgh (DC conference), Celerina (DCThera graduate school), Dunk Island and Melbourne (Antigen processing and presentation workshop and WEHI), Kobe (DC conference), Marseille (DCThera meeting). For offering unlimited and free access to high quality coffee: "do stupid things faster with more energy".

To "my" post-doc Matthias Selbach. I had my best time together with Matthias in our little office E 131b. Many thanks for all the fun, discussions, coffee breaks, ideas and advice. For his support until now. Hasta mañana.

To my co-supervisors and friends Meredith O'Keeffe and Hubertus Hochrein from Bavarian Nordic. It is always a pleasure to come over, to do experiments, to learn, even to recognize how much I still have to learn, to get motivated again, to work even harder and just to chat and drink coffee. Let's combine BN, MPIBC and Burnet! I would also like to thank in particular Ben Fancke, Barbara Bathke and Henning Lauterbach.

To my friends in the Mann lab, who have helped me with friendship, moral support and practical advice: Charo, Gabi, Tanja, Michiel, Tizi, Marcus, and Martin. Particularly to Charo, who helped through the often-tragic existence of being a PhD student in the Mann lab.

To my friends in the Fässler department: The rising stars Michl and Marc. Thank you for your great support and discussions. Viva Caffe Coretto! I would also like to thank Tim, a great colleague!

To a very special person, in all possible ways, Francesca Forner.

To the other members of the Mann lab and MPIBC family; to Theresa Schneider and Tine Klitmoeller for organizational help. To the animal technicians, especially Jeanette Biebl and Silvana Kaphengst, for taking care of my Cardif knockouts. I would also like to thank our vets Dr. Moerth and Dr. Brandstetter.

To my best friend Schlaffi, who has accompanied me with limitless friendship and support from Amberg via Tübingen via Melbourne via Basel till now in Munich. I am very proud to have such a friend.

Of course, nothing would be as it is without the continuous support of my wonderful parents, who have encouraged me to do my steps, even if these steps led far away towards Australia. I can't thank you enough. Many thanks also to my well beloved sister Tanja, my godchild Antonia and Toni.

Publications

Christian A. Luber*, Jürgen Cox*, Ben Fancke, Matthias Selbach, Jurg Tschopp, Shizo Akira, Hubertus Hochrein, Meredith O'Keeffe and Matthias Mann. Quantitative proteomics reveals subset-specific viral recognition in dendritic cells (*under revision in Immunity*)

Jürgen Cox*, **Christian A. Luber***, Nagarjuna Nagaraj and Matthias Mann. Delayed normalization and maximal peptide ratio pairing for proteome-wide label-free quantification (*under review in Nature methods*)

Francesca Forner, Chanchal Kumar, **Christian A. Luber**, Tobias Fromme, Martin Klingenspor, Matthias Mann. Mass spectrometry of brown and white fat mitochondria discovers proteome differences determining specialized metabolic functions (*submitted to Cell metabolism*)

Krüger M, Moser M, Ussar S, Thievessen I, **Luber CA**, Forner F, Schmidt S, Zanivan S, Fässler R, Mann M. (2008) SILAC mouse for quantitative proteomics uncovers kindlin-3 as an essential factor for red blood cell function. *Cell*. 134 (2): 353-364

Maitra S, Chou CF, **Luber CA**, Lee KY, Mann M, Chen CY. (2008) The AU-rich element mRNA decay-promoting activity of BRF1 is regulated by mitogen-activated protein kinase-activated protein kinase 2. *RNA*. 14 (5): 950-959

*: equal contribution

Scientific presentations

1 – 5 October 2008

    Poster presentation

    The quantitative proteome of splenic conventional dendritic cell subsets

    10th International Symposium on Dendritic Cells

    Kobe, Japan

    Poster selected for travel award

15 October 2007

    Oral presentation

    Mass spectrometry and dendritic cells

    The Walter and Eliza Hall Institute of Medical Research

    Melbourne, Australia

7 – 11 October 2007

    Oral presentation

    Quantitative proteomic investigations of mouse dendritic cells

    5th International Antigen Processing and Presentation Workshop

    Dunk Island, Australia

16 – 20 September 2006

    Poster presentation

    A phosphoproteomic approach to study migration of dendritic cells

    9th International Conference on Dendritic Cells

    Edinburgh, United Kingdom

23 - 25 February 2006

    Short oral presentation

    Phosphoproteomics in dendritic cells

    Kick-off meeting, Novartis NIBR, Vienna, Austria

Curriculum vitae

CHRISTIAN A. LUBER

DATE OF BIRTH: May 27, 1978

PLACE OF BIRTH: Hirschau, Oberpfalz

NATIONALITY: German

FAMILY STATUS: unmarried

ACADEMIC EDUCATION

7/2005 – till date	Department of Proteomics and Signal Transduction Max Planck Institute of Biochemistry, Martinsried, Germany PhD candidate *Pattern recognition receptors are subset specific in dendritic cells.* *In vivo quantitative proteomic investigations using label-free analysis* *and the SILAC mouse* Advisor: Matthias Mann
3/2005 – 6/2005	Pharma Research Basel Roche Center for Medical Genomics: Applied Immunology F. Hoffmann - La Roche, Basel, Switzerland *Immunogenicity – pilot study* Advisors: Harald Kropshofer, Anne Vogt
10/2004– 2/2005	Immunology Division The Walter and Eliza Hall Institute of Medical Research Melbourne, Australia *Subcellular fractionation of dendritic cell subsets* Advisors: Jose Villadangos, Ken Shortman
4/1998 – 8/2004	Eberhard Karls University, Tübingen, Germany Diploma in Biochemistry *Processing of protein antigens in human dendritic cells* Advisor: Hubert Kalbacher

EXPERIENCE

9/2004– 10/2004	Medical and Natural Sciences Research Center Eberhard Karls University, Tübingen, Germany Scientific Coworker in the lab of Dr. Hubert Kalbacher
10/2000– 7/2004	Institute for Physiological Chemistry Eberhard Karls University, Tübingen, Germany Teaching assistant of students in medicine in their course in chemistry

9/2000– 12/2002	Medical and Natural Sciences Research Center Eberhard Karls University, Tübingen, Germany Student assistant in the lab of Dr. Hubert Kalbacher
3/2002– 5/2002	Max Planck Institute of Biochemistry, Martinsried, Germany Internship Advisors: Luis Moroder, Robert Huber
7/2001– 9/2001	Roche Diagnostics F. Hoffmann - La Roche, Penzberg, Germany Internship

FURTHER QUALIFICATIONS

2006	GCP Workshop Erlangen, Germany
2005	Project leader and commissary for biological safety qualification §15 GenTSV

SOCIAL SERVICE

7/1997– 4/1998	Welfare Center, Hirschau, Germany Health Care Aid